Preparation and Characterization of Metalorganic Compounds as Precursors for the Preparation of Electronic Materials by Chemical Vapor Deposition

A Thesis
Presented to
The Academic Faculty

by

Henry Alney Luten III.

In Partial Fulfillment
of the Requirements for the Degree
Doctor of Philosophy in Chemistry

Georgia Institute of Technology
August 1996

Preparation and Characterization of Metalorganic Compounds
as Precursors for the Preparation of Electronic Materials
by Chemical Vapor Deposition

Approved:

William S. Rees, Jr., Advisor

Angus P. Wilkinson

E. Kent Barefield

Charles L. Liotta

W. Brent Carter

Date Approved: 24 Aug. '96

TABLE OF CONTENTS

LIST OF TABLES

LIST OF FIGURES

SUMMARY

Much interest in the area of group 2 element containing ferroelectric, superconducting and dielectric thin films has been generated by the recent observation of unique properties in these materials. MOCVD, one preferred technique of the present electronics industry, has not yet emerged as the thin film method of choice due to the demonstrable shortcomings of the available source compounds. As deposition methods move toward potential commercialization, the importance of precursors that are chemically and thermally stable at use temperature will emerge. These precursors must have high vapor pressures and purities and must also be readily available and economically competitive sources for the requisite group 2 elements. Most specifically, the challenge presented by the group 2 element charge/ionic radius ratio must be overcome to meet the vapor pressure requirements for MOCVD. This presentation entails an initial overview of the presently utilized compounds, their advantages and disadvantages. Recent findings on the coordination environment around the central metal atom have offered insight into the next generation of polydentate, monoanionic ligand design. The results of comparison studies between these new precursors and earlier compounds are presented as a model for designing future sources.

Molecular mechanics calculations have been carried out in an effort to explain the relative disparity in the vapor phase stabilities of existing barium *bis*(β-diketonate)•Lewis

base compounds. This explanation is based on the observed relationship between the charge density on the bonding oxygens of the unperturbed β-diketonate ligand and the lengths of the barium-Lewis base interactions. Reasonable agreement has been found between the developed predictive model and the known structures for a group of barium compounds: $Ba(tmhd)_2$•tetraglyme, $Ba(hfac)_2$•tetraglyme, $Ba(tfac)_2$•tetraglyme, $Ba(tdfnd)_2$•tetraglyme and $Ba(dmhd)_2$•tetraglyme (tmhd = 2,2,6,6-tetramethylheptane-3,5-dionate, hfac = 1,1,1,5,5,5-hexafluoropentane-2,4-dionate, dmhd = 5,5-dimethylhexane-2,4-dionate) tfac = 1,1,1-trifluoropentane-2,4-dionate, tdfnd = 1,1,1,2,2,3,3,7,7,8,8,9,9,9-tetradecafluorononane-4,6-dionate). This model has been used to design a number of ligands that show promise for the formation of volatile, thermally stable barium source materials for MOCVD.

The preparation of $[Y(tmhd)_3 \cdot H_2O]_2$, $Y(tmhd)_3$ and $[Y(tmod)_3]_2$ (tmhd = 2,2,6,6-tetramethylheptane-3,5-dionate; tmod = 2,2,7-trimethyloctane-3,5-dionate) are described. These compounds have been characterized by ^1H and ^{13}C NMR, IR, UV/VIS, TGA, GC/MS techniques and single crystal x-ray diffraction. The vapor pressures of the compounds are discussed in light of ligand symmetry concerns. Chemical vapor deposition experiments with these compounds produced films which were characterized by XRD, SEM, ESCA and surface profilometry. Film deposit composition and morphology are compared to deposition conditions.

Solid state molecular structure determinations have been carried out on several metalorganic compounds. Structural data, models and collection parameters are given.

CHAPTER I

GROUP 2 ELEMENT COMPOUNDS: FROM COORDINATION CHEMISTRY TO ELECTRONIC MATERIALS

The second group of the periodic table, referred to as the alkaline earth metals, is comprised of beryllium, magnesium, calcium, strontium, barium and radium. This group, in the past, also was referred to as Group II or Group 2A. The Group 2A designation is used to indicate that group 2 (IIA) is similar to group 12 (IIB) in that both are dominated in their chemistry by divalent cations. The heavier group 2 elements, Ca through Ra, have properties similar to the alkali metal (group 1) elements in that their bonding is dominated by ionic interactions. The ionic radii of the group 2 dications are smaller than those of the corresponding group 1 monocations, due to the increased nuclear charge of the group 2 ions. Like the alkali metals, reactivity increases with atomic number in the group 2 elements. Beryllium is an exception in its properties, as to a lesser extent is magnesium. The chemistry of beryllium compounds is dominated by covalent bonding. It forms stable metal carbon bonds.

There has been a significant amount of confusion about the toxicity of beryllium.[1] Numerous reports are based on incomplete research and, in a limited number of instances, have been misquoted at great length in the subsequent scientific literature. For example,

one authoritative work states, "It should be noted that not more than 500 g Be total, *in any chemical form*, should be kept in the laboratory; otherwise, in the event of a fire, beryllium compounds could be vaporized or blown about to such an extent as to constitute a hazard to the surrounding area."[2] Yet, in 1948, after a major fire and explosion in a Lorain, Ohio, beryllium manufacturing facility, which included the ignition of some 2.5 tons of Mg in the BeO processing factory, no firefighters, police, naval reserve personnel or spectators reported any symptoms of beryllium related diseases.[1]

With the data available at this point, it does not appear that ingestion of beryllium compounds presents a significant health hazard. Likewise, there is no evidence to indicate that simple skin contact with elemental beryllium, or its compounds, will result in dermatitis. The unequivocal establishment of an immunological basis for chronic beryllium disease (CBD) determined this disorder to be a pulmonary granulomatosis process. Chronic beryllium disease is a localized response to an insoluble and persistent irritant. Acute pulmonary beryllium disease is caused by airborne particulates of soluble beryllium salts, primarily $BeSO_4$ or BeF_2. This disease generally is limited to the upper respiratory tract. Although there were 30 - 60 new cases per year during the period 1942 - 1947, there have been less than ten total confirmed cases within the past 40 years. In almost every instance, it was a single isolated case resulting from accidental exposure during maintenance work at a manufacturing facility. Thus, although perhaps not as benign as its heavier congeners, Mg and Ca, the relative risk posed by Be is rather small. When compared to other inorganic compounds, such as AsH_3 which has exposure limits of 25 $\mu g\ m^{-3}$ per 30 min, the relative threat of Be can be put in perspective.

Magnesium forms stable covalent bonds with carbon, as portrayed in the rich chemistry associated with Grignard reagents. Magnesium also forms stable ionic salts which are water soluble. Radium differentiates itself from the rest of the group 2 elements due to the radioactivity of all of its isotopes. Radium-226 is the most stable isotope ($T_{1/2}$ ~ 1600 years) and is formed in the natural decay series of ^{238}U.[3] The chemical property differences of the group 2 elements can be explained by examination of the charge to radius ratio of the ions (**Table 1-1**).[3] For comparison, the charge / radius ratio for carbon is 4.4.[4] The only cations with charge densities higher than Be^{2+} are B^{3+} and H^{+}. Aluminum^{3+} is closest to Be^{2+} in charge density, and shows somewhat similar properties. Barium and radium are weaker Lewis acids than the earlier group 2 cations, due to their much larger ionic radii. The increased ionic radii, in effect, spreads their charge out, lowering the charge density at any point on their coordination spheres, thus making them weaker acids.

Table 1-1 Ionic radii and charge densities of the group 2 element dications.

Cation	Ionic Radius* (pm)	Charge / Radius ($^{e}/_{A}$)
Be^{2+}	31	6.5
Mg^{2+}	78	3.1
Ca^{2+}	106	2.0
Sr^{2+}	127	1.8
Ba^{2+}	143	1.5
Ra^{2+}	157	1.3

*Ladd Radii[3]

Group 2 elements are utilized in a broad spectrum of electronic materials, ranging from insulators to superconductors. As electronic circuitry is miniaturized to smaller and smaller dimensions, the performance level of dielectric materials used as insulating layers becomes increasingly more important. Also, capacitance-based devices, such as dynamic random access memory (DRAM) circuits, benefit from improved dielectric performance.[5] Barium titanate ($BaTiO_3$), strontium titanate ($SrTiO_3$) and the solid solution barium strontium titanium oxide ($\{Ba,Sr\}TiO_3$) (BSTO) each are oxides which show promise as high performance dielectrics.[5,6] In such DRAM architectures as those postulated for 1 Gbit and above, it is the product of the dielectric constant (ε) of the active region and the thickness of the layer (d) which forms the figure of merit. Thus, ε / d must be maximized - per memory cell volume - by achievement of 10 - 1,000 times improvement in ε over the present SiO_2 composition, unless device design can accommodate cell stacks of tens of microns in height. Such an engineering of the capacitor is not presently on the horizon. Thus, the challenge for the materials chemist is to maximize ε for the currently known BSTO composition.

In 1986 Bednorz and Müller discovered a new cuprate based superconductor with a T_c of 30 K.[7] This discovery lead to a flurry of research in the area. In 1987 Wu *et al.* discovered yttrium-barium-copper-oxide ($YBa_2Cu_3O_{7-\delta}$), also known as YBCO or 123, a cuprate-based superconductor with a T_c of 93 K.[8] The structure of YBCO is shown in **Figure 1-1**. This particularly was significant since the superconducting transition temperature is higher than the boiling point of nitrogen. In 1988 the stakes were raised

again by the discovery of the first non-rare earth-containing superconducting metal oxide (SMO) bismuth-strontium-calcium-copper-oxide ($Bi_2Sr_2CaCu_2O_{8-\delta}$), also known as BSSCO or 2212, which has a T_c of 110 K.[9] Other SMO's related to BSSCO,

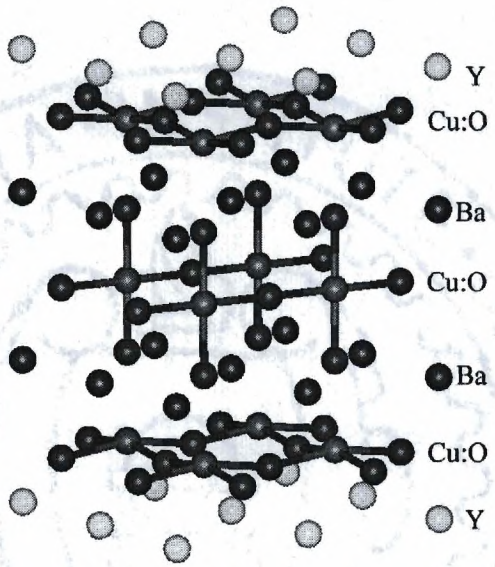

Figure 1-1. The crystal structure of YBCO.

thallium-barium-calcium-copper oxide and mercury-barium-calcium-copper oxide, have since been prepared with T_c's as high as 134 K for the thallium 2223 phase ($Tl_2Ba_2Ca_2Cu_3O_8$).[10]

Flat panel displays are a relatively active research area. One promising technology in this area is electroluminescent (EL) displays (**Figure 1-2**).[11] Electroluminescent displays are constructed on a glass substrate. An optically transparent patterned conducting layer, usually indium-tin oxide (ITO), is deposited on the glass. On

top of this conductor, a doped dielectric layer, generally a binary metal sulfide MS where M is Ca, Sr or Zn, is deposited. Pixel color is controlled by the choice of dopant, generally a rare-earth or transition metal, in the dielectric matrix. A patterned conductor is deposited on top of the dielectric layer. When a potential is applied across the two conducting layers, an electric field is generated, which excites the phosphor

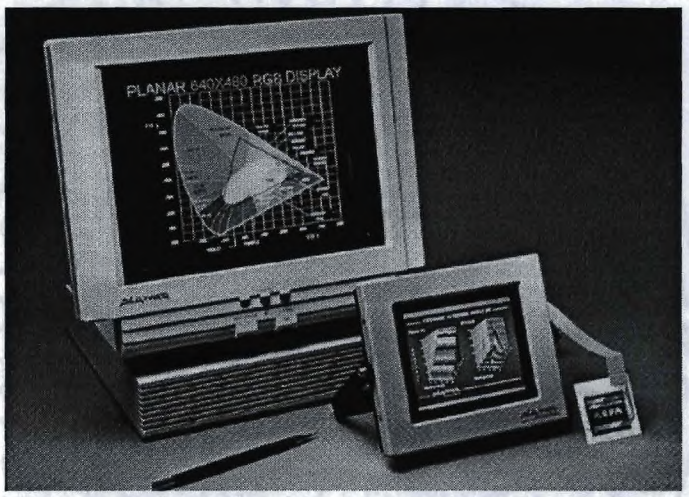

Figure 1-2. Flat panel electroluminescent displays developed by Planar, Inc.

centers (dopants) in the dielectric matrix causing them to emit light (**Figure 1-3**).[11] The advantages of EL displays over color liquid crystal displays (LCD) are many. Electroluminescent displays are not shock sensitive like liquid crystal displays. They do not require backlighting, crossed polarizers or filters. They offer a viewing angle as wide as that of a cathode ray tube-based (CRT) display, unlike the relatively narrow field of

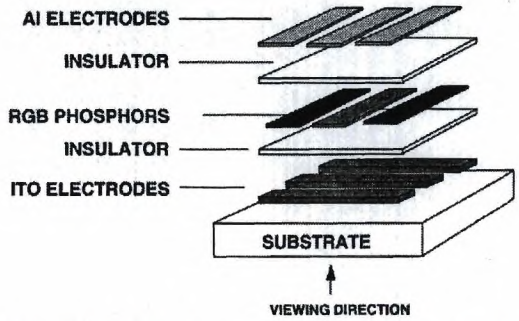

Figure 1-3. Design of a flat panel electroluminescent display.

view (45°) possible with LCD technology. Electroluminescent displays also are brighter, at present, than their LCD counterparts and have higher contrasts, allowing them to be viewed under bright light conditions such as in direct sunlight. The color scheme for pixels in a display usually is red, green and blue (RGB). Red and green phosphors are based on the mature technology of ZnS. The current challenge has been the development of a good blue phosphor. Cerium doped strontium thiogallate ($SrGa_2S_4$:Ce) functions well as a blue emitter.[12]

Magnetoresistant (MR) materials have the property that their electrical resistance varies as a function of the strength of an applied magnetic field. This effect is of great technological importance, due to its applicability to read heads for magnetic storage media, as well as sensors. Some layered and granular intermetallic materials, as well as certain doped magnetic semiconductors, show a very strong MR effect, which has been termed giant magnetoresistance (GMR). Although reported quite awhile ago for these initial compositions, this effect had not been observed for oxides until recently.[13] The

giant magnetoresistance effect particularly is pronounced in perovskite manganates of the type $La_{1-x}M_xMnO_3$ where M is a group 2 element or Pb.[14]

Each of the electronic materials discussed above has two characteristics in common: they all contain group 2 element chalcogenides (calcium, strontium or barium as an oxide or sulfide) and generally they each are utilized in thin film form. The current synthetic method of choice of the electronics industry for the preparation of thin films is chemical vapor deposition (CVD). Chemical vapor deposition is a process by which a desired material is deposited from the vapor phase onto a substrate, which usually is heated. This requires a volatile compound which can be vaporized from a heated reservoir, called an evaporator, and transported in the vapor phase by a carrier gas to the substrate (**Figure 1-4**). This source material not only must be volatile, but also must be thermally stable in the vapor phase, permitting it to arrive at the substrate before decomposition occurs. The third requirement of the source material is an accessible

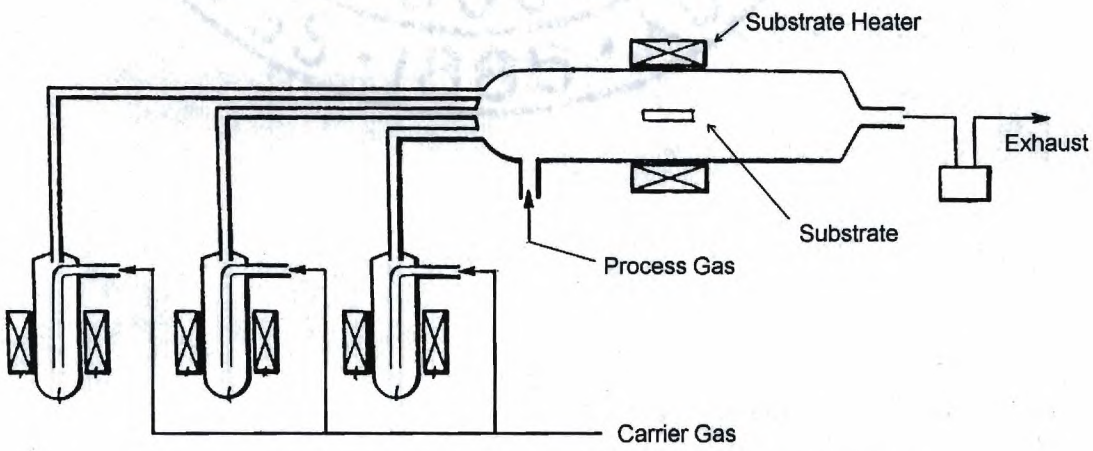

Figure 1-4. Schematic diagram of a hot walled CVD reactor.

decomposition pathway yielding the desired crystalline product in the solid state without any contaminants. One significant challenge in this area is to correlate the accessible temperature range of the substrate with the temperature necessary for generation of a crystalline film. Often, thermally limited substrates are utilized. This can be seen in the manufacture of electroluminescent displays based on SrS. A glass substrate is used, instead of quartz, to control the overall cost and mass of the display. The trade off, however, is that glass can only be heated to temperatures just above 600°C, causing complications in crystalline strontium sulfide growth.[11] In all the electronic materials described above, the elements that present a challenge to the CVD process reside in group 2. The challenge is caused simply by their low charge to radius ratio. This property makes it difficult to prepare low molecular weight precursors that are volatile.

The group 2 elements, excluding beryllium, show almost identical metalorganic and coordination chemistries. The differences which do occur are attributable to differing ionic radii. Magnesium, being the smallest, can form stable four coordinate compounds with roughly tetrahedral geometry, as well as six coordinate compounds with approximately octahedral geometry, such as those shown in **Figure 1-5**.[15,16] Calcium, being larger than magnesium, generally forms 6 and sometimes 8 coordinate compounds. Strontium forms more 8 than 6 coordinate compounds. Barium is 8 to 10 coordinate and radium is 8 to 12 coordinate. The major theme of the coordination chemistry of the group 2 elements is achievement of coordinative saturation. The elements always are divalent, requiring two monoanionic, or one dianionic, ligands to fulfill charge neutrality. Due to

the size of the group 2 dications, however, they are unstable with a coordination number (CN) of 2. The resulting compounds complete their coordination spheres either by bonding to additional Lewis base molecules, if they are available, or by bonding to the

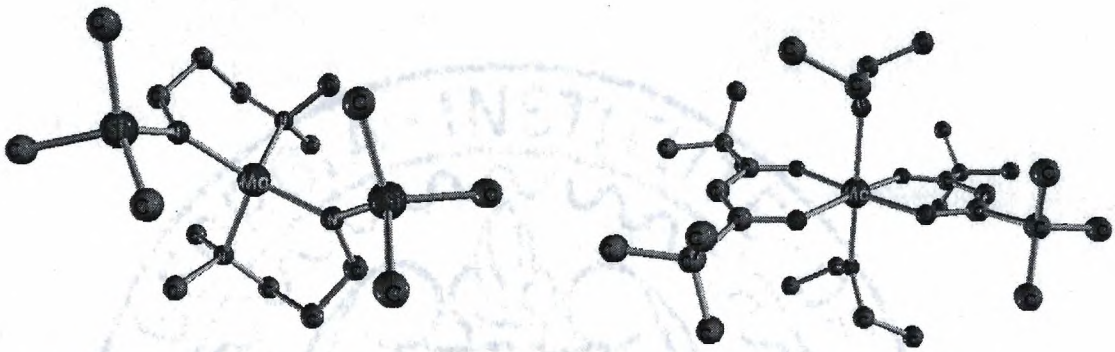

$Mg[N(TMS)CH_2CH_2CH_2NMe_2]_2$ $Mg(tmhd)_2(Et_2O)_2$

Figure 1-5. Observed coordination numbers for magnesium.[15,16]

ligands of adjacent group 2 ions, forming oligomers such as dimers, trimers, etc., or polymers (**Figure 1-6**).[17-19] Coordinative saturation can be satisfied by occupying empty coordination sites with available Lewis base moieties, or by hindering access to those sites with the steric bulk of the bound anionic ligands. It also is important to note that all group 2 organometallic compounds are thermodynamically unstable, relative to the group 2 element oxide (alkaline earth). These thermodynamically unstable species can be stabilized kinetically through coordinative saturation. This can, in some cases, physically block the attack of water and oxygen thereby giving species which are atmospherically stable.

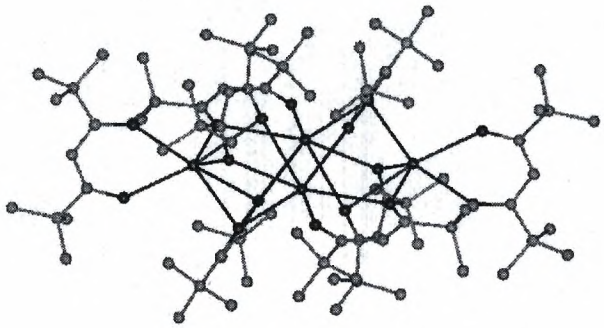

(a) $[Ba(tmhd)_2]_4$

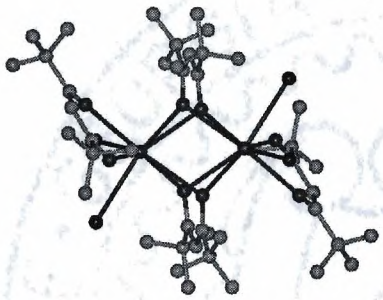

(b) $[Ba(tmhd)_2(NH_3)_2]_2$

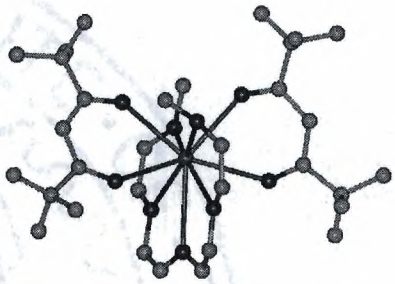

(c) $Ba(tmhd)_2$(tetraglyme)

Figure 1-6. Reduction of nuclearity by addition of Lewis base adducts.

Beryllium has a developed organometallic chemistry associated with it, due to its propensity to form covalent bonds.[3] Magnesium has a substantial organometallic chemistry. This is well represented by the general class of Grignard reagents. The stability of covalent carbon bonds to magnesium, coupled with its oxidation potential, causes magnesium to be inserted oxidatively into carbon-halogen bonds, excluding fluorine. The classic Grignard reagent, RMgX, is converted readily into the homoleptic dialkylmagnesium species through the Schlenk equilibrium (**Figure 1-7**).[3] This equilibrium can be shifted by solvent choice, or addition of Lewis base-containing

molecules. Covalent carbon bonds to the heavier group 2 elements are significantly less stable and, in many instances, compounds containing these bonds can not be isolated; however, there are a significant number of π-bound group 2 organometallic compounds.

$$2\,Mg + 2\,RX \longrightarrow 2\,RMgX \rightleftharpoons MgR_2 + MgX_2$$

Figure 1-7. Formation of a Grignard reagent and the resulting Schlenk equilibrium.

The organometallic chemistry of the late group 2 elements is dominated by the metallocenes. These are compounds based on the cyclopentadienide (deprotonated cyclopentadiene) ligand, and form sandwich structures such as the one shown in **Figure 1-8**. Again, coordinative saturation is the dominant influence on the final structure of these compounds. The simplest of the group 2 metallocenes, those based on the cyclopentadienide ($C_5H_5^-$) ligand, Cp^- for short, do not form stable monomers. The cyclopentadienide anion, when bound in an η^5 manner, occupies three coordination sites.

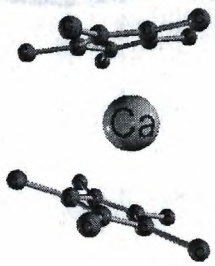

Figure 1-8. The molecular structure of $Ca(C_5Me_5)_2$.

Therefore, a divalent metal species bound to two Cp^- ligands is six coordinate. As stated earlier, this is an unstable condition for the late group 2 elements. The disparity caused by increasing ionic radii in the group 2 elements can be seen in the following trend. Calcium *bis*(cyclopentadienide) forms a polymer in which each calcium center interacts with as many as four Cp^- ligands.[20] Moving to a more sterically demanding ligand, pentamethylcyclopentadienide (Cp^{*-}), to generate the compound $Ca(Cp^*)_2$ stabilizes a monomeric product.[21] The Cp^{*-} ligand, however, is not large enough to 'cover' barium. The barium complex, $Ba(Cp^*)_2$, forms a one-dimensional polymer ribbon in the solid state.[21] To generate a monomeric barocene, the significantly larger ligand, *tetrakis*(isopropyl)cyclopentadienide, must be used. This compound, $Ba(iPr_4Cp)_2$, is a volatile monomer (**Figure 1-9**).[22] It is important here to note that the stable monomers in these cases are, in reality, metastable at best. The steric bulk of the ligands is sufficient to prevent the equally large ligands of neighboring molecules from interacting with the metal center to form intermolecular bridges. This does not mean that smaller Lewis bases are excluded from the coordination sphere. This fact is demonstrated in the extreme pyrophoric nature of this family of compounds. Water and oxygen molecules may readily approach the metal center, resulting in rapid reaction. The oligomeric examples of these compounds often can be reduced to monomers by the intermolecular addition of Lewis bases such as THF (**Figure 1-10**).[23] Rees *et al.* have incorporated Lewis donor atoms into side chains on cyclopentadiene to give ligands of the type

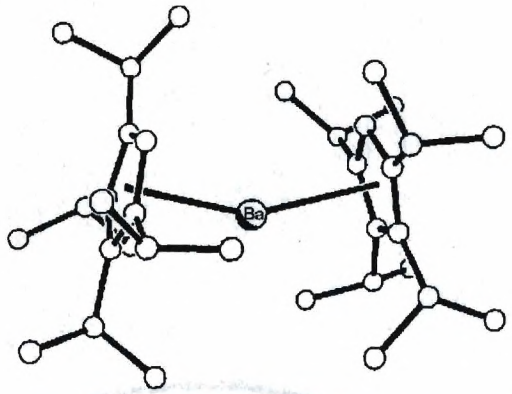

Figure 1-9. The molecular structure of $Ba(iPr_4Cp)_2$.

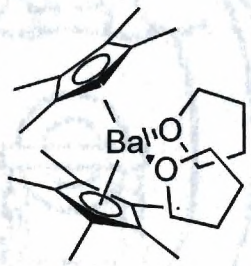

Figure 1-10. The structure of $Ba(Cp^*)_2(THF)_2$.

$C_5H_5(CH_2)_nER$, where n = 2, 3 and ER = OMe, OEt, NMe_2 or OCH_2CH_2OMe. The barium complexes of these ligands show poor vapor pressures.[24]

The use of Lewis base-containing adducts to reduce the degree of oligomerization, and thereby molecular weight, is not applicable, in general, to CVD precursors. This may be attributed to the observation that, for most complexes, the adducted neutral Lewis base molecules become dissassociated either before, or during, vaporization, thereby producing a coordinately unsaturated group 2 element compound and a highly volatile

neutral Lewis base moiety. The resultant low coordinate species oligomerize in the solid or vapor phase, leading to a reduction of overall volitility, and often reduces vapor phase stability. The reactivity of these compounds certainly would make them challenging precursors to integrate into a CVD system, but that challenge is dwarfed by a second shortcoming of these materials. Metallocenes in general seem to suffer greatly as CVD precursors due to their propensity for incorporating large quantities of carbon into the final film.[25] This property, more than any other, has prevented metallocenes of any element from becoming serious candidates as source materials for the CVD of high quality electronic materials. It is key to recognize that the inclusion of carbon is more than just a minor inconvenience for a device. The degradation of properties which results from this impurity renders the electronic material worthless for most applications.

The amide chemistry of the group 2 elements is represented, to a great extent, by one ligand: hexamethyldisilazane ($HN\{TMS\}_2$). Excepting radium, the *bis*(hexamethyldisilamide) complex (**Figure 1-11**) of each of the group 2 elements is known.[26] Beryllium and magnesium, due to their higher propensity to form covalent bonds, are known to form a wider range of amides than the heavier group 2 elements.[27] The only reported amides of the heavier group 2 elements are those based on hexamethyldisilazane. Hexamethyldisilazane (HMDZ) is unique due to the ability of the two silicons bound to the nitrogen to stabilize a negative charge on the nitrogen. This is due to donation of electron density from a p-orbital on nitrogen into empty d-orbitals on

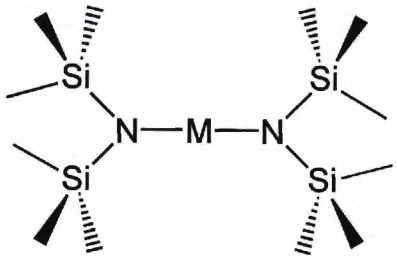

Figure 1-11. The bonding arrangement of the group 2 element amides.

silicon. This effect can be seen in the structure of the resulting compounds. The nitrogen can approach sp^2 hybridization, freeing the lone pair into a p-orbital to give maximum overlap with the d-orbitals on the silicon atoms (**Figure 1-12**). This can cause the nitrogen to approach a planar geometry. This effect is present in $Mg(HMDZ)_2(THF)_2$ as

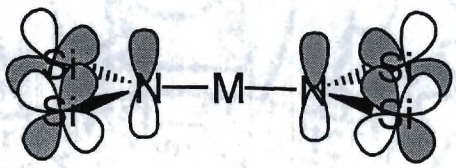

Figure 1-12. The orbital arrangement for electron donation from a filled nitrogen p-orbital in empty silicon d-orbitals.

can be seen in its Si-N-Si angles of 120.2°.[16] The beryllium complex of HMDZ is the only example of an unsolvated monomer. The native complexes of the rest of the group 2 elements each are oligomeric. These oligomers can, in some cases, be converted to monomers through the intermolecular addition of Lewis base-containing molecules (**Table 1-2**).[26]

It is interesting to note that, due to the size of the HMDZ ligand, an unsolvated dimer can be isolated for each of the group 2 elements, excluding beryllium. This again shows that, in the absence of additional Lewis bases, the steric bulk of the ligand only needs to be sufficient to prevent a bridging interaction by a ligand of an adjacent metal center. Addition of a limited number of neutral Lewis base molecules results in coordination of the Lewis bases to the dimer. Addition of an excess quantity of neutral Lewis base molecules results in monomer formation. The phosphorus- and arsenic-containing analogs of hexamethyldisilazane, hexamethyldisilaphophazane and hexamethyldisilaarsazane, respectively, also have been utilized in the formation of group 2 element compounds with similar results to the amides.[28] As with the group 2 element organometallics, there are problems with the utilization of group 2 element amides as CVD precursors. The monomeric Lewis base adducted species suffer due to the above-

Table 1-2 Coordination number and nuclearity for some group 2 element amide species.[26]

Compound	Coordination Number	Nuclearity
$Be[N(SiMe_3)_2]_2$	2	Monomeric
$[Mg\{N(SiMe_3)_2\}_2]_2$	3	Dimeric
$Mg\{N(SiMe_3)_2\}_2(THF)_2$	4	Monomeric
$[Ca\{N(SiMe_3)_2\}_2]_2$	3	Dimeric
$Ca[N(SiMe_3)_2]_2(DME)$	4	Monomeric
$[Sr\{N(SiMe_3)_2\}_2]_2$	3	Dimeric
$Sr[N(SiMe_3)_2]_2(DME)_2$	6	Monomeric
$[Sr\{N(SiMe_3)_2\}_2(dioxane)]_2$	4	Dimeric
$[Ba\{N(SiMe_3)_2\}_2]_2$	3	1-D Polymer
$[Ba\{N(SiMe_3)_2\}_2(THF)]_2$	4	Dimeric
$Ba[N(SiMe_3)_2]_2(THF)_2$	4	Monomeric

described loss of the Lewis base before or during vaporization. The inherent low coordination numbers of group 2 element amides make them less stable and open to reaction prior to decomposition at the substrate. Also, there has been some evidence of silicon incorporation into the final film, similar to the carbon incorporation seen for organometallic precursors.[29]

The alkoxide chemistry of the group 2 elements is extremely diverse. A group 2 element alkoxide of virtually any alcohol can be prepared, either by reaction of the base metal, in the case of the heavier group 2 elements, with the alcohol, or by reaction of a group 2 element organometallic compound or amide with the alcohol. Since alkoxides are only monodentate, they do not complete the coordination sphere of the heavier group 2 cations. In general, the alkoxides of the heavier group 2 elements often are polymers or higher oligomers. This is true for the simple group 2 element alkoxides utilizing methoxide, ethoxide, propoxide, etc.[30] The addition of Lewis bases, such as THF or extra protonated alcohol, generally gives oligomers such as dimers, trimers and tetramers.[26] The use of bulky ligands can allow the isolation of monomeric species such as $Ba(BHT)_2(THF)_3$ but only by incorporation of additional Lewis bases (BHT^- = 2,6-*bis*(*t*butyl)-4-methylphenoxide). The smallest of the heavy group 2 cations, Ca^{2+}, can be stabilized as a dimer by the extremely bulky ligand tritox, *tris*(*t*-Bu)methoxy, to form the complex $[Ca(tritox)_2]_2$.[31] The steric conjestion due to the bulk of this ligand is so high, however, that the molecule undergoes an elimination reaction upon sublimation, eliminating four equivalents of isobutene to give $[Ca\{OCH(tBu)_2\}_2]_3$, as shown in **Figure 1-13**.[32]

Intramolecular routes to Lewis base stabilization have been utilized. Hubert-Pfalzgraf *et al.* have utilized triethanolamine in the preparation of group 2 element alkoxides.[33] This approach, to date, has generated non-volatile oligomeric species. Buhro *et al.* have isolated the mega-cluster $Ca_9(OCH_2CH_2OMe)_{18}(HOCH_2CH_2OMe)_2$ which also is involatile.[34] Late group 2 element alkoxides of the type

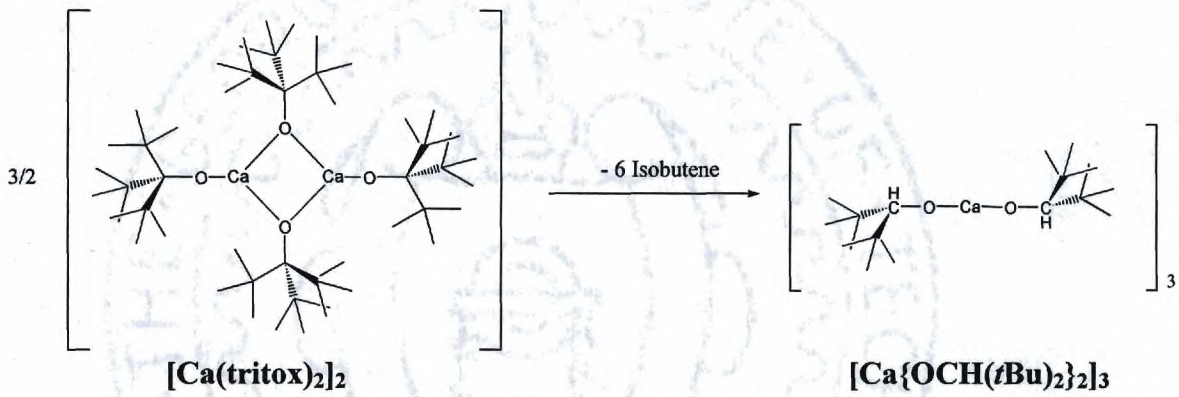

Figure 1-13. The thermal decomposition of $[Ca(tritox)_2]_2$ to $[Ca\{OCH(tBu)_2\}_2]_3$.

$M[O(CH_2CH_2O)_xR]_2$ (M = Ca, Sr, Ba; x = 2, 3; R = Me, Et, *n*-Bu, *n*-Hex) have been prepared and appear to be monomeric as determined by solution cryoscopic measurements (**Figure 1-14**).[35] In order to generate Lewis base adduct free monomers of the heavier group 2 elements, bulky alkoxide ligands bearing Lewis base substituted pendant arms have been used. The combination of steric bulk and donor functionality has been shown to yield more stable, dimeric group 2 alkoxides of the type shown in **Figure 1-15**.[32] The barium example of complex **b**, $Ba[OC(CH_2OiPr)_2tBu]_2$, has been reported to sublime at 185°C at 10^{-2} mbar and leaves a three weight percent residue when evaporated

at 600°C / 6 mbar. As with the classes of molecules described above, added neutral donors such as THF generally are lost from group 2 element alkoxides before or during vaporization. Even with increased ligand bulk and donor functionality the group 2 element alkoxides suffer as CVD precursors due to their ease of hydrolysis and due to the fact that the group 2 cations are not coordinatively saturated.

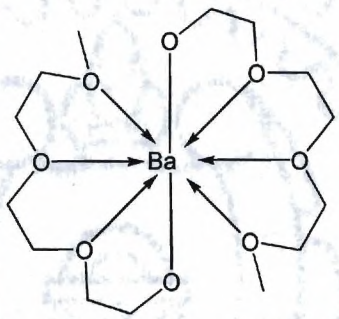

Figure 1-14. Sample barium oligoether-alkoxide.

Some researchers have utilized perfluorinated alkoxide ligands to decrease intermolecular interactions and thereby increase volatility. The barium complexes of perfluoroisopropoxide $[Ba(OCF\{CF_3\}_2)_2]_n$ and perfluorotertiarybutoxide $[Ba(OC\{CF_3\}_3)_2]_n$ have been synthesized and characterized.[36] They show a small volatility increase, relative to their hydrocarbon analogs; however, they deposit barium fluoride rather than the desired barium oxide. This requires a post-deposition hydrolysis step to form the barium oxide required by electronic applications. The perfluorinated

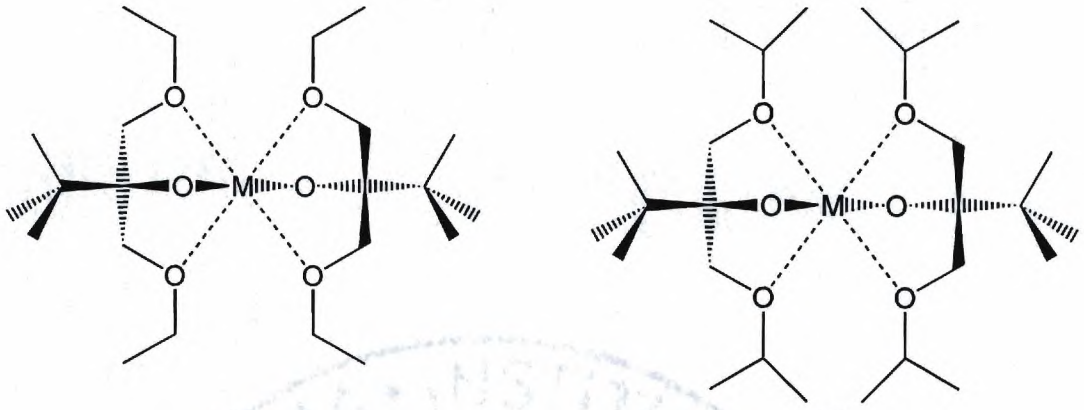

(a) (b)

Figure 1-15. Sterically demanding alkoxides bearing Lewis base containing pendant arms. (M = Ca, Sr, Ba).

group 2 element alkoxides have the same low coordination numbers and posses the same sensitivy to hydrolysis as the hydrocarbon-based alkoxides. They undergo intermolecular Lewis base loss prior to volatilization, similar to the hydrocarbon-based alkoxides. The perfluorinated group 2 element alkoxides have low volatilities and vapor phase stabilities. Although they show improved properties over their hydrocarbon-based analogs, the fluorinated group 2 element alkoxides have not yet been shown to make good CVD precursors for the deposition of device-quality group 2 element oxide-containing materials.

The carboxylate chemistry of the group 2 elements has the potential to be as diverse as the alkoxide chemistry, however, little success has been had with the application of group 2 element carboxylates to the CVD of electronic materials. The group 2 element carboxylates are, in general, involatile. There has been some work recently in the area of group 2 element dithiocarbamates ($M\{S_2CNR_2\}_2$) (M = Ca, Sr; R =

Me, Et, *n*-Bu).[37] These compounds, like their carboxylate cousins, are not volatile. The group 2 element dithiocarbamates have been shown to decompose upon heating to their respective group 2 element sulfides.[37]

The most heavily researched area of group 2 element chemistry, in respect to the CVD of electronic materials, is the group 2 element β-diketonates. The volatility and stability of metal β-diketonates in general has been well demonstrated by Sievers, who has shown that various metals can be separated chromatographically in the vapor phase as their respective β-diketonate complexes.[38] The simplest example of this ligand family is acetylacetone (2,4-pentanedione) which, upon deprotonation, is referred to simply as acac$^-$. The β-diketonate ligand is a superior ligand for several reasons. It is bidentate, occupying two coordination sites. Its negative charge is delocalized, lessening the chances of a bridging interaction. Also, its shape and enforced planar geometry tend to hold much of its steric bulk close to the metal center, giving effective coverage. The β-diketonate ligands bond through both carbonyl oxygens to the metal center, forming a six-membered MO_2C_3 ring, in which the negative charge resonates between the two carbonyl oxygens, forming a quasi-aromatic system (**Figure 1-16**). While acac$^-$ is a good ligand for many transition metal species, it is not large enough for the late group 2 elements. Only beryllium forms a monomeric species with acac$^-$, $Be(acac)_2$, in the absence of additional Lewis base adducts.[39] Also, other than beryllium, the group 2 element acac$^-$ complexes are not volatile. The most commonly utilized β-diketonate ligand in group 2 CVD precursors at present is 2,2,6,6-tetramethylheptane-3,5-dionate, abbreviated H-tmhd

when protonated and tmhd$^-$ when not. Calcium *bis*(tmhd)[40] is a trimer in the solid state, as is strontium *bis*(tmhd).[41] Barium *bis*(tmhd)[17] is a tetramer. All three are volatile, however, the barium complex suffers a lack of long term

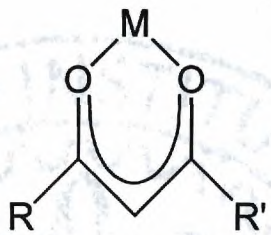

Figure 1-16. The bonding motif of β-diketonate ligands.

stability at use temperatures. These three complexes commonly are used as source materials for the CVD of group 2 oxides and sulfides; however, there still is significant room for improvement. For example, in the CVD of YBCO, yttrium *tris*(tmhd) and copper *bis*(tmhd) both have usable vapor pressures at 160°C.[42] Barium *bis*(tmhd), however, requires temperatures of 250°C or above to generate acceptable vapor phase concentrations.[43] This requires the entire reactor chain to be kept at a higher temperature to prevent the barium material from condensing. The higher temperature requirements of $[Ba(tmhd)_2]_4$, combined with its instability at use temperature, are detrimental enough to the CVD process to cause researchers to actively search for a better barium precursor.

Researchers have attempted to stabilize low molecular weight gas phase species by the addition of Lewis base adducts such as THF or ammonia to the vapor stream in CVD experiments.[44] This has led others to isolate and characterize the intermolecularly

stabilized products. The ammonia adduct of barium *bis*(tmhd), $[Ba(tmhd)_2(NH_3)_2]_2$, has been isolated and characterized.[45] Attempts at the sublimation of this compound lead to loss of the ammonia to generate $[Ba(tmhd)_2]_4$, which, in turn, sublimes at its normal temperature. Other adduct species such as $Ba(tmhd)_2$(tetraglyme),[19] $[Ba(tmhd)_2(bipy)]_2$[46] and $Ba(tmhd)_2(o\text{-phen})_2$[46] each behave in a similar manner, losing their Lewis base adducts either before or during sublimation to generate the parent $[Ba(tmhd)_2]_4$ species, which, in turn, sublimes.

Many researchers turned to perfluoroalkyl substituted β-diketonates in an attempt to decrease intermolecular Van der Waals interactions and thereby increase the volatility of the resultant barium complexes. Ligands utilized in this effort include 1,1,1,5,5,5-hexafluoropentane-2,4-dionate ($hfac^-$),[47] and 1,1,1,2,2,3,3,7,7,8,8,9,9,9-tetradecafluorononane-4,6-dionate ($tdfnd^-$).[48] These ligands (**Figure 1-17**) are successful to an extent. The group 2 element complexes of fluorinated β-diketonates in general are extremely volatile (relative to their non-fluorinated counterparts) and show good vapor phase stabilities. They still are not monomeric and still are sensitive to water.

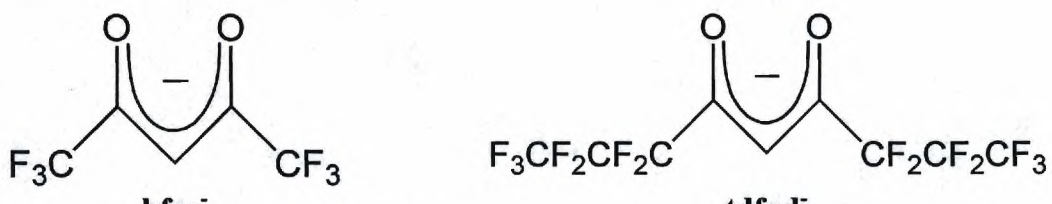

hfac⁻ **tdfnd⁻**

Figure 1-17. Example fluorinated β-diketonate ligand structures.

Addition of a Lewis base like tetraglyme (2,5,8,11,14-pentaoxopentadecane) to "$Ba(hfac)_2$" and "$Ba(tdfnd)_2$" yields $Ba(hfac)_2$(tetraglyme)[19] and $Ba(tdfnd)_2$(tetraglyme),[49] respectively (**Figure 1-18**). Both of these compounds are very volatile, sublime intact and are stable to water and oxygen. Based on these physical properties, the tetraglyme adducts should be excellent candidates for CVD source materials. They have been shown to be excellent source materials for the deposition of BaF_2. This seems, at present, to be a general trend among the group 2 element complexes containing fluorinated

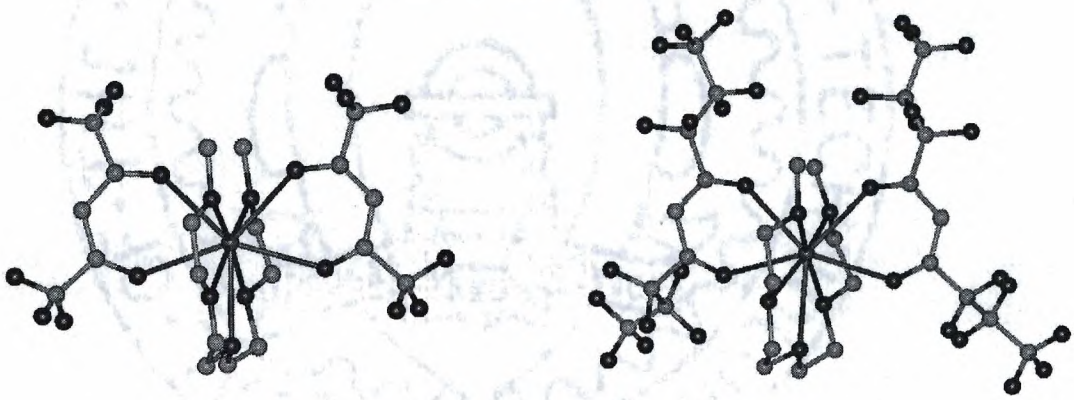

$Ba(hfac)_2$(tetraglyme) **$Ba(tdfnd)_2$(tetraglyme)**

Figure 1-18. The molecular structures of $Ba(hfac)_2$(tetraglyme) and $Ba(tdfnd)_2$(tetraglyme).[19,49]

ligands.[50] They each deposit, purely or as a significant fraction, the group 2 element difluoride. This can be converted in a post-depostion hydrolysis step to the oxide. Such a two step process, in general, is not condusive to the formation of crystalline, epitaxial films. The metal difluoride also may be reacted *in situ* (during the deposition process)

through the addition of water to the vapor stream, forming the oxide at the subtrate and copious quantities of hydrogen fluoride in the effluent. Neither of these solutions appear, at present, to be practical on an industrial scale. It may be noted that the reluctance of industry to employ this approach is driven, to a great extent, by a lack of data on the potential for such a two step process to yield state of the art devices of electronic materials. The step from demonstration of materials characterization to employment in a device manufacturing process is a large one and is not likely to be taken for reasons other than substantial improvement in device performance.

It is interesting to note that tetraglyme adducted barium complexes utilizing fluorinated β-diketonates sublime intact with no loss of the Lewis base adduct while, as discussed earlier, the seemingly isostructural $Ba(tmhd)_2$(tetraglyme) complex loses tetraglyme prior to volatilization. The cause of the apparent disparity can be found in the electronics of the two β-diketonate ligand types. As discussed earlier, $tmhd^-$, due to its electron donating groups, has a large negative charge density at the bonding carbonyl oxygens. The β-diketonate ligands with fluorinated side groups behave in an entirely different manner. Relative to tmhd *t*-butyl side groups, the fluorinated side groups are extremely electron withdrawing. This, in effect, pulls charge density out of the delocallized diketonate moiety and greatly reduces the charge density at the carbonyl oxygens. The inductive effect at the barium center is that the fluorinated β-diketonate ligands provide less electron density to the metal, making it a stronger Lewis acid, which

causes the barium center to bind Lewis bases more tightly, causing their retention in the vapor phase. This effect has been quantified in the research of Rees *et al.*[45]

Since the intermolecular stabilization of non-fluorinated barium *bis*(β-diketonates) by neutral Lewis base adducts has been shown to be ineffective for the preparation of CVD source materials, and since barium precursors bearing fluorinated ligands tend to deposit barium fluoride, a different approach to the problem is required. This approach is intramolecular stabilization. This approach takes an anionic ligand, such as a β-diketonate, and adds to it a Lewis base donor functionality. Instead of adding neutral Lewis base adducts to a complex bearing anionic ligands, Lewis base adducts are incorporated into the backbone of the anionic ligand. This approach has shown promise when applied to the barium source compound problem. The ligand 2,2-dimethyl-8-methoxyoctane-3,5-dione (Hdmmod) incorporates this design feature (**Figure 1-19**). It contains a β-diketonate moiety, as well as a methyl ether unit. The barium complex of

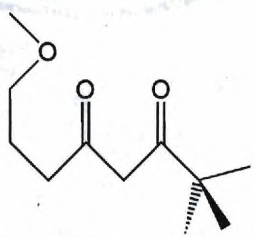

Figure 1-19. The structure of Hdmmod.

this ligand, $Ba(dmmod)_2$, is a distillable liquid.[51] The structure of the corresponding copper analog of the barium complex is shown in **Figure 1-20**.[51] Barium *bis*(dmmod) has the requisite condensed phase stability and volatility for CVD use; however, it shows less

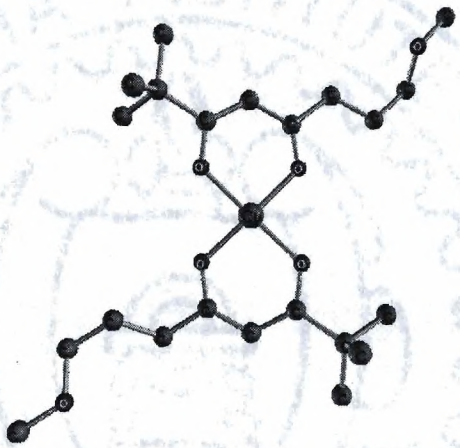

Figure 1-20. The molecular structure of $Cu(dmmod)_2$.

than acceptable vapor phase stability. Other approaches to intramolecular stabilization have been taken. Instead of adding a Lewis base to the backbone of a β-diketone, the β-diketone can be converted to a β-ketoimine with Lewis base functionalities attached to the imine group. Ligands of this type are shown in **Figure 1-21**.[52] The corresponding barium complexes of these ligands are reported to be quite air sensitive. They also have low volatilities and lack vapor phase stability.[52] This presumably is due to the instability of the metal nitrogen bond.

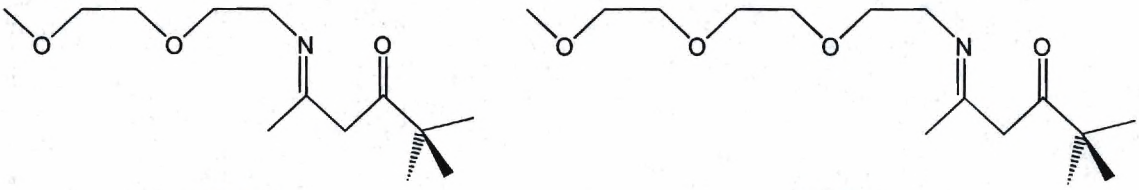

Hdiki **Htriki**

Figure 1-21. The structures of the β-ketoimines Hdiki and Htriki.

The β-diketonate class of ligand shows good promise for the formation of a suitable barium precursor for the CVD of barium chalcogenides. The volatilities and vapor phase stabilities of this class of compounds, combined with their relative chemical stabilities, make them the precursors of choice for the present materials industry. There is still significant room for improvement, and a good deal of on-going research is devoted to that task.

References

1 (a) L.B. Tepper, in *Beryllium: Biomedical and Environmental Aspects*, eds: M.D. Rossman, O.P. Preuss and M.B. Powers, Williams and Williams, San Francisco, **1991**, p. 3. (b) M.B. Powers, *ibid*, p. 9. (c) A.L. Reeves, *ibid*, p. 59.

2 (a) P.A. Everest, in *Comprehensive Inorganic Chemistry*, eds: J.C. Bailar, Jr., H.J. Emelius, R. Nyholm and A.F. Trotman-Dickenson, Permagnon Press, Oxford, **1973**, Vol. 1, p. 531. (b) R.D. Goodenough and V.A. Stenger, *ibid*, p. 591.

3. F.A. Cotton and G. Wilkinson, *Advanced Inorganic Chemistry, Fifth Edition*, John Wiley and Sons, New York, **1988**, 144.

4. Periodic Table of the Elements, Sergeant Welch Scientific Company, **1980**.

5. I.T. Kim, C.H. Lee and S.J. Park, *Jap. J. Appl. Phys.*, Part 1, **1994**, *33*, 5125.

6. S.R. Gilbert, B.W. Wessels, D.B. Studebaker and T.J. Marks, *Appl. Phys. Lett.*, **1995**, *66(24)*, 3298.

7. J.G. Bednorz and K.A. Muller, *Z. Phys. B.*, **1986**, *64*, 189.

8. M.K. Wu, J.R. Ashburn, C.J. Torng, P.H. Hor, R.L. Meng, L. Gao, Z.J. Huang, Y.Q. Wang and C.W. Chu, *Phys. Rev. Lett.*, **1987**, *58*, 908.

9. H. Meada, Y. Tanaka, M. Fukutomi and T Asano, *Jap. J. Appl. Phys.*, **1988**, L2080.

10. R.A. Kerr, *Science*, 29 March **1996**, *271*, 1804.

11. P.D. Rack, A. Naman, P.H. Holloway, S-S. Sun and R.T. Tuenge, *MRS Bulletin*, March **1996**, 49.

12. K. Tanaka, Y. Inoue, S. Okamoto and K. Kobayashi, *J. Cryst. Growth*, **1995**, *150*, 1211.

13. C.N.R. Rao and A.K. Cheetham, *Science*, 19 April **1996**, *272*, 369.

14. H. Kuwahara, Y. Tomioka, Y. Moritomo, A. Asamitsu, M. Kasai, R. Kumai and Y. Tokura, *Science*, 5 April **1996**, *272*, 80.

15. G. Kräuter, B. Neumüller and W.S. Rees, Unpublished Results.

16. H.A. Luten and W.S. Rees, Jr., Patent Pending.

17. A. Gleizes, S. Sans-Lenain and D. Medus, *C. R. Acad. Sci. Paris*, **1991**, *313*, 761.

18. W.S. Rees, M.W. Carris and W. Hesse, *Inorg. Chem.*, **1990**, *30*, 4479.

19. R. Gardiner, D.W. Brown, P.S. Kirlin and A.L. Rheingold, *Chem. Mater.*, **1991**, *3(6)*, 1053.

20. B.G. Gowenlock, W.E. Lindsell and B.J. Singh, *J. Chem. Soc., Dalton Trans.*, **1978**, 657.

21. C.J. Burns and R.A. Andersen, *J. Organometallic Chem.*, **1987**, *325*, 31.

22. R.A. Williams, K.F. Tesh and T.P. Hanusa, *J. Amer. Chem. Soc.*, **1991**, *113*, 4843.

23. R.A. Williams, T.P. Hanusa and J.C. Huffman, *Organometallics*, **1990**, *9*, 1128.

24 W.S. Rees, U.W. Lay and K.A. Dippel, *J. Organometallic Chem.*, **1994**, *483*, 27.

25. A.C. Greenwald, W.S. Rees and U.W. Lay in *Rare Earth Doped Semiconductors*, Edited by: G.S. Pomrenke, P.B. Klein and D.W. Langer (Mater. Res. Soc. Proc., 301, Pittsburg, PA. 1993) 21.

26. W.S. Rees, *Alkaline Earth Metals: Inorganic Chemistry*, in *Encyclopedia of Inorganic Chemistry, Vol. 1*, Editor in Chief: R.B. King, John Wiley and Sons, New York, **1994**, 67 - 87.

27. W.E. Lindsell, *Magnesium, Calcium, Strontium and Barium*, in *Comprehensive Organometallic Chemistry II*, Vol. 1, Ed. C.E. Housecroft, Elsevie Science Ltd., New York, **1995**, 57 - 127.

28. M. Westerhausen and W. Schwarz, *J. Organometallic Chem.*, **1993**, *463*, 51.

29. A.C. Greenwald, W.S. Rees and O. Just in *Rare Earth Doped Semiconductors*, Vol. 2, Ed. G.S. Pomrenke, P.B. Klein and D.W. Langer (Mater. Res. Soc. Proc., 301, Pittsburg, PA. 1996) In Press.

30. D.C. Bradley, R.C. Mehrotra and D.P. Gau, *Metal Alkoxides*, Academic Press, New York, **1978**, 411.

31. W.A. Herrman, R. Anwander, M. Kleine and W. Scherer, *Chem. Ber.*, **1992**, *125*, 1971.

32. W.A. Herrman, N.W. Huber and T. Priermeier, *Angew. Chem. Int. Ed. Engl.*, **1994**, *33(1)*, 105.

33. L.G. Hubert-Pfalzgraf, O. Poncelet, C. Sirio and J.C. Daran in *Chemical Processing of Advanced Materials*, Eds. L.L. Hench and J.K. West, Wiley, New York, **1992**, p. 277.

34. S.C. Goel, M.A. Matchett, M.Y. Chiang and W.E. Buro, *J. Am. Chem. Soc.*, **1991**, *113*, 1844.

35. W.S. Rees and D.A. Moreno, *Chem. Comm.*, **1991**, *24*, 1759.

36. A.P. Purdy, C.F. George and J.H. Callahan, *Inorg. Chem.*, **1991**, *30*, 2812.

37. A.P. Purdey and C.F. George, *Main Group Chemistry*, **1996**, *1*, 229.

38. R.W. Moshier and R.E. Sievers, *Gas Chromatography of Metal Chelates*, Permagnon Press, Oxford, **1965**.

39. R.C. Mehrotra, R. Bohra and D.P. Gaur, *Metal β-Diketonates and Allied Derivatives*, Academic Press, New York, **1978**, 382.

40. V.C. Arunsalem, S.R. Drake, M.B. Hursthouse, K.M.A. Malik and S.A. Miller, *Inorg. Chem.*, In Press

41. S.R. Drake, M.B. Hursthouse, D.J. Otway and K.M.A. Malik, *J. Chem. Soc., Dalton Trans.*, **1993**, 2883.

42. W.S. Rees, H.A. Luten, M.W. Carris, E.J. Doskocil and V.L. Goedken, *MRS Symp. Proc.*, **1992**, *271*, 141.

43. E.W. Berg and N.M. Hewera, *Anal. Chim. Acta*, **1972**, *60*, 117.

44. A.R. Barron, J.M. Buuriak and R. Gordon, *US. Pat.* applied for.

45. H.A. Luten, W.S. Rees, Jr., *Proc. Mater. Res. Soc. Symp.*, **1995** Fall Meeting, Boston, Mass., In Press.

46. W.S. Rees, H.A. Luten, M.W. Carris, C.R. Caballero, W. Hesse and V.L. Goedken, *Mat. Res. Soc. Symp. Proc.*, **1993**, *310*, 375.

47. A.P. Purdy, A.D. Berry, R.T. Holm, M. Fatemi and K.K. Gaskill, *Inorg. Chem.*, **1989**, *28*, 2799.

48. S.C. Thompson, D.J. Cole-Hamilton, D.D. Gilliland and M.L. Hitchman, *Adv. Mater. Opt. Electron.*, **1992**, *1*, 81.

49. J. Nash, J. Barnes, D. Cole-Hamilton, B. Richards, J. Cook and M. Hitchman, *Adv. Mater. Opt. Electron.*, **1995**, *5*, 1.

50. M.L. Hitchman, S.H. Shamlian, D.D. Gilliland, D.J. Cole-Hamilton, J.A.P. Nash, S.C. Thompson and S.C. Cook, *J. Mater. Chem.*, **1995**, *5(1)*, 47.

51. W.S. Rees, C.R. Caballero and W. Hesse, *Angew. Chem. Int. Ed. Engl.*, **1992**, *31(6)*, 735.

52. D.L. Schulz, B.J. Hinds, C.L. Stern and T.J. Marks, *Inorg. Chem.*, **1993**, *32*, 249.

CHAPTER II.

INTERMOLECULAR LEWIS BASE STABILIZATION OF BARIUM *BIS*(2,2,6,6-TETRAMETHYLHEPTANE-3,5-DIONATE)

Introduction

There is an interest in the preparation of some ferroelectric materials in thin film form by chemical vapor deposition (CVD).[1,2] One composition presently attracting attention is $BaTiO_3$. In order to achieve reasonable epitaxial growth rates at usable substrate temperatures, precursor molecules containing the elements of interest should transport in the vapor phase at processing conditions of less than 200°C and greater than 5 Torr.[3] This presents a significant problem for the case of barium. Most researchers have utilized the *bis*(β-diketonate) complexes of this group 2 element as the source of the metal. Although $Ba(fod)_2$[4] and $Ba(hfac)_2$•tetraglyme[5] each posses the requisite vapor pressure characteristics demanded for for employment in CVD, they also suffer from the primary deposition of BaF_2, and the requirement for a subsequent, hydrolytic conversion into the desired oxide form of the ferroelectric perovskite material.[6] To date, research on non-fluorine containing, high vapor pressure barium-containing compounds has focused on intermolecular coordination of Lewis bases to alkoxides[7] and cyclopentadienides.[8] In the absence of Lewis bases, hydrocarbon-based *bis*(β-diketonate species) are oligomeric.[9]

Substantial progress has been made in the utilization of these compounds in the CVD growth of superconducting metal oxides.[10]

Results and Discussion

Previous workers have added neutral β-diketone to the carrier gas stream of a CVD reactor in efforts to augment the vapor pressure of "$Ba(tmhd)_2$".[11] Other research groups have chosen H_2O,[12] THF,[13] or NH_3[14] as the additive. The compound has also been crystallized with MeOH[15] and Et_2O[16] of solvation. Although the vapor pressure of $Ba(hfac)_2$ was enhanced substantially upon complexation with tetraglyme, the comparable $Ba(tmhd)_2$ adduct has proven to be unstable toward vapor phase dissociation.[17] Likewise, the nitrogen-based adducts $[Ba(tmhd)_2 \bullet 2\ NH_3]_2$[18] (**Figure 2-1**) and $[Ba(tmhd)_2 \bullet 2\ tmeda]_2$[19] each dissociate the neutral amine in the gas phase, even though it is tightly bound both in the solid state and in solution.

A report[20] of the use of $Ba(tmhd)_2 \bullet 2$ *o*-phen (*o*-phen = 1,10-phenanthroline) in the growth of YBCO films prompted us to explore several difunctional nitrogen-centered Lewis bases. A list of the Lewis bases employed in combination with "$Ba(tmhd)_2$", and the compounds isolated in each case, is given in **Table 2-1**. The details of the preparation and characterization of the $Ba(\beta\text{-diketonate})_2 \bullet L_x$ compounds is given in the experimental section. Of the seven Lewis base molecules utilized, only *o*-phen and bipy yielded Lewis base coordinated products.

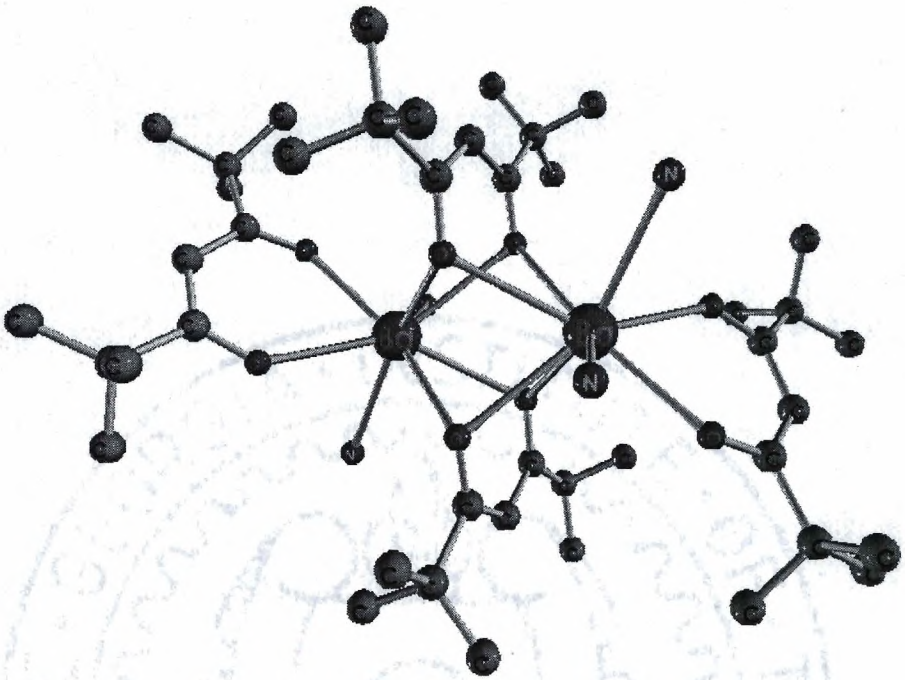

Figure 2-1. The molecular structure of $[Ba(tmhd)_2 \cdot 2\ NH_3]_2$

$Ba(tmhd)_2$•2 *o*-phen. The isolated product was an off-white powder with a benzene solubility too low for cryoscopic molecular weight determination. The proton NMR spectrum indicates one coordination environment for both $tmhd^-$ and *o*-phen, and integrates in a manner as to indicate a stoichiometry of one *o*-phen to each $tmhd^-$ ligand. Thermogravimetric analysis of $Ba(tmhd)_2$•2 *o*-phen (**Figure 2-2**) shows one weight loss event, seemingly indicating intact sublimation of the compound (K_1 in **Figure 2-3**). Low pressure sublimation of $Ba(tmhd)_2$•2 *o*-phen, however, shows decomposition of the adduct species in the solid state (K_2 in **Figure 2-3**), accompanied by concomitant sublimation of two species(K_4 and K_5 in **Figure 2-3**). Analysis of the sublimate showed

o-phen enrichment, indicating loss of coordinated *o*-phen in the solid state followed by sublimation of the two species at different rates.

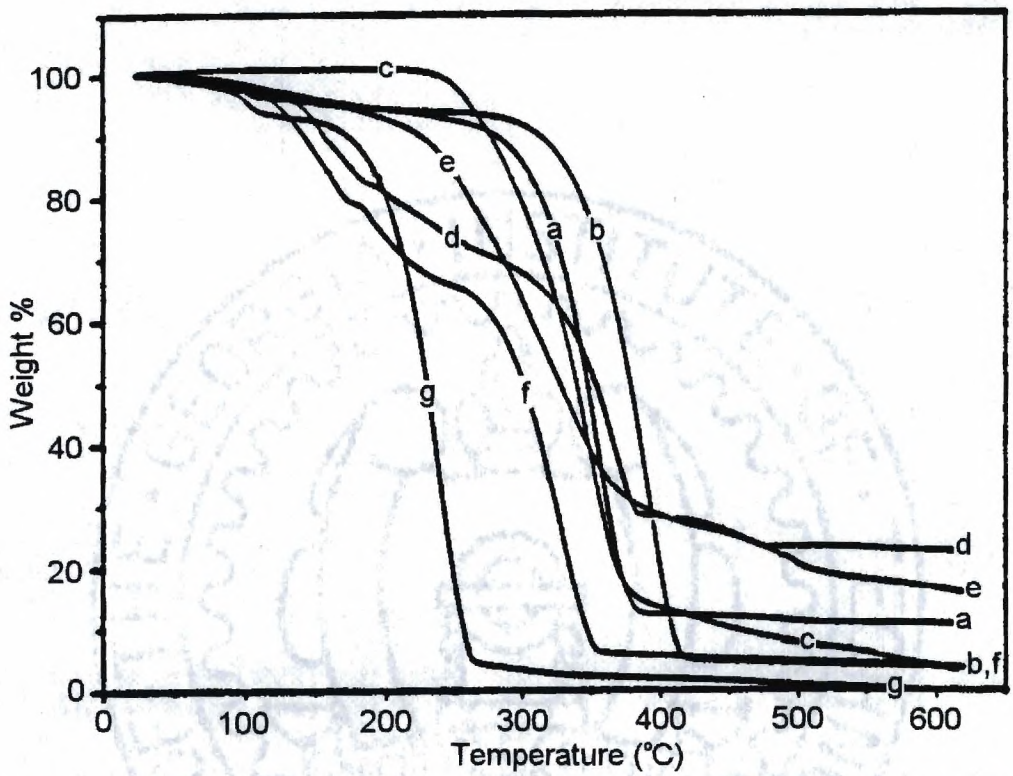

Figure 2-2. Thermogravimetric traces of: a) $[Ba(tmhd)_2]_4$, b) $[Ba(tmhd)_2{\bullet}2NH_3]_2$, c) $Ba(tmhd)_2{\bullet}2o$-phen, d) $[Ba(tmhd)_2{\bullet}bipy]_2$, e) stoichiometric mixture of $[Ba(tmhd)_2]_4$ and *o*-phen, f) stoichiometric mixture of $[Ba(tmhd)_2]_4$ and bipy, g) *o*-phenanthroline.

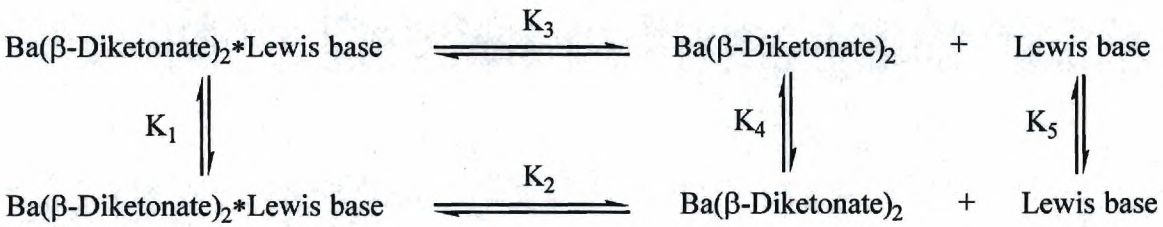

Figure 2-3. Solid state and vapor phase equilibria for Lewis base containing barium *bis*(β-diketonate) species.

Table 2-1. Combination of $Ba(tmhd)_2$ with difunctional amine based Lewis base molecules.

Lewis Base	Abbreviation	Isolated Product
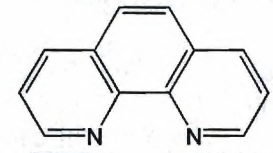	*o*-phen	$Ba(tmhd)_2$•2 *o*-phen
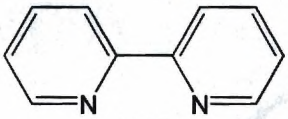	bipy	$[Ba(tmhd)_2$•bipy$]_2$
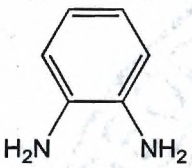	opda	$[Ba(tmhd)_2]_4$
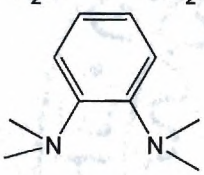	tmopda	$[Ba(tmhd)_2]_4$
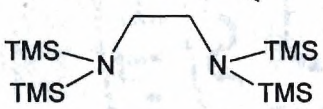	ttmseda	$[Ba(tmhd)_2]_4$
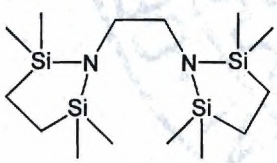	btmdsacpe	$[Ba(tmhd)_2]_4$
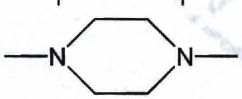	dmp	$[Ba(tmhd)_2]_4$

$[Ba(tmhd)_2$•bipy$]_2$. The isolated product was a white powder with a slight benzene solubility. Solution cryoscopic measurements identified the compound as a monomer in solution. Proton NMR was consistant with a single coordination environment for both the $tmhd^-$ and bipy ligands. Integration of the signals gave a stoichiometry of one bipy molecule to two $tmhd^-$ ligands. Thermogravimetric analysis (**Figure 2-2**) showed two

weight loss events; the initial event being loss of coordinated bipy, followed by sublimation of $[Ba(tmhd)_2]_4$ at its normal temperature. Low pressure sublimation verified this observation showing sublimation of bipy to give a residue of pure $[Ba(tmhd)_2]_4$. Subsequent to our initial publication of these data, Drosdov *et al.* published the crystal strucure of $[Ba(tmhd)_2 \bullet bipy]_2$ (**Figure 2-4**).[21]

Mixtures of $[Ba(tmhd)_2]_4$ and *o*-phen, and $[Ba(tmhd)_2]_4$ and bipy were prepared with stoichiometries matching the isolated compounds. Themogravimetric analysis of these mixtures (**Figure 2-2**) showed close matches to the traces of the two legitimate compounds lending credence to the conclusion that loss of the Lewis base is occuring, in the solid state, prior to sublimation.

Conclusions

The rather large ionic radius for barium (146 pm),[3] combined with its propensity to adopt coordination numbers of 8 - 12, presents a significant challenge to the synthetic chemist. The divalent cation demands utilization of low valent, multidentate anionic ligands (intramolecular stabilization) and/or the incorporation of additional neutral ligands (intermolecular stabilization) to inhibit cluster formation. In the case of "$Ba(tmhd)_2$", intermolecular stabilization via Lewis base incorporation does not seem to be a viable solution. The Lewis acidity of the barium center in these species is not strong enough to retain the Lewis base molecules in the vapor phase and thereby prevent oligomerization.

Experimental

$Ba(tmhd)_2$ •2*o*-phen. In a 250 mL Schlenk flask were combined 1.00 g (7.30 mmol) of barium metal, 2.82 g (15.30 mmol) of H-tmhd (2,2,6,6-tetramethylheptane-3,5-dione), 5.25 g (29.10 mmol) of *o*-phenanthroline and 100 mL of THF (distilled from Na / benzophenone). With rapid stirring, anhydrous $NH_{3\,(g)}$ (passed over KOH) was bubbled through the mixture. The solution was warmed to 40°C and the reaction was allowed to proceed for 5 hours. The solution was transferred by cannulation under $N_{2(g)}$ atmosphere into another flask leaving the unreacted barium metal behind. The flask containing the solution was sealed and placed in a freezer at -20°C and a pale, beige precipitate formed. This precipitate was recrystallized from a minimum amount of hot toluene (distilled from Na) to give 4.67 g (5.40 mmol) of $Ba(tmhd)_2$ •2*o*-phen, 74% based on barium. **Characterization: mp:** 216.5°C. **^{1}H NMR:** (300 MHz, positive δ downfield referenced to $Si(CH_3)_4$ = 0 ppm utilizing residual C_6D_5H = 7.15 ppm in solvent C_6D_6) 9.38 [d, 2H, *o*-phen], 7.41 [d, 2H, *o*-phen], 7.11 [s, 2H, *o*-phen], 6.93 [d, 2H, *o*-phen], 5.81 [s, 1H, tmhd], 1.25 [s, 18H, tmhd]. **^{13}C{^{1}H} NMR:** (75 MHz, positive δ downfield referenced to $Si(CH_3)_4$ = 0 ppm utilizing $CDCl_3$ = 77.0 ppm) 199 [tmhd], 151 [*o*-phen], 146 [*o*-phen], 136 [*o*-phen], 129 [*o*-phen], 123 [*o*-phen], 77 [tmhd], 41[tmhd], 28 [tmhd]. **IR (nujol):** 3040(vw), 3020(vw), 2847(vs), 1612(w), 1583(s), 1522(w), 1501(m), 1489(m), 1417(vs), 1349(m), 1261(w), 1226(vw), 1221(m), 1195(vw), 1173(w), 1168(w), 1134(w), 1119(w), 1095(vw), 1022(vw, br),857(m, sh), 841(m, sh), 785(w, sh), 769(w, sh), 762(w, sh), 748(vw), 730(m, sh), 712(w, sh). **UV/VIS:** $c = 1.44 \times 10^{-6}$ M, λ_{max} = 263 nm, ε = 5.87

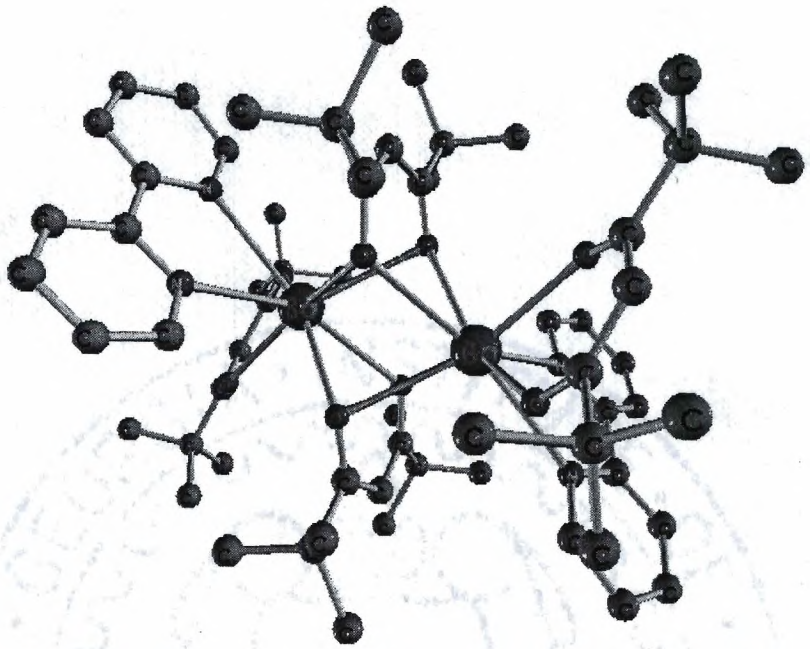

Figure 2-4. Molecular structure of $[Ba(tmhd)_2 \bullet bipy]_2$.

x 10^{-4} M^{-1} cm^{-1}, λ_{max} = 231 nm, $\varepsilon = 10.98 \times 10^{-4}$ M^{-1} cm^{-1}. **TGA:** (see **Figure 2-2**).

Sublimation. A sublimator equipped with a dry-ice/acetone cooled cold finger was charged with 0.50 g (0.579 mmol) of $Ba(tmhd)_2 \bullet 2$ *o*-phen. The sublimator was evacuated to 10^{-5} Torr and warmed slowly. Sublimation occured from 220 to 260°C. After one hour, 0.478 g of sublimed material was recovered from the cold finger, leaving a residue of 0.017 g. The ^{1}H-NMR of the sublimate showed it to be *o*-phenanthroline enriched, indicating decomposition of the compound in the solid state and unequal sublimation rates of the decomposition products.

$[Ba(tmhd)_2 \bullet bipy]_2$. Under a N_2 atmosphere, 1.32 g (9.60 mmol) of barium metal was combined with 80 cc of anhydrous Cabosil^{Tm} (dried at 100°C / 0.01 Torr for 48 hours) in

a 250 mL flask equipped with a magnetic stir bar and a dry-ice/acetone cooled condenser. Into this mixture was condensed 125 mL of anhydrous $NH_{3(l)}$ (passed over KOH), completely dissolving the barium. The $NH_{3(l)}$ was then allowed to evaporate slowly with stirring, leaving a barium metal coating on the Cabosil^{Tm}. The flask was evacuated to remove any residual NH_3. To the resulting grey solid was added 80 mL of hexane (distilled from $LiAlH_4$) followed by 2.68 g (14.5 mmol) H-tmhd and 5.68 g (36.4 mmol) 2,2'-dipyridil in 20 mL of toluene (distilled from Na). Rapid gas evolution was evident. The reaction mixture was stirred for 3 hours and then filtered through a Schlenk frit. The frit was rinsed with an additional solution of 20 mL toluene and 20 mL hexane. The solvents were removed under vacuum to give a white solid. The solid was recrystallized from a minimum amount of hot hexane to give 4.26 g (4.93 mmol) of $Ba(tmhd)_2$ •bipy, 89% based on H-tmhd. **Characterization: mp:** 157.3°C. **^{1}H NMR:** (300 MHz, positive δ downfield referenced to $Si(CH_3)_4$ = 0 ppm utilizing residual C_6D_5H = 7.15 ppm in solvent C_6D_6) 8.66 [d, 1H, bipy], 8.15 [d, 1H, bipy], 7.11 [td, 1H, bipy], 6.71 [td, 1H, bipy], 5.84 [s, 1H, tmhd], 1.28 [s, 18H, tmhd]. **^{13}C{^{1}H} NMR:** (75 MHz, positive δ downfield referenced to $Si(CH_3)_4$ = 0 ppm utilizing $\underline{C}D_3C_6D_5$ = 20.4 ppm) 200 [tmhd], 157 [bipy], 150 [bipy], 137 [bipy], 124 [bipy], 121 [bipy], 90 [tmhd], 42 [tmhd], 29 [tmhd]. **IR (nujol):** 3085(vw), 3045(vw), 2847(vs), 1581(s), 1564(s), 1523(w), 1480(m), 1435(w), 1416(vs), 1352(m), 1318(vw), 1259(vw,br), 1237(vw), 1217(w), 1194(vw), 1169(w), 1148(w), 1121(m), 1086(vw), 1057(w), 1037(w, sh), 1022(w, br), 1001(m, sh), 949(w), 929(w), 862(w), 790(w), 757(m), 739(w, sh). **UV/VIS:** $c = 1.30 \times 10^{-6}$ M, λ_{max}

= 236 nm, $\varepsilon = 13.17 \times 10^{-4}$ $M^{-1}cm^{-1}$, $\lambda_{max} = 284$ nm, $\varepsilon = 29.55 \times 10^{-4}$ M^{-1} cm^{-1}. **TGA:** (see **Figure 2-2**). **MW:** (benzene cryoscopy) obs. 748 g/mol (calc. monomer: 660 g/mol). **Sublimation.** A sublimator equipped with a dry-ice/acetone cooled cold finger was charged with 0.75 g (1.40 mmol) of the $[Ba(tmhd)_2 \bullet bipy]_2$. The sublimator was evacuated to 10^{-4} Torr and heated slowly. At approximately 70°C a white solid, identified as bipy (mp, ^{1}H-NMR), had sublimed onto the cold finger. This solid was allowed to migrate to the top of the cold finger before the finger was cooled. The remainder of the solid in the bottom of the sublimator sublimed from 160 to 220°C over the period of one hour and was identified as pure $[Ba(tmhd)_2]_4$ by ^{1}H-NMR and mp.

All other Preparations. The preparations involving the Lewis base molecules that did not yield a Lewis base coordinated product upon isolation were run in a method analogous to the $[Ba(tmhd)_2 \bullet bipy]_2$ preparation. The product isolated in each case was characterized by ^{1}H-NMR and identified as pure, authentic $[Ba(tmhd)_2]_4$.

References

1. L.A. Wills, B.W. Wessels, D.S. Richeson and T.J. Marks, *Appl. Phys. Lett.*, **1992**, *60*, 41.

2. P.C. Buskirk, R. Gardiner and P.S. Kirlin, *J. Mater. Res.*, **1992**, *7*, 542.

3. G.B. Stringfellow, *Organometallic Vapor-Phase Epitaxy: Theory and Practice*, Academic Press, New York, **1989**.

4. fod (7,7-dimethyl-1,1,1,2,2,3,3-heptafluorooctane-4,6-dionate).

5. (a) hfac (1,1,1,5,5,5-hexafluoropentane-2,4-dionate), (b) tetraglyme (2,5,8,11,14-pentaoxopentadecane).

6. (a) K. Timmer, K. Spee, A. Mackor, H.A. Meinema, A.L. Spek and P. van der Sluis, *Inorg. Chim. Acta*, **1991**, *190*, 190; (b) C.I.M.A. Spee, E.A. van der Zouwen-Assink, K. Timmer, A. Mackor and H.A. Meinema, *J. Phys. IV.*, **1991**, *1(C2)*, 295; (c) G. Malandrino, D.S. Richeson, T.J. Marks, D.C. DeGroot, J.L. Schindler and C.R. Kannewurf, *Appl. Phys. Lett.*, **1991**, *58*, 182; (d) J.M. Zhange, B.W. Wessels, D.S. Richeson, T.J. Marks, E.C. Degroot and C.R. Kannewurf, *J. Appl. Phys.*, **1991**, *69*, 2743; (e) S.J. Duray, D.B. Buchholtz, S.N. Song, D.S. Richeson, J.B. Ketterson, T.J. Marks and R.P.H. Chang, *Appl. Phys. Lett.*, **1991**, *59*, 1503; (f) R. Gardiner, D.W. Brown, P.S. Kirlin and A.L. Rheingold, *Chem. Mater.*, **1991**, *59*, 1503; (g) A.L. Spek, P. van der Sluis, K. Timmer and H.A. Meinema, *Acta Cryst.*, **1990**, *C46*, 1741.

7. (a) W.S. Rees, Jr. and D.A. Moreno, *J. Chem. Soc., Chem. Commun.*, **1991**, 1759; (b) W.S. Rees, Jr. and D.A. Moreno, in *Spectroscopy and Structure of Molecules and Nuclei*, edited by N.R. Johnson, W.N. Shelton and M.A. El-Sayed, World Scientific, **1992**, pp. 367 - 374.

8. (a) W.S. Rees, Jr. and K.A. Dippel, in *Proceedings of the International Conference on the Ultrastructure Processing of Ceramics, Glasses, Composites, Ordered Polymers, and Advanced Optical Materials*, Wiley, New York, **1992**, pp. 327 - 332; (b) W.S. Rees, Jr. and K.A. Dippel, *Organic Preparations and Procedures International*, **1991**, *24*, 531.

9. (a) A. Gléizes, S. Sans-Lenain and D. Médus, *C. R. Akad. Sci. Paris*, **1991**, *313II*, 761; (b) W.S. Rees, Jr., M.W. Carris and W. Hesse, *Inorg. Chem.*, **1991**, *30*, 1164.

10. (a) W.S. Rees, Jr., Y.S. Hascicek and L.R. Testardi, in *Better Ceramics Through Chemistry V.*, edited by M.J. Hampden-Smith, W.G. Klemperer and C.J. Brinker, *Mater. Res. Soc. Proc.*, **1992**, *271*, 925 - 931; (b) W.S. Rees, Jr., in *Proceeding of the Fourth Florida Microelectronics and Materials Conference*, edited by R. Rasmussen, University of South Florida Press, **1992**, p. 83; (c) W.S. Rees, Jr. and A.J. Barron, *NASA Review Series*, edited by A. Hepp, **1993**.

11. P.H. Dickinson, T.H. Geballe, A. Sanjurjo, D. Hildebrand, G. Craig, M. Zisk, J. Collman, S.A. Banning and R.E. Sievers, *J. Appl. Phys.*, **1989**, *66*, 444.

12. S. Matsuno, F. Uchikawa and K. Yoshizaki, *Jap. J. Appl. Phys.*, **1990**, *29L*, 947.

13. a) J. Zhao, K.H. Dahmen, H.O. Marcey, L.M. Tonge, T.J. Marks, B.W. Wessels and C.R. Kannewurf, *Appl. Phys. Lett.*, **1988**, *53*, 1750. b) J. Zhao, H.O. Marcey, L.M. Tonge, T.J. Marks, B.W. Wessels and C.R. Kannewurf, *Physica C*, **1989**, *159*, 710.

14. A.R. Barron, J.M. Buriak, L. Chetham and R. Gordon, *Abstract 343 HTS, 177th Meeting of the Electrochemical Society*, Montreal, Canada, **1990**.

15. A. Gléizes, S. Sans-Lenain, D. Médus and R. Morancho, *C. R. Acad. Paris*, **1991**, *312II*, 983.

16. P. Zanella, G. Rosseto, A. Polo, F. Benetollo and M. Porchia, *Polyhedron*, **1992**, *11*, 979.

17. R. Gardiner, D.W. Brown, P.S. Kirlin and A.L. Rheingold, *Chem. Mater.*, **1991**, *3*, 1503.

18. W.S. Rees, M.W. Carris and W. Hesse, *Inorg. Chem.*, **1991**, *30*, 1164.

19. tmeda = N,N,N',N'-tetramethylethylenediamine.

20. H. Zama, K. Sakai and S. Oda, *Jap. J. Appl. Phys.*, **1992**, *31L*, L1243.

21. A. Drozdov and S. Troyanov, *Polyhedron*, **1993**, *12(24)*, 2973.

CHAPTER III.

BARIUM *BIS*(β-DIKETONATE)•TETRAGLYME COMPLEXES AS POTENTIAL CVD PRECURSORS FOR ELECTRONIC MATERIALS

Introduction

Much can be learned from existing research aimed at the preparation of superconducting metal oxides (SMO's). The discovery of the general class of cuprate based high T_c superconductors has led to a virtual explosion of research in a number of fields aimed at development of synthetic methods suitable for the production of superconducting devices.[1] One active field has been research aimed at the production of high-quality thin films suitable for use in microwave cavities, integrated circuit interconnects and Josephson junctions.[2] Organometallic chemical vapor deposition (OMCVD) is an attractive method for the preparation of these films. The advantage of OMCVD over competing methods (*eg.*, molecular beam epitaxy, laser ablation, sputtering or evaporation) is its ability to combine high rates of deposition on irregularly shaped large area substrates at low temperature with adaptability in regard to compositional control over a broad range for multiple sources.[3] The fact that many of the SMO's contain group 2 elements has been a source of difficulty in OMCVD, due to the lack of suitably volatile precursors, particularly in the case of barium.[4]

Development of precursors suitable for OMCVD of group 2 element containing materials has focused mainly on the use of previously prepared substituted acetylacetonate ($acac^-$) complexes (**Figure 3-1**).[5] A commonly utilized barium precursor is $Ba(tmhd)_2$ (R = R'= *t*-Bu). Drawbacks of this precursor are that it is a tetramer in the solid state and shows limited thermal stability at its use temperature.[5] A series of sufficiently volatile

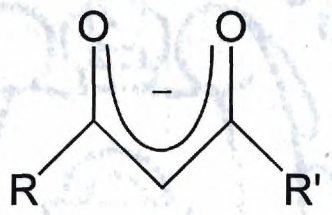

Figure 3-1. Structure of β-diketonate ligands.

precursors have been developed through the use of fluorinated substituents: $Ba(tfac)_2$ (R = CF_3, R' = Me),[6] $Ba(hfac)_2$ (R = R' = CF_3),[6] $Ba(fod)_2$ (R = C_3F_7, R' = *t*-Bu).[6] These precursors were shown to be well suited to the direct deposition of BaF_2 films, but require the addition of substantial quantities of H_2O into the reactor system in order to prepare SMO compositions.[6] Residual fluorine concentrations of approximately 100 ppm still are seen in even the very best water soaked films.[6] It is not known what effect this has on the electrical properties of the film. It is preferable, therefore, to develop volatile precursors lacking fluorine.

Results and Discussion

A variety of intermolecular neutral Lewis base adducts have been used in addition to the acac$^-$ based ligands to form compounds of the type: $Ba(tmhd)_2 \cdot L_x$ where L is a mono- or oligo-ether such as tetraglyme (2,5,8,11,14-pentaoxopentadecane).[7] Little success has been had here due to a lack of vapor phase stability. These neutral adducts tend to dissociate from the barium atom either before, or during, sublimation, producing a thermally unstable barium species in the vapor phase. It has been noted, however, that a number of fluorinated barium diketonates retain their oligoether adducts, in this case glymes, in the vapor phase. There are two effects potentially responsible for the stability differences of the fluorinated compounds. The first is a Van derWaals effect of mutual fluorine repulsion decreasing the solid state intermolecular cohesive forces. The second is an electronic effect. The electron withdrawing effect of fluorinated substituents lowers the negative charge density on the oxygens of the diketonate. This effect has been quantified through molecular mechanics and ZINDO calculations.[8] The bonding of barium to heteroatoms can be thought of as mainly electrostatic in nature. This creates a scenario where an electron density change on the oxygens of the diketonate is observed at the neutral adduct as a consequence of changing the total negative charge density available to offset the cationic charge of barium. Lowering the charge density on the diketonate oxygens makes the (now more positive) barium center a stronger Lewis acid, causing it to bind the neutral adduct more tightly. This effect is demonstrated in the change in barium-oxygen interatomic distances in these Ba(β-diketonate)$_2$•tetraglyme compounds, relative to the effective charge on the β-diketonate ligand. Effective charge

here is defined to be the sum of the partial charges on the two bonding oxygens of the diketonate ligand. The data set being examined consists of five barium β-diketonate tetraglyme adduct species whose structures differ only in the identities of the terminal R-groups of the β-diketonate ligands as shown in **Figure 3-1**. The structures and abbreviations for these β-diketonate ligands are shown in **Figure 3-2**. The solid state

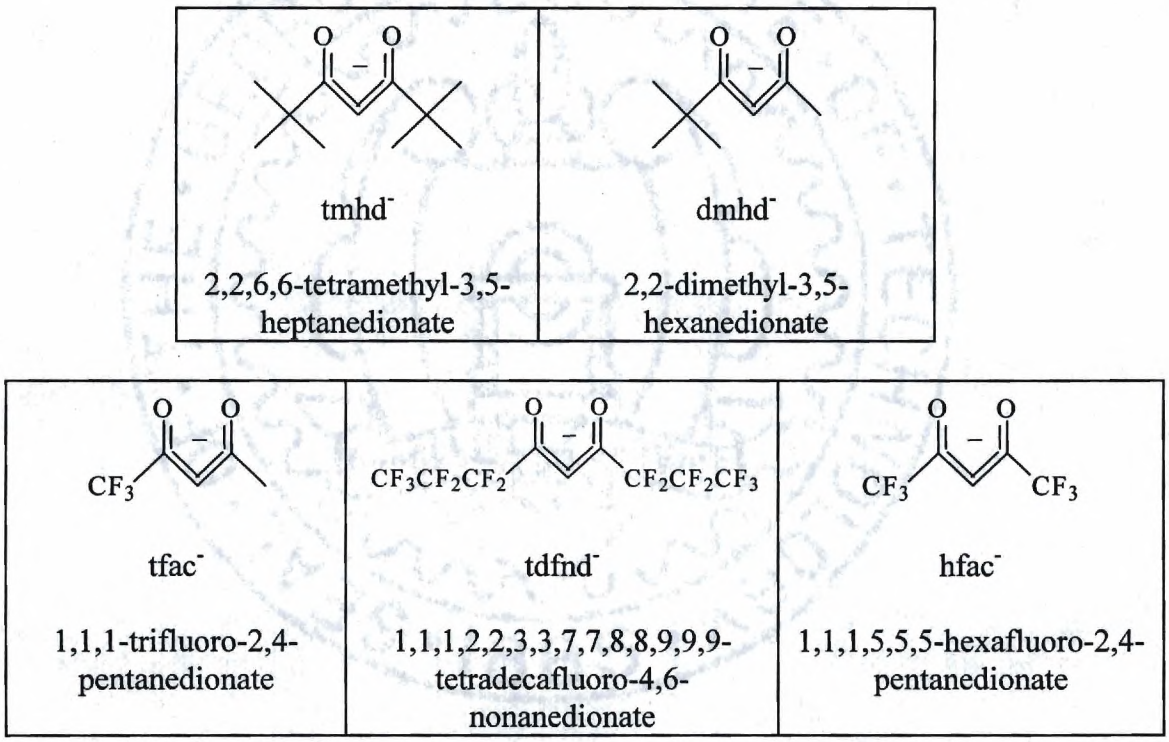

Figure 3-2. Representative β-diketonate structures.

structures of the barium *bis*(β-diketonate)•tetraglyme complexes, as determined by single crystal x-ray diffraction, are shown in **Figure 3-3**. It is important to note that the MO_9 cores of these complexes are virtually superimposable (**Figure 3-4**). By probing the

response of both the barium-diketonate and barium-tetraglyme interatomic distances to changes in the effective charge on the β-diketonate (**Figure 3-6**), one observes that a decrease in charge has a significant effect on the relative interatomic distances present within the complexes.

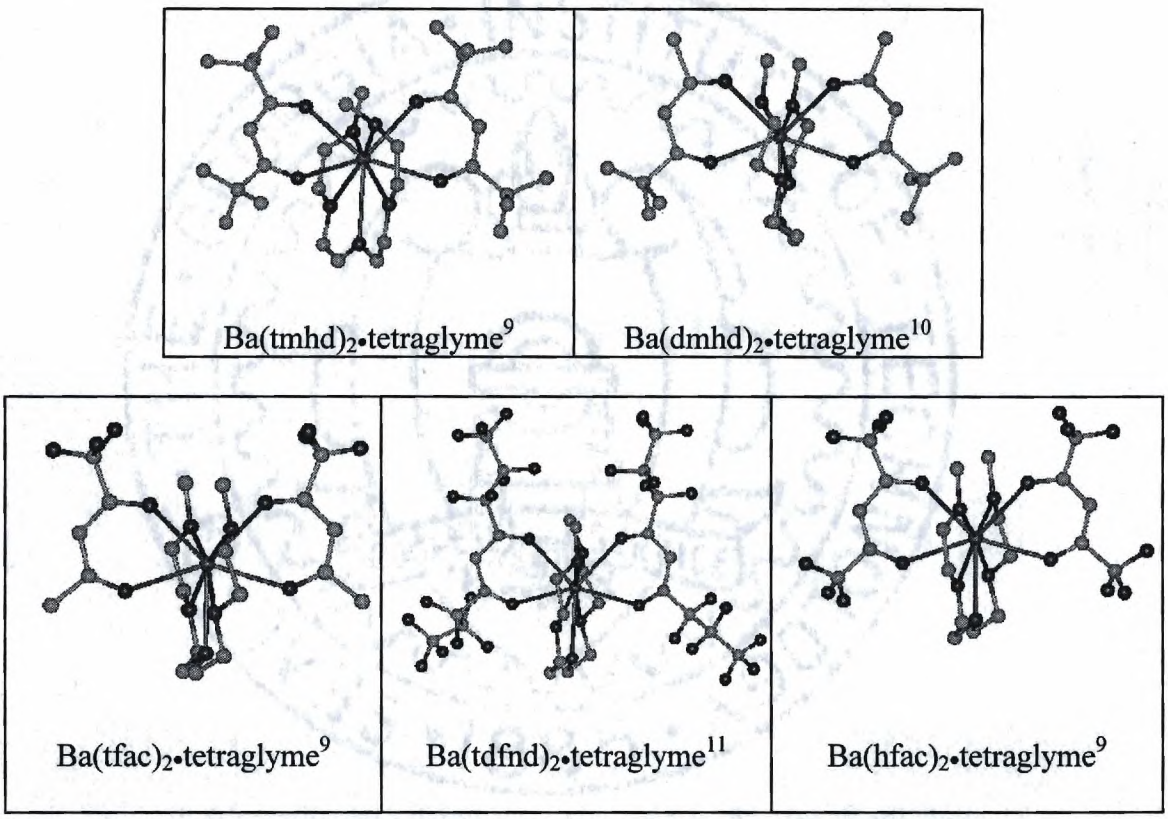

Figure 3-3. Ba(β-diketonate)$_2$•tetraglyme compound structures.

As the partial charge on the oxygens of the diketonate increases, the barium β-diketonate interatomic distances decrease. Conversely, as the Ba-diketonate interatomic distances increase, the barium tetraglyme oxygen atom interatomic distances decrease. Therefore, the advantage of using fluorinated diketonates is that their lower effective

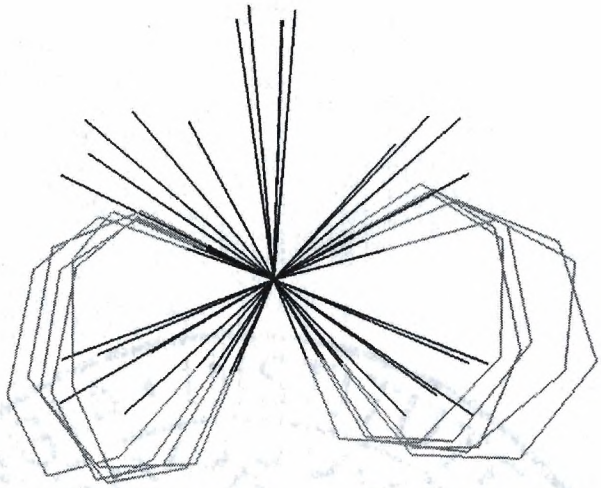

Figure 3-4. Superimposed images of the MO_9 cores of the examined barium complexes. The three ring carbons of the diketonate are included and the oxygens of the diketonate rings are a lighter color for clarity.

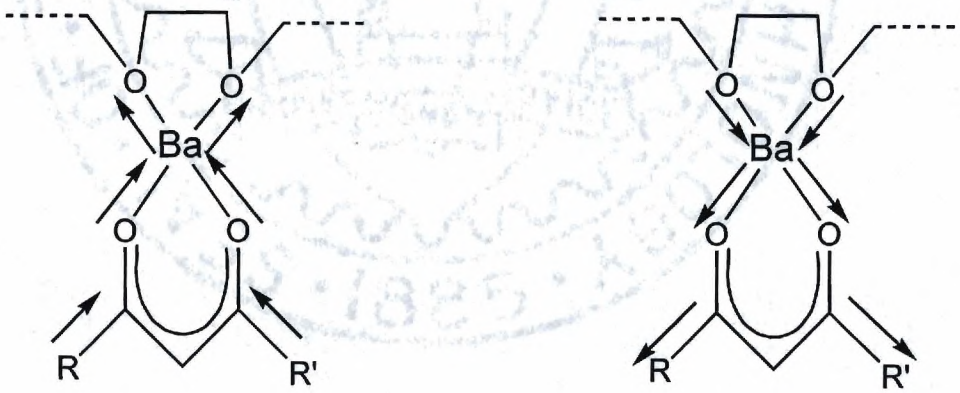

Figure 3-5. Inductive effects observed in these species.

charges cause the barium center to become a stronger Lewis acid, consequently drawing the glyme's oxygen atoms closer to the metal center (**Figure 3-5**). The thermal stability data correlates well with the effective charge data shown in **Figure 3-6** in the following

manner: The barium complexes of those β-diketonate ligands with effective charges more negative than $tfac^-$ lose tetraglyme prior to (or during) sublimation, producing a thermally unstable vapor phase species. The barium complexes of those β-diketonate ligands with

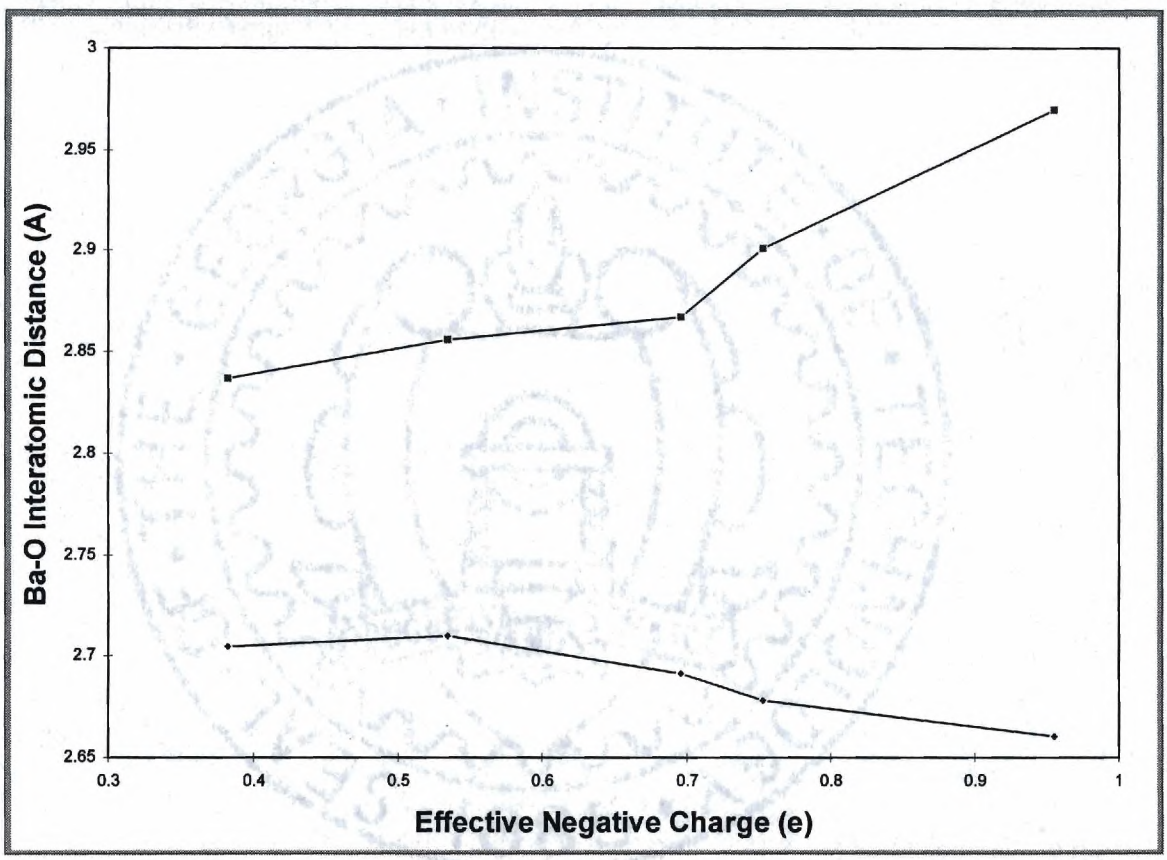

Figure 3-6. Ba-O interatomic distances versus effective charge of the β-diketonate. The top data (squares) represent the average tetraglyme O-Ba interatomic distance for each compound. The bottom data (diamonds) represent the average diketonate O-Ba interatomic distance for each compound.

effective charges less negative than $tfac^-$ sublime intact and show good volatility and stability. It has been reported that $Ba(tfac)_2$•tetraglyme itself sublimes intact, although not

in 100% yield.[12] As discussed earlier, however, fluorinated ligands present challenges in the direct deposition of group 2 element containing metal oxides.

There are other, more effective, routes to lowering the charge donated by the diketonate. One promising route is through heteroatom substitution for the oxygens on the diketonates. For ease of comparison, a tmhd$^-$ backbone will be used. Each oxygen in tmhd$^-$ holds a partial charge of -0.377 (e$^-$) (**Figure 3-7a**) giving a total partial charge on

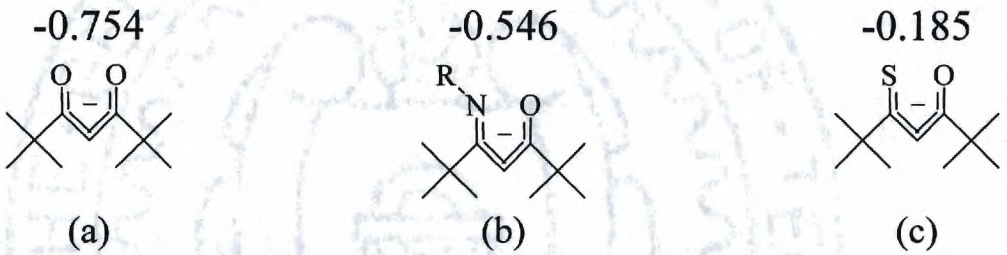

Figure 3-7. Effective charges of various heteroatom substituted β-diketonate ligands.

both oxygens, in other words an effective charge, of -0.754 (e$^-$). Subtitution of an alkyl-bearing nitrogen for one of these oxygens to give a β-ketoimine (**Figure 3-7b**) lowers the effective charge (O+N) to -0.546 (e$^-$). In an elegant example of ligand design, two barium *bis*(β-ketoiminate) compounds were prepared and studied by Marks *et al.*;[12] however, they showed thermal instability, presumably as a consequence of the inherent instability of the metal imine bond. Substitution of sulfur for oxygen would seem more promising. Replacement of one oxygen would lower the effective charge to -0.185 (e$^-$) (**Figure 3-7c**). The preparation of monothio-β-diketones from several typical β-diketones is known.[13]

Monothio-2,2,6,6-tetramethyl-3,5-heptanedione (**Figure 3-7c**), referred to from here on as H-stmhd, was prepared by the method of Chaston *et al.*[14] The barium tetraglyme complex of the stmhd$^-$ ligand, Ba(stmhd)$_2$•tetraglyme, has been prepared by reaction of barium metal with the protonated ligand in toluene, using a catalytic amount of EtOH. The compound shows extreme x-ray sensitivity allowing only unit cell information (primitive monoclinic, a = 13.18Å, b = 19.13Å, c = 16.00 Å, β = 93.52°) to be obtained; however, this data is consistant with the structural motif of the other compounds of its type. One can ascertain from its TGA trace (**Figure 3-8**) that

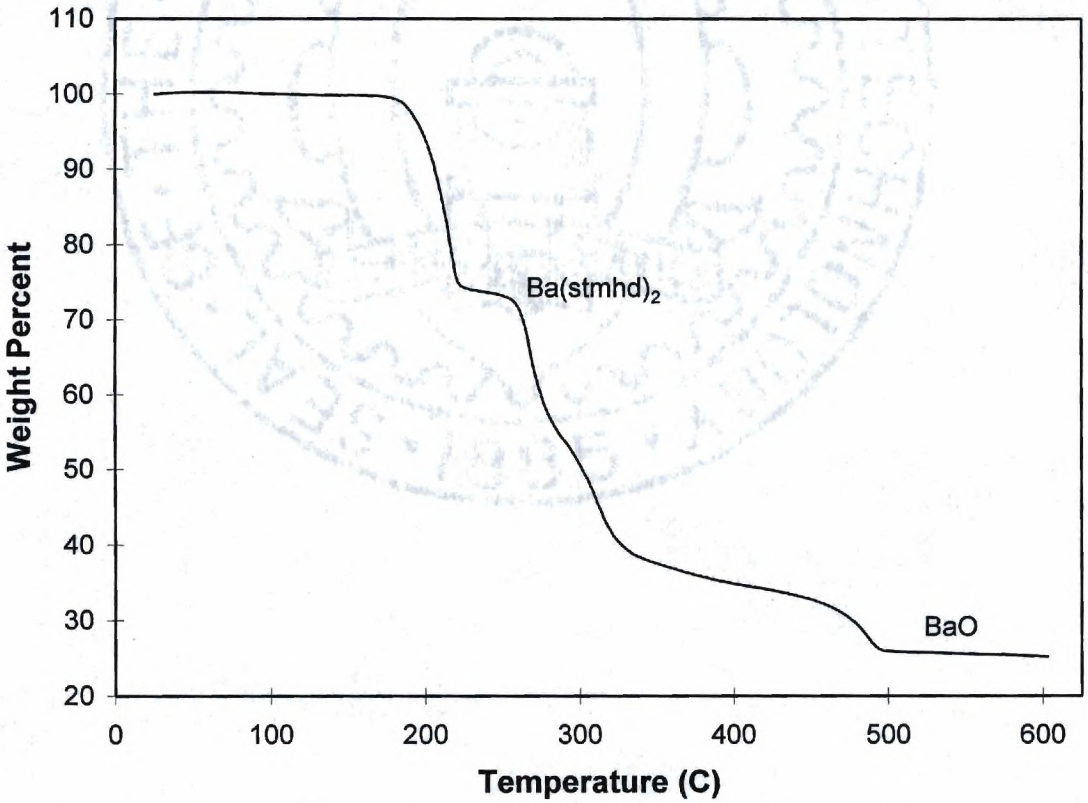

Figure 3-8. TGA of Ba(stmhd)$_2$•tetraglyme showing loss of tetraglyme followed by decomposition to BaO.

$Ba(stmhd)_2$•tetraglyme is not volatile. It does not retain the tetraglyme and sublime. This does not fit the predictive model based on the ligand's effective charge. The model, however, assumes a delocalized charge in an aromatic system. We believe that this is not the case for this ligand. It is more likely that the charge is localized on the sulfur forming a β-thioketoenolate as shown in **Figure 3-9**. This particular localized system is calculated to have an effective charge of -0.697 (e^-).

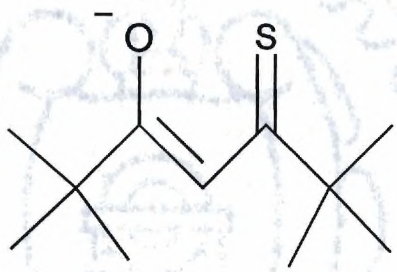

Figure 3-9. Proposed β-thioketoenolate structure.

The model would predict loss of tetraglyme prior to sublimation for a β-diketonate complex with this effective charge. Also, it is not surprising that BaO is formed, since the compound is, in effect, a substituted barium alkoxide.

Conclusions

The relative Lewis acidity of the metal center in a barium *bis*(β-diketonate)•tetraglyme complex is a function of the effective charge of the β-diketonate ligand, whereby, the effective charge is defined as the sum of the calculated partial

charges residing on the bonding atoms of the ligand. The primary advantage of fluorinated β-diketonate ligands is that the fluorinated side groups are electron withdrawing and lower the partial charge density at the binding oxygens of the ligand, thereby enhancing the metal center's Lewis acidity resulting in the metal's enhanced ability to bind neutral Lewis bases (*eg.* tetraglyme) more strongly. Substitution of the oxygens of the β-diketonate with heteroatoms of lower electronegativity should influence the barium center in a similar manner, provided that the substitution retains the β-diketonate's charge delocalization in the resultant bidentate moiety.

Experimental

Monothio-2,2,6,6-tetramethylheptane-3,5-dione (H-sthd). H-sthd was prepared by the method of Chaston *et al.*[14] The crude orange oil containing residual H-tmhd was purified by column chromatography utilizing flash silica gel as the stationary phase and hexanes as the mobile phase. This yielded the purified orange oil described by Chaston *et al.* **Characterization: ^{1}H NMR:** (300 MHz, positive δ downfield referenced to $Si(CH_3)_4$ = 0 ppm utilizing residual $CHCl_3$ = 7.24 ppm in solvent $CDCl_3$) 6.69 [s,1H, -CO-C**H**=CSH-], 1.27 [s, 9H, $(CH_3)_3$C-CSH=], 1.22 [s, 9H, $(CH_3)_3$-CO-]. **^{13}C{^{1}H} NMR:** (75 MHz, positive δ downfield referenced to $Si(CH_3)_4$ = 0 ppm utilizing residual C_6D_5H = 128.0 ppm in solvent C_6D_6) 215.7 [*t*Bu-**C**SH=CH-], 197.2 [*t*Bu-**C**O-CH-], 107.4 [-CO-**C**H=CSH-], 44.8 [$(CH_3)_3$**C**-CSH=], 40.0 [$(CH_3)_3$**C**-CO-], 30.1 [($CH_3)_3$C-CSH=], 27.1 [($CH_3)_3$C-CO-].

Ba(sthd)$_2$•tetraglyme. Under an argon purge, 0.555g (2.50 mmol.) of anhydrous tetraglyme (distilled from Na), 1.00g (5.00 mmol.) of monothio-2,2,6,6-tetramethylheptane-3,5-dione and 0.34g (2.50 mmol.) of barium metal were combined in a 250 ml. Schlenk flask containing 50 ml. of anhydrous toluene (distilled from Na / benzophenone) and a magnetic stir bar. The mixture was stirred and 10 drops of anhydrous ethanol (distilled from CaO) were added. The mixture was warmed to 60°C for 24 hours. While the solution was still warm it was Schlenk filtered through washed Celite into another flask. The solvent was then stripped by evacuation to give a yellow solid. **Characterization: mp:** 149°C. **^{1}H NMR:** (400 MHz, positive δ downfield referenced to Si(CH$_3$)$_4$ = 0 ppm utilizing residual C$_6$D$_5$H = 7.15 ppm in solvent C$_6$D$_6$) 7.04 [s, 2H, -CS-C**H**-CO-], 3.40 [br, tetraglyme], 3.29 [m, tetraglyme], 3.21 [m, tetraglyme], 3.17 [s, 12H, tetraglyme], 1.59 [s, 18H, (C**H**$_3$)$_3$C-CS-], 1.30 [s, 18H, (C**H**$_3$)$_3$C-CO-]. **^{13}C{^{1}H} NMR:** (100 MHz, positive δ downfield referenced to Si(CH$_3$)$_4$ = 0 ppm utilizing residual C$_6$D$_5$H = 128.0 ppm in solvent C$_6$D$_6$) 207.0 [*t*Bu-**C**S-CH-], 200.0 [*t*Bu-**C**O-CH-], 110.6 [-CO-**C**H-CS-], 71.4 [tetraglyme], 70.5 [tetraglyme], 70.3 [tetraglyme], 70.0 [tetraglyme], 58.6 [tetraglyme], 44.8 [(CH$_3$)$_3$**C**-CS-], 42.4 [(CH$_3$)$_3$**C**-CO-], 32.1 [(**C**H$_3$)$_3$C-CS-], 28.5 [(**C**H$_3$)$_3$C-CO-]. **TGA: Figure 3-8. Elemental Analysis:** Calc'd: C 50.7%, H 8.0%; Found: C 50.3%, H 7.9%.

Ba(dmhd)$_2$•tetraglyme. Under an argon purge, 1.12g (5.10 mmol.) of anhydrous tetraglyme (distilled from Na), 1.44g (10.1 mmol.) of 5,5-dimethylhexane-2,4-dione and 0.70g (5.1 mmol.) of barium metal were combined in a 250 ml. Schlenk flask containing

50 ml. of anhydrous toluene (distilled from Na / benzophenone) and a magnetic stir bar. The mixture was stirred and 10 drops anhydrous ethanol (distilled from CaO) were added. The mixture was then warmed to 60°C for 24 hours. While the solution was still warm it was Schlenk filtered through washed Celite into another flask. The solvent was then stripped by evacuation to give a colorless solid. **Characterization: mp:** 87°C (dec.). **^{1}H NMR:** (400 MHz, positive δ downfield referenced to $Si(CH_3)_4$ = 0 ppm utilizing residual C_6D_5H = 7.15 ppm in solvent C_6D_6) 5.57 [s, 2H, -CO-C**H**-CO-], 3.37 [m, tetraglyme], 3.26 [s, tetraglyme], 3.26 [m, tetraglyme], 2.07 [s, 6H, C**H**$_3$-CO-], 1.29 [s, 18H, (C**H**$_3$)$_3$C-CO-]. **^{13}C{^{1}H} NMR:** (100 MHz, positive δ downfield referenced to $Si(CH_3)_4$ = 0 ppm utilizing residual C_6D_5H = 128.0 ppm in solvent C_6D_6) 219.8 [CH_3-**C**O-CH-], 188.4 [*t*Bu-**C**O-CH-], 93.6 [-CO-**C**H-CO-], 71.7 [tetraglyme], 70.6 [tetraglyme], 70.3 [tetraglyme], 58.9 [tetraglyme], 40.8 [(CH_3)$_3$**C**-CO-], 29.4 [**C**H$_3$-CO-], 29.1 [(**C**H$_3$)$_3$C-CO-]. **Elemental Analysis:** Calc'd: C 48.6%, H 7.5%; Found: C 48.0%, H 7.7%.

References

1. J.G. Bednorz, K.A. Mueller, *Z. Phys. B*, **1986**, *64*, 189-193.

2. T. Venkatesan, X.D. Wu, A. Inam, M.S. Hegde, E.W. Chase, C.C. Chang, P. England, D.M. Hwang, R. Krchnavek, J.B. Wachman, W.L. McLean, R. Levi-Setti, J. Chabala, Y.L. Wang, In *Chemistry of High-Temperature Superconductors II*, edited by D.L. Nelson and T.F. George, ACS Symposium Series 377 (American Chemical Society, Washington, DC, 1988), pp. 234-264.

3. G.B. Stringfellow, *Organometallic Chemical Vapor Phase Epitaxy: Theory and Practice*, (Academic Press: New York, 1989).

4. A.R. Barron, *Strem Chem.* **1990**, *12* (Oct), 1-9.

5. L.M. Tonge, D.S. Richeson, T.J. Marks, J. Zhao, J. Zhang, B.W. Wessels, H.O. Marcy, C.R. Kannewurf, In *Electron Transfer in Biology and the Solid State: Inorganic Compounds with Unusual Properties, Part III*, edited by M.K. Johnson, R.B. King, D.M. Kurtz, Jr., C. Kutal, M.L. Norton, R.A. Scott, ACS Advances in Chemistry Series 226, (American Chemical Society, Washington, DC, 1990) pp. 351-368.

6. M.L. Hitchman, S.H. Shamlian, D.D. Gilliland, D.J. Cole-Hamilton, J.A.P. Nash, S.C. Thompson, S.C. Cook, *J. Mater. Chem.* **1995**, *5(1)*, 47-52; M.L. Hitchman, Spring Meeting, European Materials Research Society, **1996**, Abstract # F-VIII.2.

7. S.R. Drake, S.A.S. Miller, D.J. Williams, *Inorg. Chem.* **1993**, *32*, 3227-3235.

8. H.A. Luten, W.S. Rees, Jr., work to be published: utilizing Biosym's (4.0) InsightII and Discovery3 software and esff forcefields for the MM2 calculations and Biosym's ZINDO software for energy minimization and partial charge calculations on the MM2 minimized free anionic ligands using the software default settings.

9. R. Gardiner, D. Brown, P. Kirlin, A. Rheingold, *Chem. Mater.* **1991**, *3*, 1053.

10. H.A. Luten, D.J. Otway, W.S. Rees, Jr., Manuscript in Preparation.

11. J. Nash, J. Barnes, D. Cole-Hamilton, B. Richards, J. Cook, M. Hitchman, *Adv. Mater. Opt. Elec.* **1995**, *5*, 1.

12. D.L. Schultz, B.J. Hinds, C.L. Stern, T.J. Marks, *Inorg. Chem.* **1993**, *32*, 249-250.
13. Saul Patai, *The Chemistry of the Functional Groups, The Chemistry of the Carbonyl Group*, edited by Saul Patai (Interscience Publishers: New York, 1966), pp. 919-959.

14. S.H.H. Chaston, S.E. Livingstone, T.N. Lockyer, V.A. Pickles, J.S. Shannon, *Aust. J. Chem.* **1965**, *18*, 673.

CHAPTER IV.

THE PREPARATION AND STRUCTURAL CHARACTERIZATION OF, AND CHEMICAL VAPOR DEPOSITION STUDIES WITH, CERTAIN YTTRIUM *TRIS*(β-DIKETONATE) COMPOUNDS

Introduction

A wide variety of materials contain yttrium. Materials such as yttria, Y_2O_3, or yttria-stabilized zirconia, YSZ, are of interest due to their structural properties.[1] Optoelectronic yttrium-containing materials, for example yttrium aluminum or iron garnet, YAG and YIG, respectively, are employed widely in the field of lasers.[2] Rare earth element doped Y_2O_3 samples exhibit a sharp emission at 612 nm, in the red region of phosphors.[3] The perovskite phase material $YTiO_3$ is an ambient condition semiconductor with a band gap of 0.22 eV and it displays ferromagnetic ordering.[4] Perhaps the electronic material which contains the second member of the group 3 elements that has generated the highest level of activity is the superconducting metal oxide $YBa_2Cu_3O_{7-\delta}$.[5,6] Recently, $YAlO_3$ has been proposed as a compatable substrate for the deposition of $YBa_2Cu_3O_{7-\delta}$.[7] It possesses both a good crystal lattice and coefficient

of thermal expansion match with the superconducting material, as well as displaying excellent dielectric properties. The initial publication on this material described its preparation in a thin film form by means of chemical vapor deposition, CVD.[7]

There are numerous advantages of CVD over alternative methods for depositing thin films of electronic materials.[8] In particular, the potential for combination of rapid and uniform application of coatings on uneven substrates having large surface areas with the integration into existing semiconductor-based technology has contributed heavily to the motivation for such investigations.[9] One specific target at the present is the fabrication of a multichip module, MCM, containing superconducting interconnects.[10] Several approaches have led to some success in this and related areas.[11,12] For the achievement of CVD of any yttrium-containing material, the primary chemical issue is identification of a suitable chemical precursor compound for the metal of interest.[8,9]

Certain β-diketonate[13] complexes of some elements are known to be sufficiently volatile to be successfully applied toward the thermal deposition of the requisite material.[14,15] For example, recent results have been reported for $Ag(hfac)PMe_3$,[16] $[(hfac)Ag(COD)]_2$,[17] $Bi(L)_3$ for L = $tfac^-$, $hfac^-$, or fod^-,[18] $Ce(L)_4$ for L = $tmhd^-$ or $tfdmhd^-$ and both of the respective *o*-phen adducts,[19] $[Bi(tmhd)_3]_2 \cdot 0.5\ Htmhd$,[20] CuL_2 for L = $acac^-$ or $tmhd^-$,[21,22] $[Ba(tmhd)_2 \cdot 2NH_3]_2$,[23] $Ba(dmmod)_2$,[24] and $Ba(L)_2$•tetraglyme for L = $tfac^-$, $hfac^-$, $tdfnd^-$ or $tmhd^-$.[25-28] Particularly noteworthy among the numerous precursors for the selective deposition of copper is the family of Cu^{+1} ligand-stabilized β-diketonate

compounds, LCu(L'), with L' representing a β-diketonate moiety and L being a neutral Lewis base such as a phosphine, phosphite, alkene, or alkyne.[29]

The preparation of a general class of compounds, $M(tmhd)_3$ for M = Sm, Eu, Gd, Tb, Dy, Ho or Er, was described over a quarter of a century ago.[30] The solid state structures have been determined for $Er(tmhd)_3$,[31] $[Pr(tmhd)_3]_2$,[32] and $Dy(tmhd)_3 \cdot H_2O$.[33] In light of the discussion surrounding the advantages or disadvantages associated with the presence or absence of water in the growth ambient for CVD of $YBa_2Cu_3O_{7-\delta}$,[34-36] and the reports of the successful utilization of $Y(tmhd)_3$ in CVD of electronic materials,[5, 7, 37-39] it was of interest to explore the role of water in this composition, and the effect, if any, it had on subsequent CVD use. A preliminary report of some of these studies has appeared,[37,40] simultaneously with comparable work from the research group of Gleizes.[41,42]

Results

Ligands:

Htmhd. A modification of a previous method[43] was employed and optimized to permit the isolation of high purity (>98% by GC/MS) material in high yield (>90%, based on pinacolone charged as a reactant) following a simple and rapid workup of the crude reaction mixture.

Htmod. Substantial economic benefit was realized by a change in the reactants, relative to a previous method.[44] Each method relies upon a traditional Claisen

(Eq. 4-1)

(Eq. 4-2)

i) Conditions: 2 NaH / DME / 80°C

condensation between an ester and a methyl ketone. They differ only in the penultimate location of the terminal groups present in the β-diketone product. The benefit is realized in the relative cost of the two routes, each leading to an identical product.* Additionally, economics plays a major role in the selection between H-tmhd and H-tmod when such flexibility is present (H-tmhd = $95.77 / mol; H-tmod = $46.57 / mol). The structures of H-tmhd and H-tmod are illustrated in **Figure 4-1**.

Hydrous Metal Ligand Complexes:

$[Y(tmhd)_3 \bullet H_2O]_2$. This compound was prepared following minor modification of a previously published general route to compounds of the formula $M(tmhd)_3$, where M represents a trivalent lanthanide, or pseudolanthanide, ion.[45] Following a workup described in the literature, this method consistently yielded a hydrated product.

(a) (b)

Figure 4-1. The structures of the protonated ligands: a) 2,2,6,6-tetramethylheptane-3,5-dione (H-tmhd); b) 2,2,7-trimethyloctane-3,5-dione (H-tmod).

$Y(tmod)_3 \bullet H_2O$. Attempts to prepare this product in an analogous manner to $[Y(tmhd)_3 \bullet H_2O]_2$ consistently resulted in the isolation of anhydrous material.

Anhydrous Metal Ligand Complexes:

$Y(tmhd)_3$. A preliminary screening of several known methods for dehydration of hydrated transition metal coordination compounds resulted in the selection of the one represented by **Eq. 4-3**. This method consistently produced anhydrous material. Although other methods were found to be mildly successful, the degree of reproducibility was highest with that represented here.

$$[Y(tmhd)_3 \bullet H_2O]_2 \xrightarrow{\text{Sublimation}} Y(tmhd)_3$$

(Eq. 4-3)

$[Y(tmod)_3]_2$. Following the initial preparation of this compound, analogous to that utilized as described above in the synthesis of $[Y(tmhd)_3 \bullet H_2O]_2$, the compound

which was isolated in good yield on a regular basis was determined by analytical techniques to have a formula and properties which corresponded to those expected for an anhydrous composition.

Characterization of Precursor Compounds:

NMR: $^{13}C\{^{1}H\}$. The observed spectra for $[Y(tmhd)_3 \bullet H_2O]_2$ and $Y(tmhd)_3$ each correlated well with those expected for the ~O_h symmetry present within each compound. The case, however, of $[Y(tmod)_3]_2$ rendered a substantial surprise (**Figure 4-2**). The observation of two independent resonances for the carbonyl carbons adjacent to the *iso*-butyl end of the β-diketonate ligand presented indications that there was more than one binding mode present in solution under static conditions.

UV/VIS. Absorption spectra have been published for "$Y(tmhd)_3$",[46] and it appears that such data correspond to $[Y(tmhd)_3 \bullet H_2O]_2$. Although undoubtedly the chromophore present in such a species is localized within the β-diketonate moiety, some contribution may arise from the ancillary ligands present on the d^0 metal.

Mass Spectral Data. The predominant mass peak observed corresponds to a *t*-Bu fragment (m/e = 57 amu). Additionally, mass units which corresponded to ML_3 and ML_2 are evident among the data (L = β-diketonate ligand).

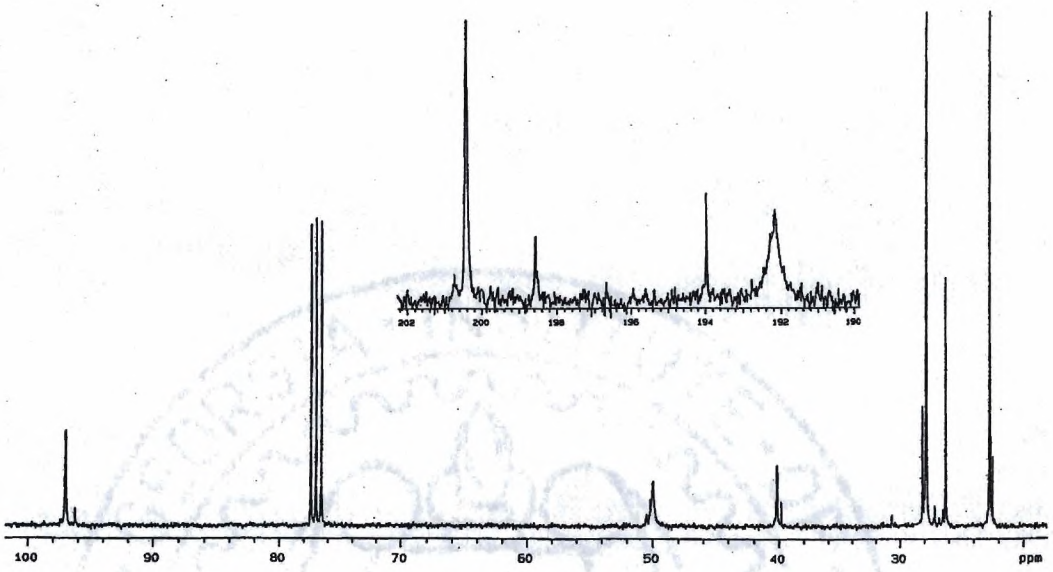

Figure 4-2. $^{13}C\{^{1}H\}$NMR spectrum of $[Y(tmod)_3]_2$.

Structural Examination. There are three fundamental solid state structural motifs displayed by trivalent lanthanide or pseudolanthanide β-diketonate complexes. For the anhydrous case, six-coordinate monomeric[30] and seven-coordinate dimeric[33] species have been reported previously. Likewise, monomeric, hydrated, seven-coordinate moieties are known for some of these elements as well. The nominal coordination number for each metal center in the anhydrous dimer also is seven. The separation observed between Y and O(1') of 2.42Å in the structure of $[Y(tmod)_3]_2$ lies outside the range typically found for M-O interatomic distances which are attributed to bonding interactions (2.23 to 2.35 Å). Likewise, it is 0.07 Å (3%) above the sum of the covalent radii of the two elements (Y: 1.62 Å; O: 0.73 Å).[47]

Structure of $[Y(tmhd)_3 \cdot H_2O]_2$. Previous $M(tmhd)_3 \cdot H_2O$ structures have been reported for Dy and Eu.[32] The vapor phase structure of $Y(tmhd)_3$, determined by gas phase electron diffraction (GPED), has been reported (**Figure 4-3**).[48] Subsequent to our initial report of the structure determination for $[Y(tmhd)_3 \cdot H_2O]_2$ (**Figure 4-4**),[37] Gleizes[42] also published comparable results. The units within the crystallographic cell are arranged as dimeric species. This is the result of hydrogen bonding between the protons of the water ligand (O7) and the carbonyl oxygens of two independent β-diketonate ligands on the second metal center (O1' and O6'). Consistent with this explaination, it is observed that the Y-O interatomic distances for these three interactions (2.35, 2.35 and 2.32 Å, respectively) substantially are longer than those portrayed by the other four such moieties

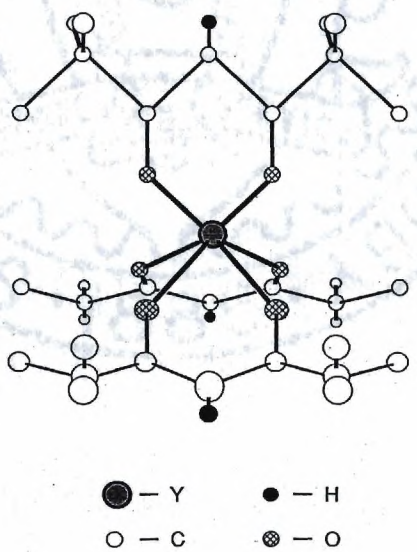

Figure 4-3. The structure of $Y(tmhd)_3$ as determined by gas phase electron diffraction.[48] Protons have been omitted for clarity.

(2.22 - 2.26 Å). Although some minor deviation is noted here from the duplication of our preliminary report by others,[42] qualitative agreement exists between the two data sets. Structural data is given in **Table 4-1**.

These M-O distances may be compared with those found for $Y(tmhd)_3$ (2.128-2.298 Å),[42] $[Pr(tmhd)_3]_2$ (2.38-2.44, terminal; 2.46-2.59, bridging),[32] $Er(tmhd)_3$ (2.21 Å)[31] and $Dy(tmhd)_3 \cdot H_2O$ (2.22-2.36, β-diketonate; 2.36 Å, H_2O).[33] Additionally $[Y(tmod)_3]_2$, described in more detail below, has a range of 2.23-2.29 Å. Thus, it may be concluded

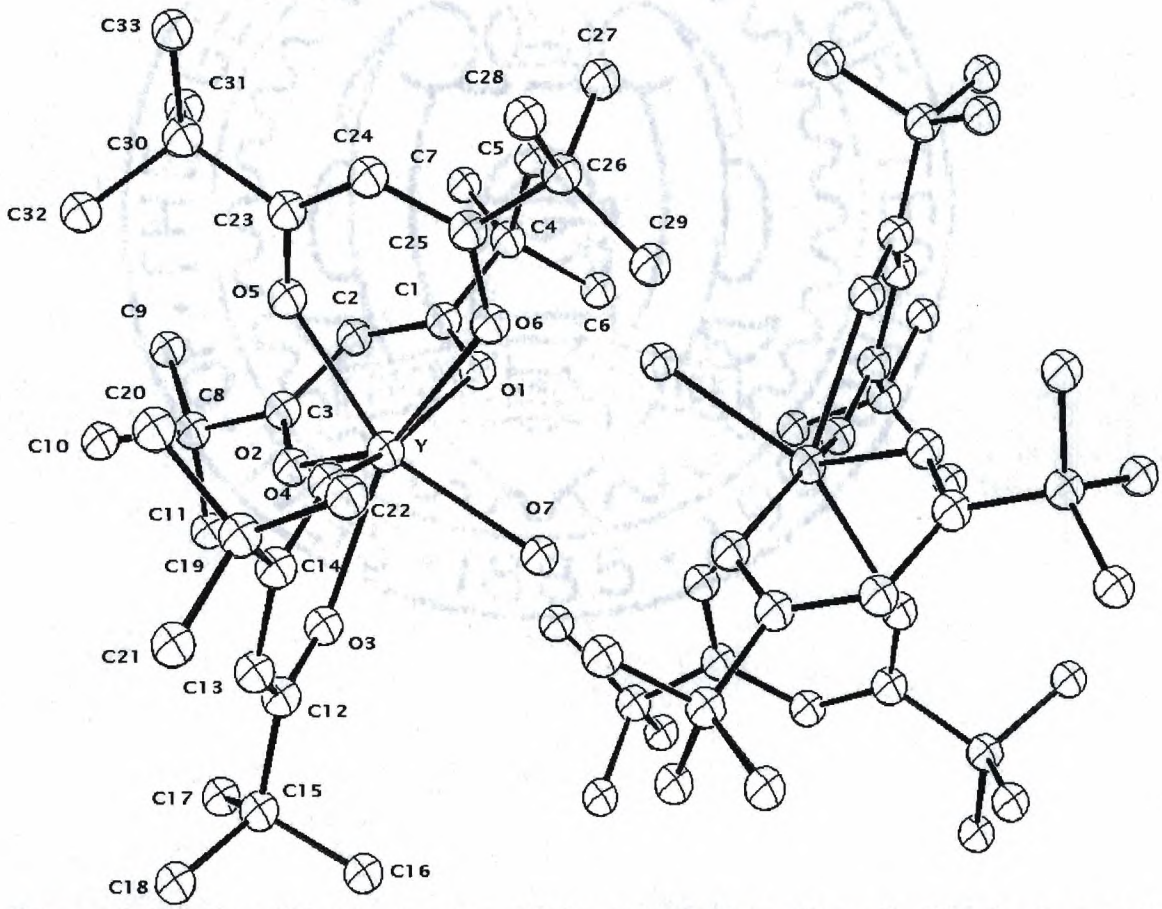

Figure 4-4a. The solid state structure of $[Y(tmhd)_3H_2O]_2$ as determined by single crystal X-ray diffraction. Hydrogen atoms are omitted for clarity.

that the present data break down into two general categories of Y-O interatomic distances. Those having contacts within 2.12 - 2.29 Å (those at the low end are unusually short and suprisingly are seen in only one report)[46] may be termed as traditional terminal M-O units. Those within the range of 2.32 - 2.35 Å belong to oxygen atoms which occupy bridging positions between two yttrium centers.

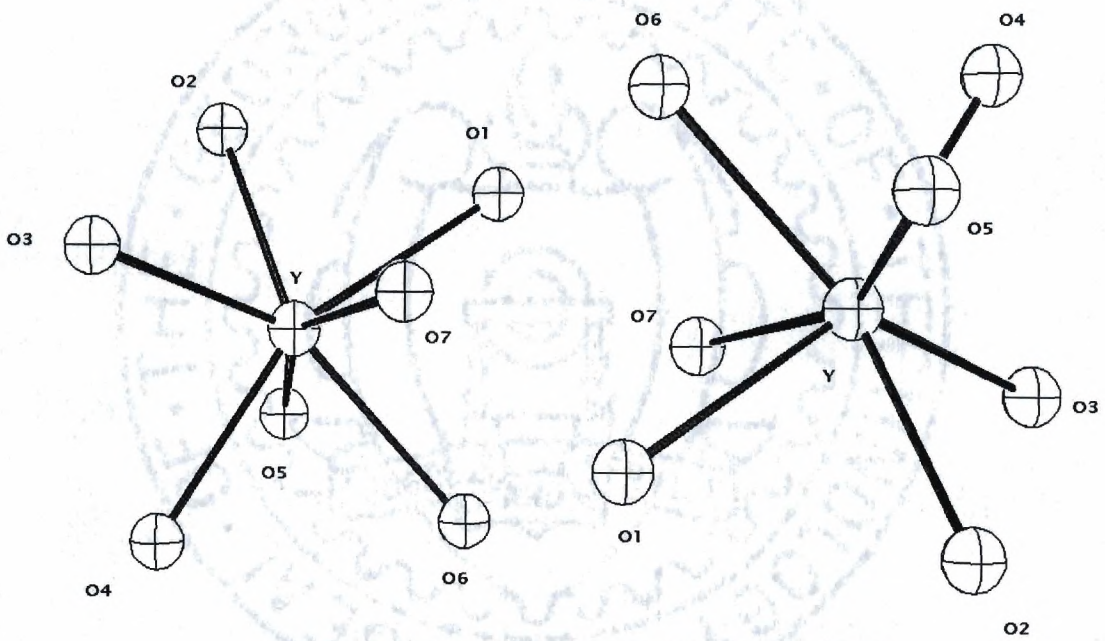

Figure 4-4b. The M_2O_{14} core of $[Y(tmhd)_3H_2O]_2$.

The localized geometry around the metal center in $[Y(tmhd)_3{\bullet}H_2O]_2$ is seven coordinate. It is neither a regular pentagonal bipyramid nor a monocapped octahedron. Perhaps the closest approximation of its structure is that of a distorted monocapped

Table 4-1. Structural data for $[Y(tmhd)_3 \cdot H_2O]_2$.

Interatomic Distances	
Atoms	**Distances (Å)**
Y-O(1)	2.35 (1)
Y-O(2)	2.24 (1)
Y-O(3)	2.25 (1)
Y-O(4)	2.26 (1)
Y-O(5)	2.22 (1)
Y-O(6)	2.32 (1)
Y-O(7)	2.35 (1)
O(1)-C(1)	1.28 (2)
O(2)-C(3)	1.28 (2)
O(3)-C(12)	1.24 (2)
O(4)-C(14)	1.29 (2)
O(5)-C(23)	1.23 (2)
O(6)-C(25)	1.29 (2)
C(1)-C(2)	1.36 (3)
C(1)-C(4)	1.51 (3)
C(2)-C(3)	1.43 (3)
C(3)-C(8)	1.50 (3)
C(4)-C(5)	1.53 (4)
C(4)-C(6)	1.52 (3)
C(4)-C(7)	1.57 (3)
C(8)-C(9)	1.49 (4)
C(8)-C(10)	1.52 (4)
C(8)-C(11)	1.50 (3)
C(12)-C(13)	1.46 (3)
C(12)-C(15)	1.49 (3)
C(13)-C(14)	1.33 (3)
C(14)-C(19)	1.54 (3)
C(15)-C(16)	1.51 (4)
C(15)-C(17)	1.50 (4)
C(19)-C(20)	1.51 (3)
C(19)-C(21)	1.54 (5)
C(19)-C(22)	1.50 (4)
C(23)-C(24)	1.36 (3)
C(23)-C(30)	1.56 (2)
C(24)-C(25)	1.37 (3)
C(25)-C(26)	1.53 (3)
C(26)-C(27)	1.44 (7)
C(26)-C(28)	1.49 (4)
C(26)-C(29)	1.53 (4)
C(30)-C(31)	1.51 (4)
C(30)-C(32)	1.53 (3)
C(30)-C(33)	1.50 (4)

Interatomic Angles	
Atoms	**Angles (Deg)**
O(1)-Y-O(2)	73.8 (4)
O(1)-Y-O(3)	128.3 (4)
O(1)-Y-O(4)	156.8 (5)
O(1)-Y-O(5)	89.7 (4)
O(1)-Y-O(6)	78.5 (5)
O(1)-Y-O(7)	80.1 (3)
O(2)-Y-O(3)	76.1 (4)
O(2)-Y-O(4)	126.1 (5)
O(2)-Y-O(5)	80.0 (3)
O(2)-Y-O(6)	142.3 (4)
O(2)-Y-O(7)	117.6 (4)
O(3)-Y-O(4)	72.7 (4)
O(3)-Y-O(5)	124.7 (4)
O(3)-Y-O(6)	141.6 (4)
O(3)-Y-O(7)	78.1 (4)
O(4)-Y-O(5)	83.2 (4)
O(4)-Y-O(6)	78.33 (5)
O(4)-Y-O(7)	97.5 (3)
O(5)-Y-O(6)	74.7 (4)
O(5)-Y-O(7)	155.5 (4)
O(6)-Y-O(7)	81.4 (3)
O(1)-C(1)-C(2)	124 (2)
O(1)-C(1)-C(4)	116 (2)
O(2)-C(3)-C(2)	122 (1)
O(2)-C(3)-C(8)	116 (2)
O(3)-C(12)-C(13)	120 (2)
O(3)-C(12)-C(15)	120 (2)
O(4)-C(14)-C(13)	126 (2)
O(4)-C(14)-C(19)	112 (2)
O(5)-C(23)-C(24)	125 (1)
O(5)-C(23)-C(30)	114 (2)
O(6)-C(25)-C(24)	122 (2)
O(6)-C(25)-C(26)	117 (1)

Fractional Coordinates

Atom	x/a	y/b	z/c
Y	0.04685 (6)	0.19150 (4)	0.31138 (4)
O(1)	-0.1429 (5)	0.1672 (3)	0.4728 (3)
O(2)	-0.1139 (5)	0.2929 (4)	0.2533 (3)
O(3)	0.0821 (4)	0.1658 (3)	0.1633 (3)
O(4)	0.2621 (4)	0.1994 (3)	0.2076 (3)
O(5)	0.0659 (5)	0.3432 (4)	0.3031 (4)
O(6)	0.1332 (5)	0.1439 (3)	0.4435 (3)
O(7)	0.0427 (6)	0.0072 (3)	0.3892 (3)
C(1)	-0.2385 (7)	0.2346 (5)	0.4912 (5)
C(2)	-0.2762 (8)	0.3176 (6)	0.4102 (7)
C(3)	-0.2183 (7)	0.3435 (5)	0.2939 (5)
C(4)	-0.3066 (13)	0.2193 (5)	0.6106 (5)
C(5)	-0.2074 (7)	0.2218 (6)	0.6511 (5)
C(6)	-0.3640 (9)	0.1130 (7)	0.6802 (5)
C(7)	-0.4228 (18)	0.3046 (7)	0.6294 (7)
C(8)	-0.2769 (9)	0.4293 (6)	0.2122 (7)
C(9)	-0.3695	0.5093 (12)	0.2503 (10)
C(10)	-0.1679 (10)	0.4919 (8)	0.1080 (9)
C(11)	-0.3344 (10)	0.3758 (9)	0.1798 (6)
C(12)	0.1694 (9)	0.1614 (5)	0.0778 (4)
C(13)	0.3027 (7)	0.1770 (4)	0.0501 (4)
C(14)	0.3372 (7)	0.1976 (5)	0.1123 (5)
C(15)	0.1395 (14)	0.1350 (5)	0.0064 (4)
C(16)	0.1295 (12)	0.0168 (9)	0.0617 (8)
C(17)	0.0116 (22)	0.1909 (14)	-0.0023 (12)
C(18)	0.2463 (12)	0.1638 (8)	-0.1103 (5)
C(19)	0.4775 (8)	0.2193 (7)	0.0779 (7)
C(20)	0.4727 (9)	0.3300 (8)	0.0632 (10)
C(21)	0.5675 (13)	0.2156 (8)	-0.0347 (7)
C(22)	0.5321 (9)	0.1420 (7)	0.1656 (6)
C(23)	0.1261 (7)	0.3705 (5)	0.3349 (4)
C(24)	0.1932 (7)	0.3035 (6)	0.4023 (5)
C(25)	0.1935 (10)	0.1954 (5)	0.4565 (5)
C(26)	0.2589 (6)	0.1312 (6)	0.5417 (5)
C(27)	0.1767 (19)	0.1476 (12)	0.6409 (9)
C(28)	0.3876 (8)	0.1675 (9)	0.5044 (9)
C(29)	0.2849 (17)	0.0151 (13)	0.5621 (13)
C(30)	0.1274 (9)	0.4926 (5)	0.2858 (6)
C(31)	-0.0134 (15)	0.5329 (8)	0.3295 (9)
C(32)	0.1714 (9)	0.5384 (6)	0.1589 (5)
C(33)	0.2142 (9)	0.5274 (7)	0.3120 (6)

trigonal antiprism, with the top represented by the (O1, O2, O3) plane, the bottom depicted by the (O4, O5, O6) plane, and the face bounded by (O1, O3, O6) being capped by O7.

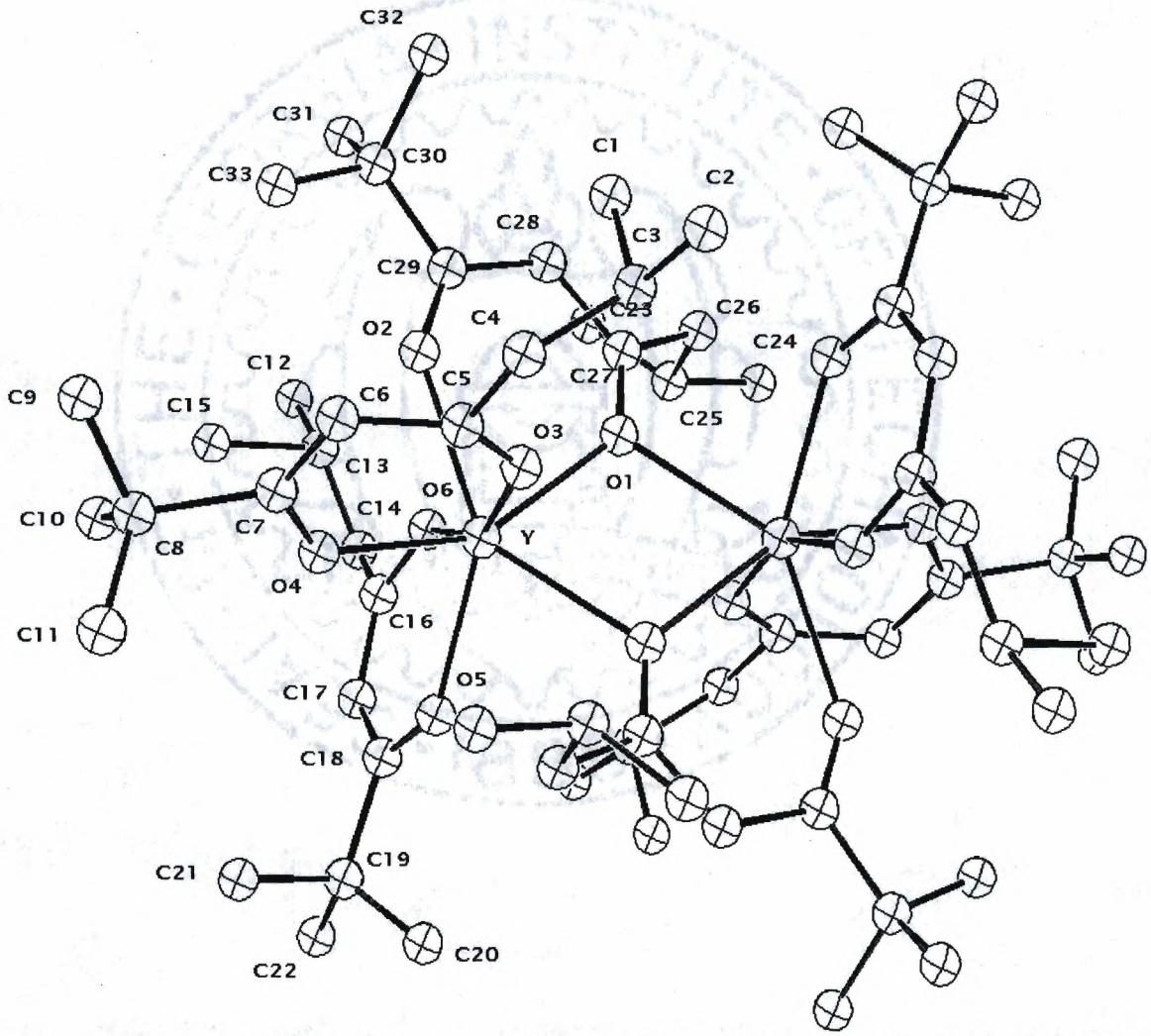

Figure 4-5a. The solid state structure of $[Y(tmod)_3]_2$ as determined by single crystal X-ray diffraction. Hydrogen atoms are omitted for clarity.

Structure of $[Y(tmod)_3]_2$. By far, the most common motif observed for the class of compounds comprising tmhd$^-$ ligation with trivalent lanthanide cations is the dimeric unit. Such moieties are known for Pr, Sm, Eu, Gd, Tb and Dy.[30] The most interesting feature of the present structure (**Figure 4-5**) is the notation of ligand bridging preference. The least sterically demanding end of the unsymmetrical β-diketonate ligand (O1) bridges the two metals, while the more sterically conjested component goes to a terminal (O2) position. Structural data is given in **Table 4-2**. With minor deviation, this is the same basic structural unit displayed by $[Pr(tmhd)_3]_2$.[32] The asymetry present in the bridging

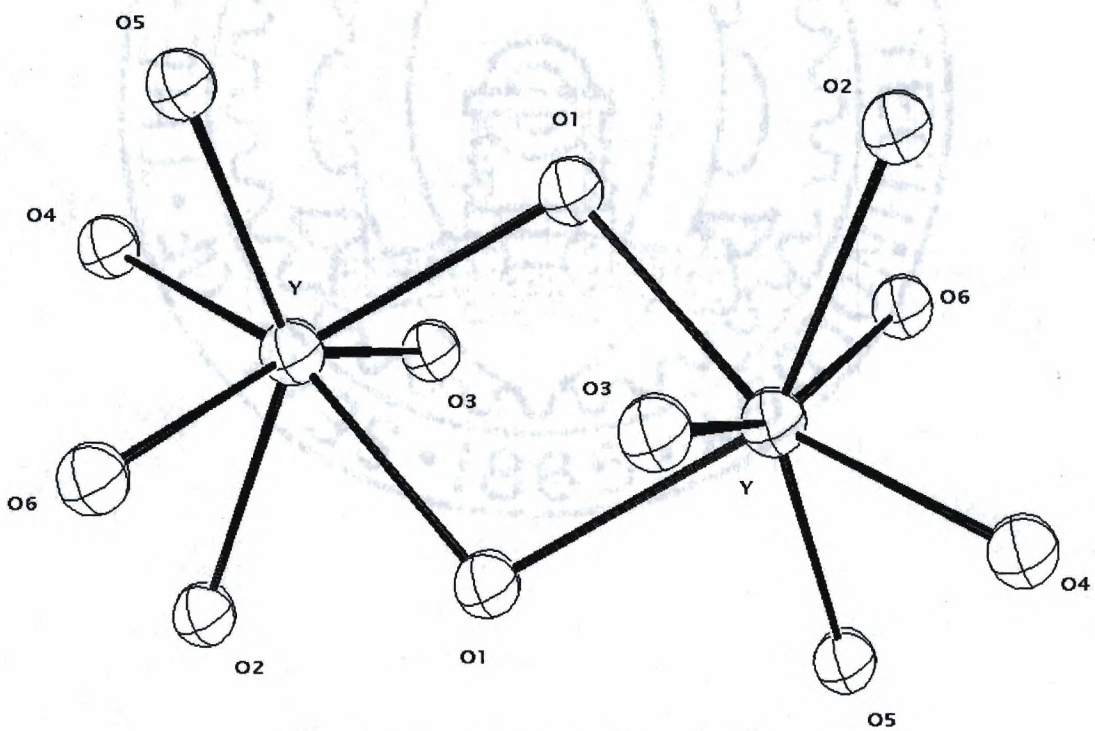

Figure 4-5b. The M_2O_{12} core of $[Y(tmod)_3]_2$.

unit is portrayed in the interatomic distances found on each side of the molecule. For the Y-O1 interaction (to the metal bound to O2 of the same ligand) a distance of 2.29 Å is found, while the Y'-O1 interaction is observed to be 2.42 Å. This increase of >5% also is evident, albeit to a lesser degree, in the $[Pr(tmhd)_3]_2$ structure. The pertinent distances for that case are 2.47 and 2.59 Å. The most striking difference, however, between the two examples is a display of apparent dimensional reversal for the Pr example. Thus, the

Table 4-2. Structural data for $[Y(tmod)_3]_2$.

Interatomic Distances		Interatomic Angles	
Atoms	Distances (Å)	Atoms	Angles (Deg)
Y-O(1)	2.29 (1)	O(1)-Y-O(1')	73.8 (3)
Y-O(2)	2.28 (1)	O(1)-Y-O(2)	74.7 (3)
Y-O(3)	2.26 (1)	O(1)-Y-O(3)	89.9 (3)
Y-O(4)	2.27 (1)	O(1)-Y-O(4)	151.9 (3)
Y-O(5)	2.23 (1)	O(1)-Y-O(5)	126.6 (3)
Y-O(6)	2.25 (1)	O(1)-Y-O(6)	81.8 (3)
Y-O'(1)	2.42 (1)	O(1')-Y-O(2)	139.6 (3)
O(1)-C(27)	1.22 (1)	O(1')-Y-O(3)	77.2 (3)
O(2)-C(29)	1.17 (1)	O(1')-Y-O(4)	123.1 (3)
O(3)-C(5)	1.25 (2)	O(1')-Y-O(5)	78.3 (3)
O(4)-C(7)	1.30 (2)	O(1')-Y-O(6)	120.2 (3)
O(5)-C(18)	1.25 (2)	O(2)-Y-O(3)	78.2 (3)
O(6)-C(16)	1.29 (2)	O(2)-Y-O(4)	79.4 (3)
C(1)-C(3)	1.46 (2)	O(2)-Y-O(5)	141.8 (3)
C(2)-C(3)	1.49 (2)	O(2)-Y-O(6)	78.9 (3)
C(3)-C(4)	1.52 (2)	O(3)-Y-O(4)	74.3 (4)
C(4)-C(5)	1.50 (2)	O(3)-Y-O(5)	126.7 (4)
C(5)-C(6)	1.42 (2)	O(3)-Y-O(6)	157.0 (4)
C(6)-C(7)	1.36 (2)	O(4)-Y-O(5)	80.9 (4)
C(7)-C(8)	1.65 (2)	O(4)-Y-O(6)	103.7 (4)
C(8)-C(9)	1.51 (2)	O(5)-Y-O(6)	74.5 (4)
C(8)-C(10)	1.48 (3)	Y-O(1)-Y'	106.3 (3)
C(8)-C(11)	1.54 (2)	O(3)-C(5)-C(4)	119 (2)
C(12)-C(13)	1.38 (4)	O(3)-C(5)-C(6)	125 (2)
C(13)-C(14)	1.38 (3)	O(4)-C(7)-C(6)	127 (2)
C(13)-C(15)	1.59 (4)	O(4)-C(7)-C(8)	107 (2)
C(14)-C(16)	1.49 (2)	O(6)-C(16)-C(14)	115 (2)
C(16)-C(17)	1.34 (2)	O(6)-C(16)-C(17)	125 (2)
C(17)-C(18)	1.40 (2)	O(5)-C(17)-C(18)	123 (1)
C(18)-C(19)	1.51 (2)	O(5)-C(18)-C(19)	117 (2)

C(19)-C(20)	1.39 (3)	O(1)-C(27)-C(26)	125 (2)
C(19)-C(21)	1.55 (3)	O(1)-C(27)-C(28)	123 (2)
C(19)-C(22)	1.52 (2)	O(2)-C(29)-C(28)	124 (1)
C(23)-C(25)	1.52 (2)	O(2)-C(29)-C(30)	121 (2)
C(24)-C(25)	1.53 (2)		
C(25)-C(26)	1.54 (2)		
C(26)-C(27)	1.47 (2)		
C(27)-C(28)	1.43 (2)		
C(28)-C(29)	1.49 (2)		
C(29)-C(30)	1.51 (2)		
C(30)-C(32)	1.55 (3)		
C(30)-C(33)	1.46 (2)		
C(30)-C(31)	1.38 (2)		

Fractional Coordinates

Atom	x/a	y/b	z/c
Y	0.4789 (1)	0.1102 (1)	0.04140 (9)
O1	0.5598 (5)	0.0430 (7)	-0.0522 (4)
O2	0.4942 (7)	0.2139 (6)	-0.0465 (5)
O3	0.3270 (7)	0.0979 (7)	-0.0204 (5)
O4	0.3766 (9)	0.2160 (7)	0.0860 (5)
O5	0.5072 (8)	0.0875 (6)	0.1605 (5)
O6	0.6392 (7)	0.1591 (7)	0.0655 (6)
C1	0.295 (2)	0.1158 (19)	-0.1918 (11)
C2	0.131 (2)	0.0383 (15)	-0.2017 (12)
C3	0.215 (1)	0.0701 (14)	-0.1518 (9)
C4	0.173 (1)	0.1234 (15)	-0.0897 (8)
C5	0.252 (1)	0.1475 (11)	-0.0319 (9)
C6	0.242 (1)	0.2328 (12)	-0.0032 (9)
C7	0.300 (1)	0.2581 (11)	0.0559 (9)
C8	0.282 (1)	0.3463 (13)	0.1046 (10)
C9	0.232 (2)	0.4089 (8)	0.0516 (12)
C10	0.384 (2)	0.3818 (19)	0.1280 (20)
C11	0.211 (2)	0.3267 (17)	0.1654 (10)
C12	0.883 (2)	0.3244 (18)	0.0445 (15)
C13	0.794 (1)	0.2792 (16)	0.0612 (12)
C14	0.795 (1)	0.2139 (15)	0.1128 (9)
C15	0.726 (2)	0.3596 (14)	0.0849 (15)
C16	0.691 (1)	0.1773 (11)	0.1244 (9)
C17	0.661 (1)	0.1576 (14)	0.1919 (8)
C18	0.569 (1)	0.1158 (13)	0.2084 (7)
C19	0.538 (1)	0.1045 (12)	0.2869 (9)
C20	0.491 (2)	0.0244 (19)	0.2951 (10)
C21	0.462 (1)	0.1779 (20)	0.3056 (13)
C22	0.626 (2)	0.1092 (17)	0.3438 (10)
C23	0.858 (1)	0.1113 (15)	-0.0972 (13)
C24	0.874 (1)	-0.0474 (14)	-0.1131 (11)
C25	0.802 (1)	0.0247 (10)	-0.0891 (10)
C26	0.699 (1)	0.0184 (12)	-0.1322 (8)

C27	0.616 (1)	0.0690 (11)	-0.1001 (7)
C28	0.609 (1)	0.1541 (11)	-0.1303 (8)
C29	0.541 (1)	0.2224 (10)	-0.1000 (8)
C30	0.542 (1)	0.3085 (11)	-0.1396 (8)
C31	0.636 (2)	0.3500 (12)	-0.1444 (14)
C32	0.498 (3)	0.3003 (14)	-0.2184 (13)
C33	0.472 (1)	0.3661 (13)	-0.1017 (13)

longer of the two interactions for Pr exists between the bridging O atom and the metal atom bound to the other end of the same ligand, while the shorter distance is seen to be for the bridging interaction to the second metal center. The structure of $[Y(tmod)_3]_2$ may be compared to $[Bi(tmhd)_3]_2$,[20] which is similiar.

Thermal Analysis. Comparative TGA plots for each of the compounds utilized in the present study are summarized in **Figure 4-6**. In general, all precursors investigated proved to be successful in transporting yttrium in the vapor phase; however, the relative merits of $[Y(tmod)_3]_2$ place it as the strongest one of the class.

Characterization of Deposited Films:

XRD. All samples examined (**Table 4-3**) either were amorphous or contained diffraction lines which could be indexed satisfactorily as Y_2O_3 (JCPDS file # 41-1105). Representative diffraction data are shown in **Figure 4-7**.

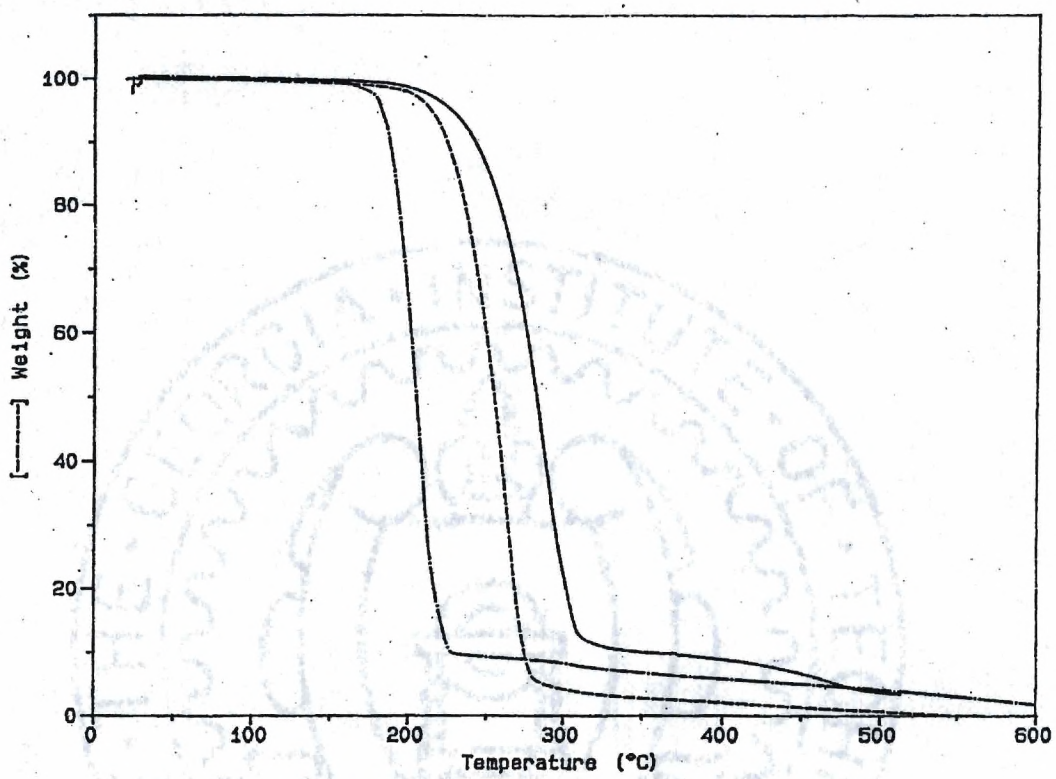

Figure 4-6. TGA traces of $Y(tmhd)_3$ [—]; $[Y(tmod)_3]_2$ [----]; and $[Y(tmhd)_3H_2O]_2$ [—].

Table 4-3. Relative crystallinity of the deposited films as determined by X-ray diffraction.

	$[Y(tmhd)_3 \cdot H_2O]_2$ Precursor
Deposition Atmosphere	**Crystallinity of Film**
N_2	Amorphous Yttrium
N_2 / H_2O	Amorphous Yttrium
O_2	Crystalline Yttria
O_2 / H_2O	Crystalline Yttria
H_2	Amorphous Yttrium
H_2 / H_2O	Amorphous Yttrium

$[Y(tmod)_3]_2$ Precursor

Deposition Atmosphere	Crystallinity of Film
N_2	Amorphous Yttrium
N_2 / H_2O	Amorphous Yttrium
O_2	Amorphous Yttria
O_2 / H_2O	Amorphous Yttria
H_2	Amorphous Yttrium
H_2 / H_2O	Amorphous Yttrium

$Y(tmhd)_3$ Precursor

Deposition Atmosphere	Crystallinity of Film
N_2	Amorphous Yttrium
N_2 / H_2O	Amorphous Yttrium
O_2	Crystalline Yttria
H_2	Amorphous Yttrium

ESCA. The data (**Figure 4-8**) indicate that the films for the present investigation fall into two groups: those containing approximately 1.5 oxygen atoms per yttrium atom, and those containing none or almost none. The former group comprises those films deposited under oxygen, either hydrous or anhydrous, whereas the latter group consists of all other thin film growth runs.

SEM. The data in **Figure 4-9** indicate two predominate growth modes. Surface nucleation and growth, without evidence for migration, is displayed for the case of b, c, d, I and j. Contrasting this mechanism, a, e, f, g, k, m and p appear to have a fairly dense, smooth structure. This presumably is due to the presence of a high kinetic term for surface mobility.

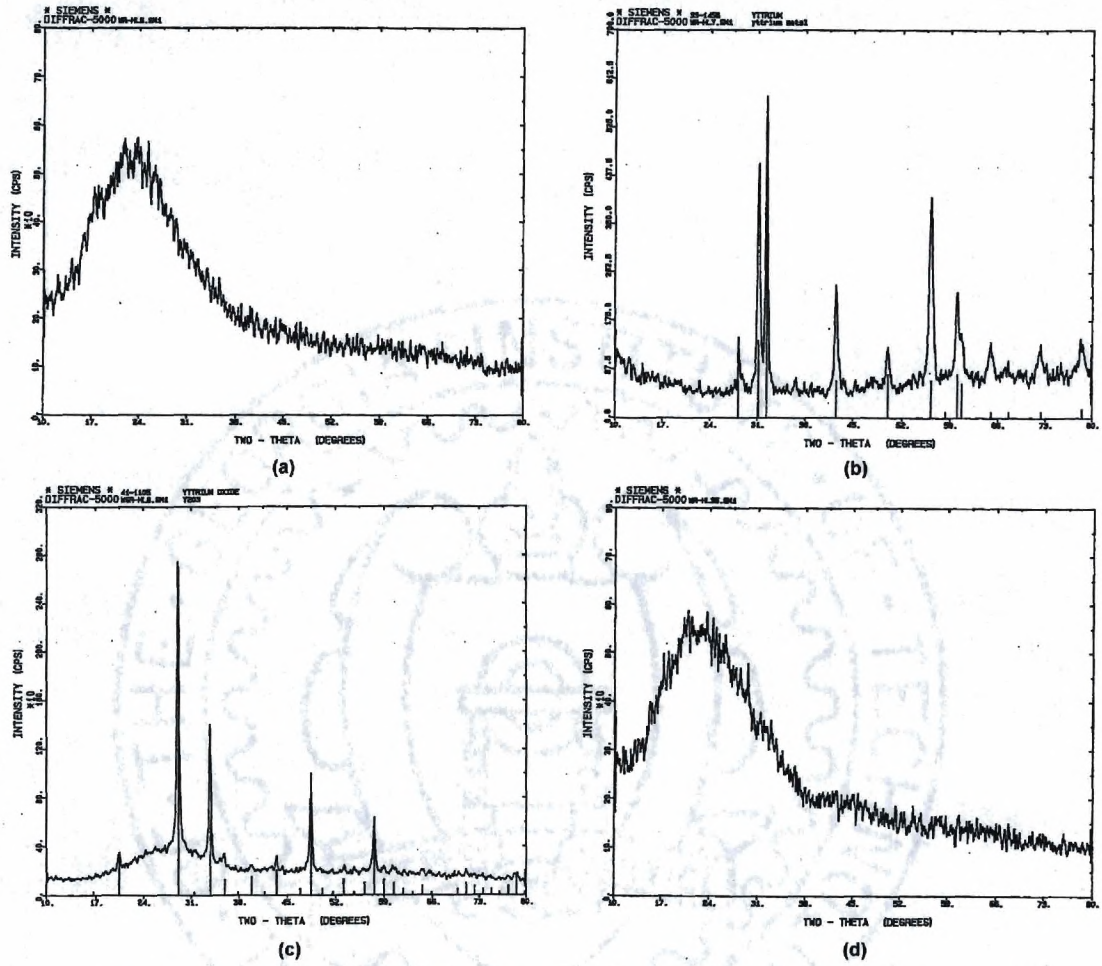

Figure 4-7. Representative x-ray diffraction patterns: (a) clean substrate, (b) crystalline yttrium standard, (c) crystalline Y_2O_3, (d) amorphous yttrium.

Profilometry. The data (**Figure 4-10**) support the conclusions reached based on SEM photomicrographs. In certain instances, the surface roughness is less than 0.2 kÅ, a good value for such compositions.

$[Y(tmod)_3]_2$ Precursor:

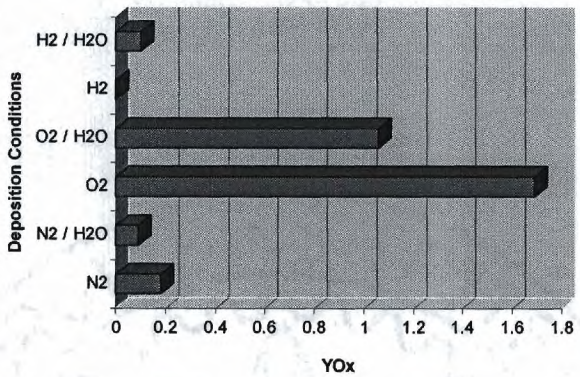

$[Y(tmhd)_3 \cdot H_2O]_2$ Precursor:

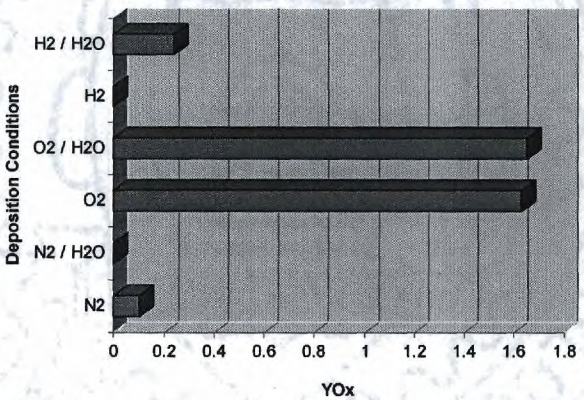

$Y(tmhd)_3$ Precursor:

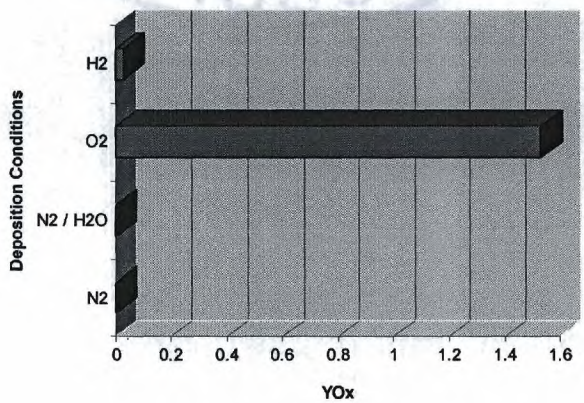

Figure 4-8. Film Y:O stoichiometry data based on ESCA analysis, expressed as YO_x.

Discussion

The Role of Water. As a consequence of its intrinsic nature, CVD concerns itself with compounds in the vapor phase. Nevertheless, with minor exceptions, the vapor phase structures of precursor compounds remain unelucidated. A rare opportunity presents itself for $Y(tmhd)_3$ in that vapor phase data (**Figure 4-3**) are available for comparison with solid state information. It is the latter of these which is obtained most often and many vapor phase correlations have been attempted from extrapolation of such structural data. Although frequently considered an "innocent," or a "spectator" ligand, the occupant of the seventh coordination site in $[Y(tmhd)_3 \cdot H_2O]_2$ does play a role in the chemistry of this CVD precursor.

The intermolecular hydrogen bonds present in the structure of $[Y(tmhd)_3 \cdot H_2O]_2$ contribute significantly to the heat of vaporization for this compound. Additionally, as seen in the TGA data (**Figure 4-6**), the vapor phase transport of the two species $\{[Y(tmhd)_3 \cdot H_2O]_2$ and $Y(tmhd)_3\}$ differ. Thus, although it would appear from ESCA data that water has no significant role in film composition, clearly solid state reactions involving it as a ligand would implicate its "guilt" as a source of vapor pressure reduction, and earn a word of caution to avoid its presence in rigorous precursor preparations and purifications. Lastly, the role of water in surface mophology is noteworthy (**Figure 4-10**). Comparable results have been observed for $Cu(tmhd)_2$ and $Cu(acac)_2$ in a previous investigation.[22]

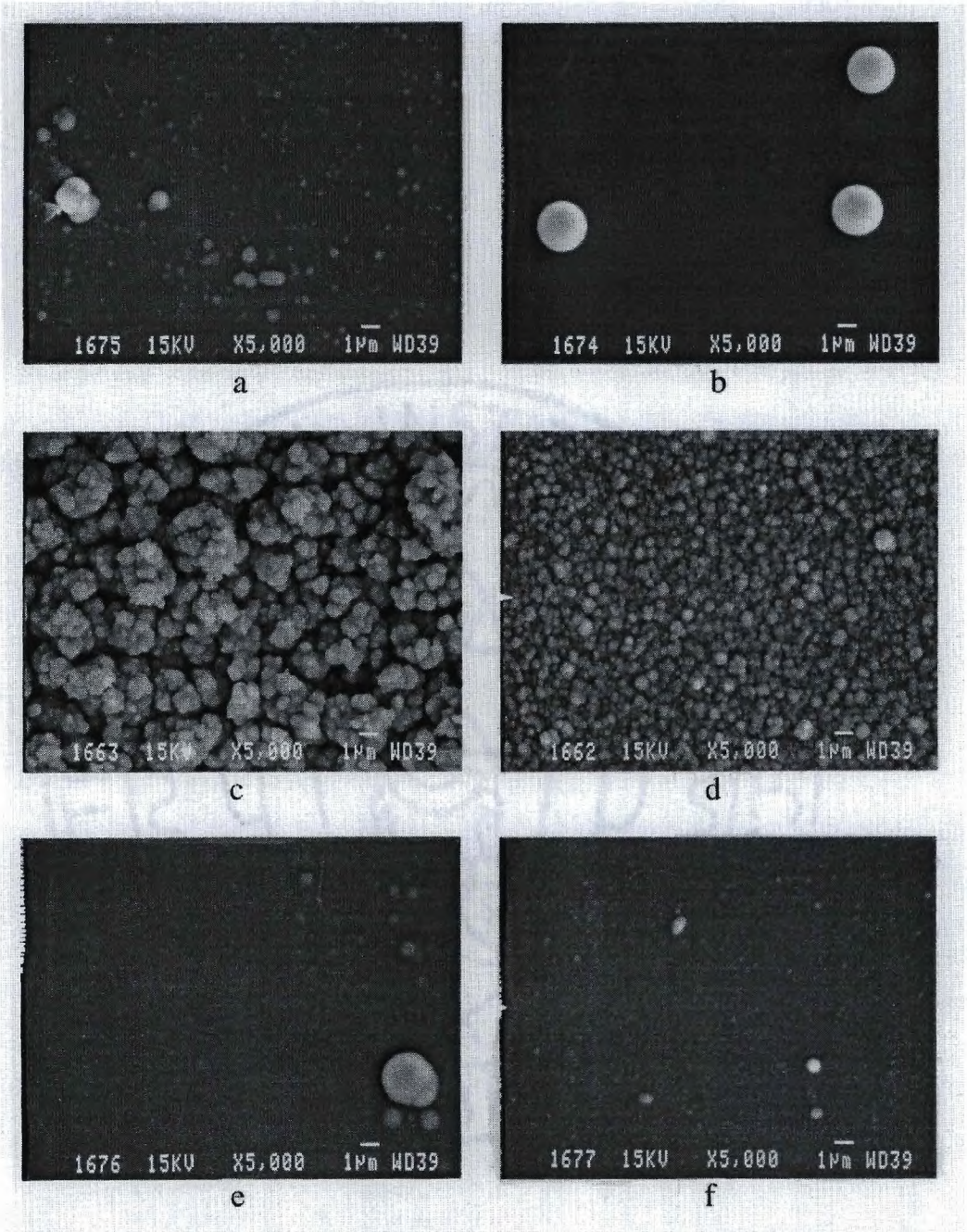

Figure 9a. SEM micrographs of the deposited thin films. Key: a) - f) are films grown from the $[Y(tmod)_3]_2$ precursor under the following growth conditions: a) N_2, b) N_2 / H_2O, c) O_2, d) O_2 / H_2O, e) H_2, f) H_2 / H_2O.

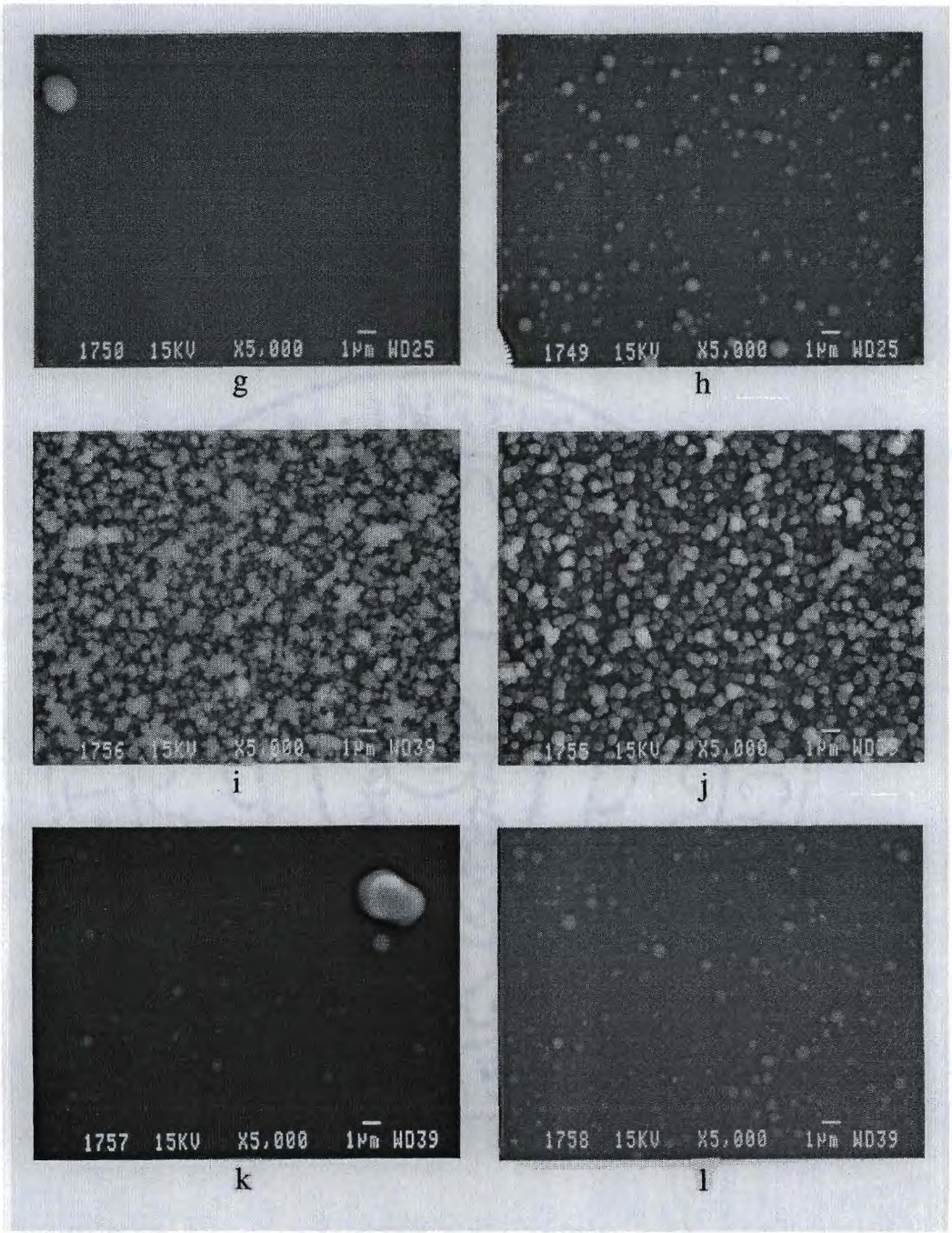

Figure 9b. SEM micrographs of the deposited thin films. Key: g) - l) are films grown from the $[Y(tmhd)_3 \cdot H_20]_2$ precursor under the following growth conditions: g) N_2, h) N_2 / H_2O, i) O_2, j) O_2 / H_2O, k) H_2, l) H_2 / H_2O.

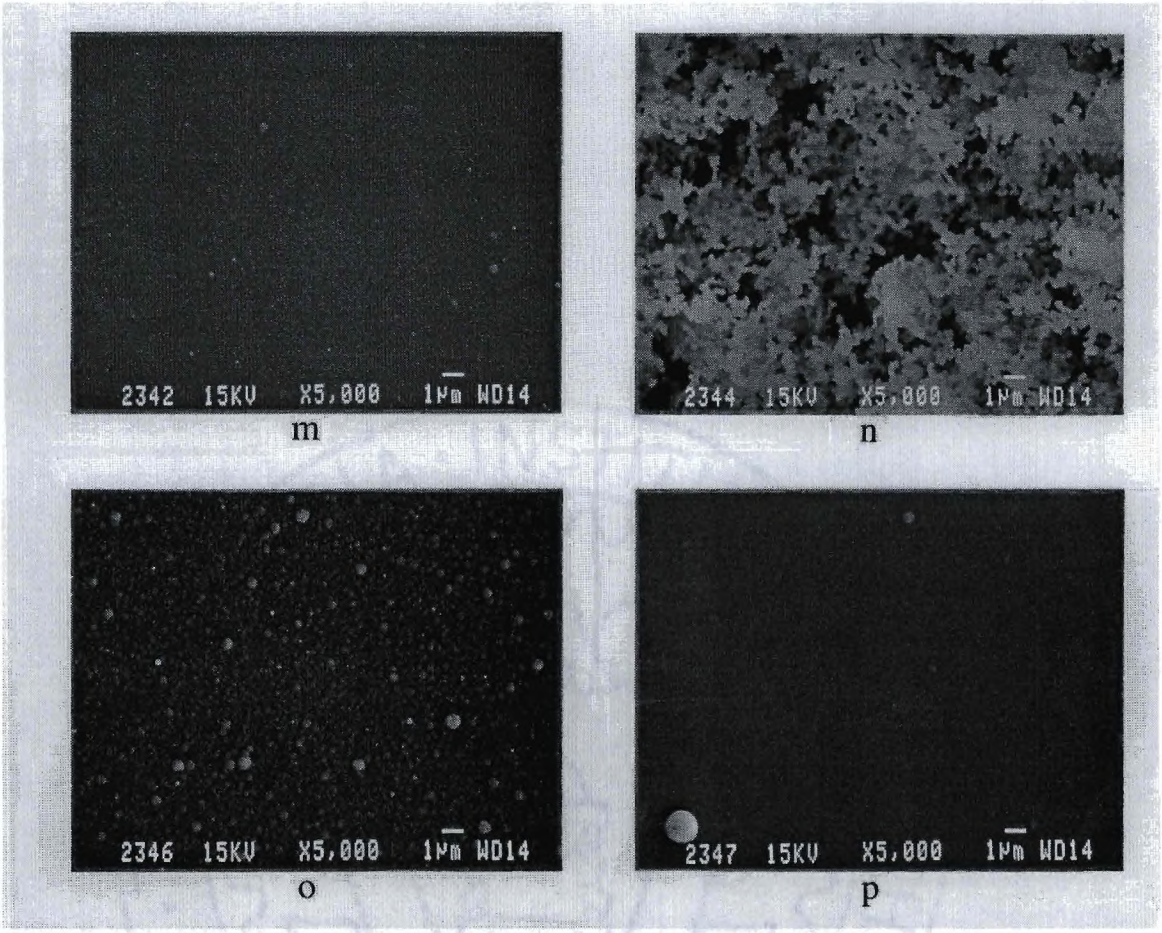

Figure 9c. SEM micrographs of the deposited thin films. Key: m) - p) are films grown from $Y(tmhd)_3$ under the following conditions: m) N_2, n) O_2, o) N_2 / H_2O, p) H_2.

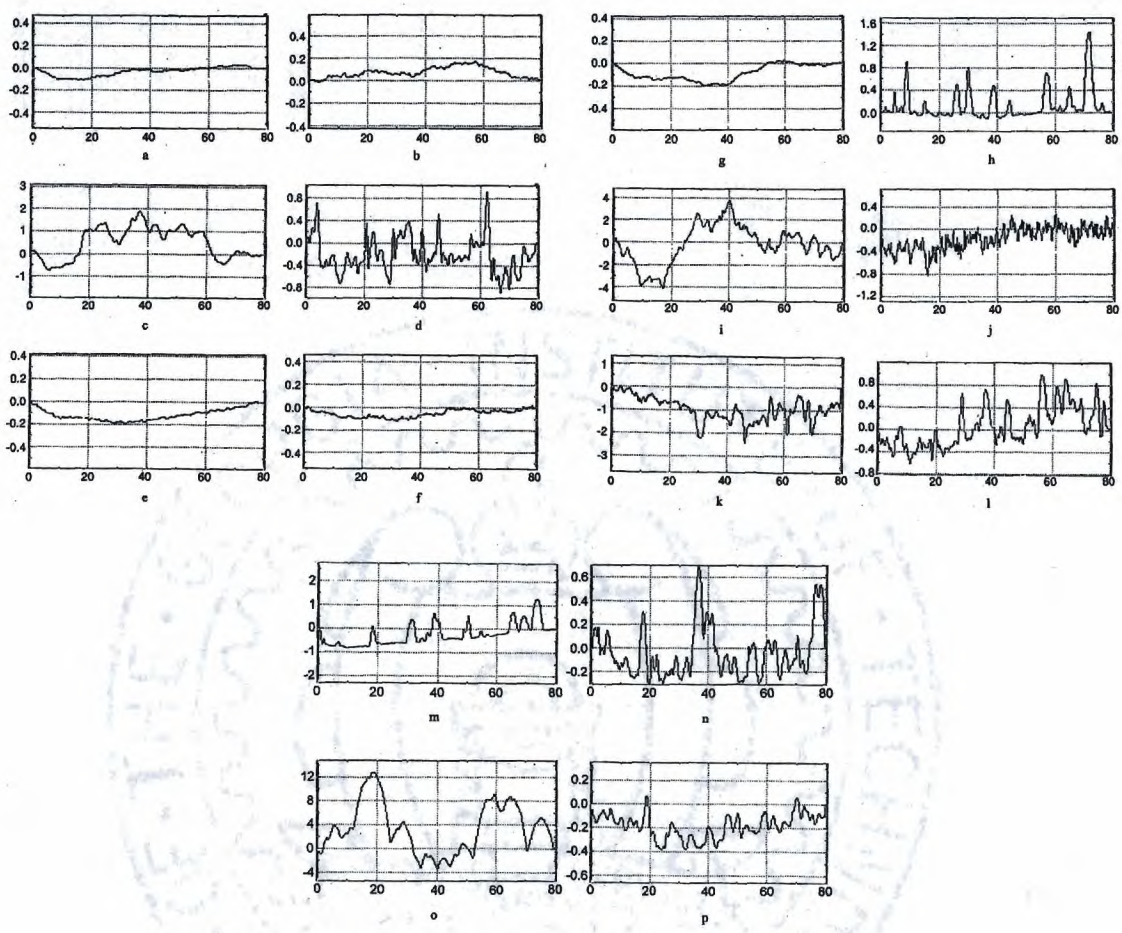

Figure 4-10. Surface profilometry traces of the deposited thin films; horizontal scale in μm and vertical scale in Å•10^3. Key: a) - f) are films grown from the $[Y(tmod)_3]_2$ precursor under the following growth conditions: a) N_2, b) N_2 / H_2O, c) O_2, d) O_2 / H_2O, e) H_2, f) H_2 / H_2O. g) - l) are films grown from the $[Y(tmhd)_3•H_2O]_2$ precursor under the following conditions: g) N_2, h) N_2 / H_2O, i) O_2, j) O_2 / H_2O, k) H_2, l) H_2 / H_2O. m) - p) are films grown from $Y(tmhd)_3$ under the following conditions: m) N_2, n) N_2 / H_2O, o) O_2, p) H_2.

Structural Control: Monomer vs. Dimer. As mentioned above, the ionic radius of the metal center appears to be a governing variable in this matter. This dependence is demonstrated in the following series of compounds: $Er(tmhd)_3$,[31] $Dy(tmhd)_3•H_2O$[33] and $[Pr(tmhd)_3]_2$.[32] The ionic radii of these three trivalent cations are

0.88 Å, 0.91 Å and 1.01 Å, respectively.[47] As the metal ion becomes larger, the β-diketonate ligands are spread out farther, making more space available for a ligand to fill a seventh coordination site. Erbium, being the smallest, is too sterically crowded to allow another ligand to coordinate. Dysprosium is slightly larger, generating sufficient space for a small ligand, H_2O, to coordinate. Praseodinium, the largest of this series, has enough uncovered surface area to permit a carbonyl oxygen from the β-diketonate ligand of a neighboring complex to coordinate by bridging the two metal centers. This bridging interaction is congested sterically, however it is favored over hydration, due to the increased charge density of the anionic β-diketonate ligand. On this basis, the present inability to hydrate $[Y(tmod)_3]_2$ may be explained. Steric crowding around the metal center is reduced in this instance not by changing the ionic radius of the metal, but by modification of the spatial requirements of the ligand. This slight lessening in the steric size of the *iso*-butyl end of the tmod$^-$ ligand, relative to a *tert*-butyl group, not only reduces the crowding around the metal center, but also reduces the steric congestion involved in the bridging interaction. The net effect is that dimerization is favored over hydration. It is interesting to note that the bridges, while favored, are strained. This is displayed by the long bridging Y-O interatomic distance of 2.42Å, as compared to an average of 2.26 Å for the non-bridging interactions. This strain developed with the tmod$^-$ ligand also would explain why $Y(tmhd)_3$, with its larger ligand, does not form dimers in the absence of H_2O.

Additional insight may be gleened on the topic of choice of bridging end for an unsymmetrical β-diketonate ligand by comparison of the partial charge present on each oxygen (**Figure 4-11**). An electrostatic based model would predict that the largest residual negative charge would prefer to reside between two positively charged metal locations. For tmhd$^-$, each oxygen has a partial charge of -0.377 (e); whereas, for tmod$^-$, the *i*-Bu end has a partial charge of -0.374 (e) versus a charge of -0.368 for the -*t*Bu end (Based on ZINDO single point calculations). This confirms the choice for bridging position to be based both on steric and electronic effects in the present case.

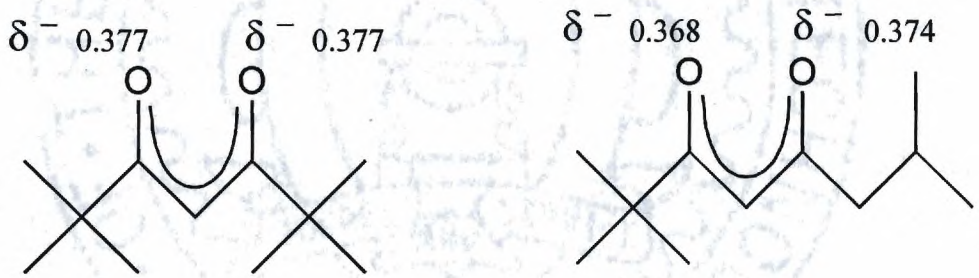

Figure 4-11. Partial charges present at the oxygen atoms of the two β-diketonate ligands.

^{13}C {^{1}H} NMR. Two signals are observed for each of the proton-decoupled carbon resonances of $[Y(tmod)_3]_2$ in its solution NMR in C_6D_6. These signals are products of the different chemical environments of the terminal and bridging ligands. The relative intensities of these signals are in agreement with the two to one relationship of the terminal to bridging ligands of the dimer observed for this compound in the solid state.

MS. A ligand pruning and expulsion mechanism is apparent from the data available (**Scheme 4-1**). In such a transformation, the primary step is the pruning of the terminal *t*-Bu groups from the β-diketonate ligands, followed by expulsion of the C_3HO_2 unit. This is consistent with data recently obtained by another research effort.[49]

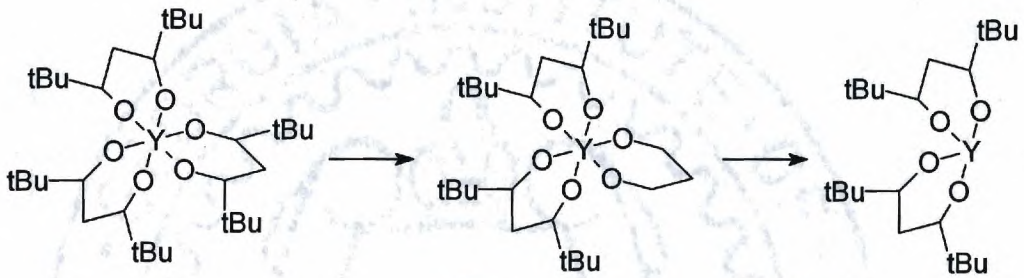

Scheme 4-1

ESCA. This clearly indicates the initial deposition of yttrium and its subsequent oxidation to Y_2O_3, under certain conditions. The observation of the deposition of oxygen-free yttrium under an inert growth ambient is noteworthy. In general, previous workers had assumed that highly electropositive metals would not behave in this manner. In light of the present results, it may be possible to understand the growth of MS from $M(tmhd)_2$ (M = Ca, Sr) in an ambient of H_2S. It would seem consistent with the data that this process is a two step sequence, with the initial deposition of M°, subsequently followed by sulfurization of the element to MS.[50] To our knowledge, no previous reports present data to support the notion that oxygen-free electropositive metals can be deposited from metal β-diketonate precursors. The extent of this finding is undergoing

examination in our laboratories. This observation is consistent with the mechanism proposed (**Scheme 4-1**) and parallels that observed for copper by this research group,[21] and reconfirmed by independent work.[51]

TGA. The basic information is contained in **Figure 4-6**. As is evidenced by the differing weight loss profiles for each of the hydrous and anhydrous samples for an invarient ligand set, the water of hydration is retained under these transport measurment conditions.

The Role of Ligand Symmetry in Vapor Pressure Control. The correlation between dipole moment, intermolecular forces and vapor pressure is well documented. In creating ligands of low symmetry, one needs to be aware of this constraint and steer toward the induction of low molecular dipole moment. Likewise, the vapor pressure correlation of branching ratio in hydrocarbons equally is documented abundantly. A delicate balance must be achieved here in order to induce weak solid state molecular packing, by disruption of symmetry due to entanglement, without generating high molecular weights. Several examples of this motif exist. For example, Meinema *et al.* have stabilized monomeric $Y(tmhd)_3$ through the use of a neutral Lewis base to form $Y(tmhd)_3$•4-*t*Bu-PyNO, which sublimes intact and shows a marked improvement in vapor pressure over $[Y(tmhd)_3•H_2O]_2$.[52] Marks has lowered the melting point and enhanced the vapor pressure of $Ba(hfac)_2$•L compounds by relying on asymmetry in the oligodentate ether ligand.[53] Also, the vapor pressure of barium compounds containing unsymmetrical fluorinated β-diketonate ligands, in addition to oligodentate ethers, substantially is higher than the comparable examples for symmetrical ligands.[54]

Conclusions

The role of ligand symmetry in some yttrium *tris*(β-diketonate) complexes has been examined. This factor influences both the observed solid state structures and, indirectly, the relative vapor pressures of the resultant compounds. An exploration of the role of carrier gas on the CVD deposits from these species has shown that it is a primary thermal decomposition product to yield yttrium metal, and a subsequent oxidation produces yttria. From mass spectral data, a ligand pruning and expulsion mechanism is proposed as the primary mode of decomposition. An excellent review of CVD of some superconducting materials from one of the leading laboratories in this area can be found in reference 55.

Experimental Section

General Information. All gases (Air Products) were of high (99.999 %) purity and used without further purification. All solvents were reagent grade, available from commercial suppliers, and purified by standard literature techniques. Dimethoxyethane (Fisher Chemical Co.) was twice distilled: first from sodium, and second from sodium/potassium alloy under N_2. Pinacolone (Aldrich Chemical Co.) was distilled, and trimethyl acetic acid and isovaleric acid (Aldrich Chemical Co.) were analysed by GC-MS and ^{1}H-NMR and used as received. Distilled H_2O was obtained from an in-house system. Sodium hydride (Aldrich Chemical Co., 60 % w/w in mineral oil) was washed with 6 x 75 ml of hexane per 25 g of dispersion, dried under vacuum, and stored under an inert atmosphere. Reagant grade NaOH, anhydrous Na_2SO_4 and $MgSO_4$ (Fisher Chemical Co.) were used as received. All deuterated solvents (Cambridge Isotope

Laboratories, Inc.) were stored over 4 Å molecular sieves and used without further purification. Carbon tetrachloride (Fisher Chemical Co.) was distilled and stored over 4 Å molecular sieves. IR spectra were obtained in solution cells with NaCl windows in CCl_4 (*vs.* CCl_4) on a Perkin Elmer 983 spectrometer and are reported in cm^{-1}. UV/VIS spectra were taken as hexane solutions (*vs.* hexane) in 1 cm quartz cells on a Cary-14 Conversion, On Line Instruments Systems, Inc. spectrometer and are reported in nm. Gas chromatographs/mass spectra were obtained with a Hewlet-Packard GC 5890 Series II equipped with a split-flow injected, 12 m x 0.2 mm, cross-linked, polydimethylsiloxane gum, capillary column interfaced to a Hewlet-Packard MS 5971 A mass spectrometer under a He gas flow with a 70 eV EI ion source and are reported as m/e^+. ^1H NMR (300 MHz) and $^{13}C\{^1H\}$ NMR (75 MHz) spectra were recorded on a Varian Gemini-300 spectrometer and processed on a Sun 4/110 data station using vxr-5000 software. Chemical shifts are reported in ppm on a + δ scale upfield with resonances from the NMR solvents serving as internal standards for the ^1H (residual $CHCl_3$ in $CDCl_3$ δ = 7.24 ppm) and ^{13}C ($CDCl_3$ δ = 77.0 ppm) spectra. Thermogravimetric analyses were recorded on a Dupont Systems' TA Instruments 951 thermogravimetric analyzer with a N_2 purge rate of 10 sccm and were processed using Thermal Analyst 2100 System software. Melting points were measured on a Mel-Temp II apparatus with a J type thermocouple using a Fluke 51 K/J digital thermometer in open topped capillary tubes and are uncorrected. Chemical vapor deposition was performed in a Lindberg model 55035 tube furnace with a 20 mm I.D. quartz tube using a Lindberg 847 digital temperature

controller. The temperature zones were mapped out with a Cole Parmer Digi-Sense digital thermometer with a type K thermocouple. Gas flows were measured with size 2 and 3 Manostat mass flow controllers, utilizing glass beads, uncorrected for viscosity, and calibrated for temperature. Surface profilometry traces were obtained on a Tencor Instruments Alpha-Step 200 profilometer with a stylus pressure of 25 mg and a scan speed of 10 μm/sec over a distance of 300 μm. Scanning electron micrographs were acquired on a JEOL SEM and deposit compositions were determined with a Perkin Elmer PHI-5100 ESCA system. ESCA samples were surface cleaned by argon sputtering with a Perkin Elmer Model 04-303A differential ion gun. X-ray diffraction data were obtained with a Siemens Diffrac-5000 automated powder diffraction system interfaced with vendor-supplied JCPDS peak search and match software. Partial charges were calculated on a Silicon Graphics Indigo-2 data station utilizing the Biosym Discover3 package with ESFF forcefields.

Preparations:

2,2,6,6-tetramethylheptane-3,5-dione (Htmhd). This is a modification of the method of Adams *et al.* involving a change in the order of reactant addition.[43] Under $N_{2(g)}$, 11.0 g (0.46 mol) of NaH and 400 ml of DME were added to a 1 liter, three-necked, round-bottomed flask. The flask was equipped with a reflux condenser, an over-head shaft paddle stirrer, and a pressure equalizing delivery funnel charged with 15.7 g (0.157 mol) of pinacolone and 44.6 g (0.343 mol) of ethyl pivalate diluted with 30 ml of DME. The flask was heated to the reflux temperature and the contents of the addition funnel were added drop-wise (at 1 drop/sec.). Upon completion of the addition, the solution was

allowed to reflux for an additional 7 hours. The reaction mixture was cooled to 0°C then 50 ml of 12 **M** HCl was added slowly with rapid stirring, followed by addition of 100 ml of H_2O and 100 ml of pentane. The resulting mixture was warmed to ambient temperature and allowed to stir for 0.5 hour. The solution was transferred to a 1 liter separatory funnel. The organic layer was washed with 3 x 75 ml aliquots of H_2O, dried over anhydrous $MgSO_4$ for 12 hours, gravity filtered, and distilled at 6 torr. The fraction collected at 72 - 73°C was identified as pure (GC/MS), authentic Htmhd. Yield: 22.8 g (0.124 mol), 90% based on pinacolone. **Characterization Data:** ^{1}**H NMR:** 5.70 [s, 2H, CH_2], 1.24 [s, 18H, CH_3]. ^{13}**C{**^{1}**H} NMR:** 201.9 [CO], 90.7 [CH_2], 39.3 [ipso C], 27.2 [CH_3]. **MS:** {(fragment); LH = Htmhd} 184(LH), 169(LH - CH_3), 127(LH - *t*Bu), 111(LH - *t*Bu - O), 97(*t*Bu-CO-C), 85(*t*Bu-CO), 69(*t*Bu-C), 57(*t*Bu). **solution IR:** (4000 - 400 cm^{-1}, in CCl_4 *vs.* CCl_4 reference, NaCl plates) 2960 (vs) [CH], 1685 (vs, sh), 1600 (vs) [CO], 1460 (s) [CH], 1440 (s), 1350 (s, sh) [CH_3], 1275 (m) [CCH_3], 1210 (m, sh), 1190 (m, sh), 1120 (m) [$CHCCH_3$], 940 (w) [CH_3], 860 (m, sh) [CCCO]. **UV/VIS:** (750 - 200 nm, hexane *vs.* hexane reference) λ_{max} = 275.4, c = 2.22 x 10^{-5} **M**, ε = 1.01 x 10^4 M^{-1} cm^{-1}.

2,2,7-trimethyloctane-3,5-dione (Htmod). This compound was prepared in a manner identical to that described above for Htmhd, substituting ethyl isovalerate for ethyl pivalate and was distilled at 44°C and 0.2mm Hg. This is the 'inverse' of the Sievers *et al.* preparation.[44] Yield: 39.34 g (0.213), 93% based on pinacolone. **Characterization Data:** ^{1}**H NMR:** 5.54 [s, 1H, CH], 2.12 [d, 2H, CH_2], 2.06 [t, 1H,

CH], 1.13 [s, 9H, CH_3], 0.91 [d, 6H, CH_3]. **$^{13}C\{^1H\}$ NMR:** 201.5 [*t*Bu-CO], 194.4 [*i*Bu-CO], 95.8 [**C**$(CO)_2$], 47.6 [CH_2], 39.0 [ipso C], 27.0 [$(\mathbf{C}H_3)_3C$], 26.0 [CH], 22.2 [$(\mathbf{C}H_3)_2CH$]. **MS:** {(fragment); LH = Htmod} 184(LH), 169(LH - CH_3), 156(LH - C_2H_4), 141(LH - *i*Pr), 127(LH - Bu), 111(LH - Bu - O), 97(Bu-CO-C), 85(Bu-CO), 71(Pr-CO), 57(Bu), 43(Pr). **solution IR:** 2964(vs), 2932(s), 2904(m), 2868(m), 1598(vs, br), 1568(vs), 1544(s), 1528(m), 1524(m), 1520(m), 1510(m), 1496(m), 1488(m), 1472(m), 1458(s), 1424(m), 1360(m), 1218(m). **UV/VIS:** λ_{max} = 275, c = 3.26 x 10^{-4} **M**, ε = 9.48 x 10^3 $\mathbf{M}^{-1}$ cm^{-1}.

$Y(NO_3)_3 \cdot 3.35\ H_2O$. Caution: This reaction is rather exothermic. The yttrium oxide must be added slowly in order to maintain a controllable reaction rate.

To a 400 ml beaker containing 188 ml of 6 **M** nitric acid and a magnetic stirring bar, 50 g (0.22 mol) of 99.9 % Y_2O_3 (Strem Chemicals) was added over a 30 minute period. Once the addition was complete, the beaker was covered with a watch glass and heated on a steam bath until all of the solid was dissolved. At this point, the watch glass was removed and the solution was concentrated by evaporation on a steam bath at ambient pressure to 100 ml. Upon cooling, a mass of white solid precipitated.

The solid was collected by suction filtration on a coarse porosity fritted glass disk and transferred to a clean 400 ml beaker and dissolved in a minimum amount of 1 **M** HNO_3. This solution again was concentrated as above to 100 ml. The beaker was placed in an ice/water bath and with constant manual stirring a white solid began to precipitate. Before the solid hardened, it was collected by vacuum filtration on a coarse porosity frit.

The highly hydrated solid was dried for two days in a desiccator over concentrated H_2SO_4. The reaction afforded 80 g (0.24 mol) of $Y(NO_3)_3 \cdot 3.35\ H_2O$, 55 % yield based on Y_2O_3. The degree of hydration was determined by the product's TGA trace.

Diyttrium hexakis(2,2,6,6-tetrametylheptane-3,5-dionate) dihydrate [{Y(tmhd)$_3$ •H$_2$O}$_2$]. To a 1 l Erlenmyer flask containing a magnetic stir bar, 115 g (0.62 mol) of Htmhd and 400 ml of 95% ethanol, 25 g (0.62 mol) of NaOH in 100 ml of H_2O were added over 30 minutes with rapid stirring. A solution of 80 g (0.24 mol) of $Y(NO_3)_3 \cdot 3.35\ H_2O$ dissolved in 125 ml of H_2O then was added dropwise. Upon this addition, a white precipitate formed immediately. After stirring for 12 hours, the majority of the ethanol was removed by rotary evaporation. To the remaining solution 500 ml of H_2O were added and it again was allowed to stir for 12 hours. The white/yellow solid that precipitated was collected on a suction frit and air dried for 3 hours. The solid was ground to a powder with a mortar and pestle and placed in a desiccator at ambient temperature and 10^{-3} mm Hg for 24 hours. The semi-dry solid was dissolved in hexane and dried over Na_2SO_4 for 24 hours. The pale yellow solution was gravity filtered and the filtrate was evaporated to dryness on a rotary evaporator. The resulting white powder was recrystallized from hexane. The white needle-like crystals were collected on a suction frit and allowed to air dry. A second crop of crystals was harvested from the mother liquor by further concentration on a rotary evaporator to one-fourth the initial volume. The combined solids again were ground to a powder and placed in a round-bottomed flask. The flask was evacuated to 0.01 mm Hg and heated at 110°C for 7 hours to remove all of the hexane and any remaining Htmhd. Yield: 105 g (0.16 mol) of

$[Y(tmhd)_3 \cdot H_2O]_2$, 77% based on Htmhd. **Characterization Data:** mp 170.9°C. **MW:** (benzene cryoscopy) obs. 607 g/mol (cal. monomer: 657 g/mol). **MS:** {(fragment); L = tmhd, M = parent ion-H_2O} 638(M), 623(M-Me), 581(M-*t*Bu), 455(M-L), 313(YLC_2HO), 184(LH), 146(Y*t*Bu), 127(LH-*t*Bu), 57(*t*Bu), 42(*t*Bu-Me). **^{1}H NMR:** 5.71 [s, 1H], 1.16 [s, 18H]. **^{13}C{^{1}H} NMR:** 201.7 [CO], 91.7 [CH], 40.5 [*ipso* C], 27.9 [CH_3]. **solution IR:** 2960, 1590, 1570, 1550, 1500, 1445, 1400, 1355. **UV/VIS:** λ_{max} = 275, c = 2 x 10^{-5} **M**, ε = 4.02 x 10^4 M^{-1} cm^{-1}. **TGA:** (**Figure 4-6**).

Yttrium tris(2,2,6,6-tetrametylheptane-3,5-dionate) [Y(tmhd)$_3$]. A sublimator equipped with a dry-ice cold finger was charged with 3.0 g (0.0046 mol) of $[Y(tmhd)_3 \cdot H_2O]_2$. After evacuation to 5 x 10^{-5} torr, the sublimator was heated to 187°C, the cold finger was cooled to -78°C and the $Y(tmhd)_3$ was allowed to sublime for 70 minutes. The white solid was scraped off the cold finger in an inert atmosphere glove box to yield, 2.75 g (0.0043 mol), 93%, of $Y(tmhd)_3$, based on the initial charge of $[Y(tmhd)_3 \cdot H_2O]_2$. **Characterization Data:** mp 168.4°C. **MW:** (benzene cryoscopy) obs. 661 g/mol (cal. monomer: 639 g/mol). **TGA:** (**Figure 4-6**).

Diyttrium hexakis(2,2,7-trimethyloctane-3,5-dionate) [{Y(tmod)$_3$}$_2$]. To a 250 ml Erlenmeyer flask containing a magnetic stirring bar, 10 g (0.054 mol) of Htmod and 40 ml of 95% ethanol, 3.1 g (0.055 mol) of KOH in 9.0 ml of H_2O were added slowly with rapid stirring. A solution of 6.93 g (0.0181 mol) of $Y(NO_3)_3 \cdot 3.35\ H_2O$ dissolved in 33 ml of H_2O was added dropwise. Upon addition of this solution a white precipitate formed immediately. The mixture was allowed to stir for 12 hours and then

approximately 90% of the ethanol was removed by rotary evaporation. To the remaining solution, 50 ml of H_2O were added and the mixture was again allowed to stir for 12 hours. The impure $[Y(tmod)_3]_2$ was collected by gravity filtration and allowed to air dry. The resultant white solid was dissolved in hexane, dried over anhydrous Na_2SO_4 for 24 hours, gravity filtered, and the filtrate was evaporated to dryness yielding a white powder which was recrystallized from hexane to yield 7.7 g (0.006 mol, 66%) of enhanced purity $[Y(tmod)_3]_2$. A sublimator equipped with a dry ice cold finger was charged with 7.7 g (0.006 moles) of the recrystallized $[Y(tmod)_3]_2$. A thin layer of glass wool was placed on top of the white powder. After evacuation to 1 x 10^{-5} mm Hg, the sublimator was heated to 180°C, the cold finger was cooled to -78°C, and the intermediate purity $[Y(tmod)_3]_2$ was allowed to sublime for 2 hours as the temperature was slowly increased to 245°C. The white solid was scraped off the cold finger to yield 6.8 g (0.005 mol, 89%), of purified $[Y(tmod)_3]_2$, based on the initial charge of recrystallized $[Y(tmod)_3]_2$. **Characterization Data:** mp 185.8°C. **MW:** (benzene cryoscopy) obs. 1,126 g/mol (calc. dimer: 1,277 g/mol). **MS:** {(fragment); L = tmod, M = monomer parent ion} 638(M), 581(M-Bu), 455(M-L), 281($YO_4C_{10}H_8$), 207($YO_4C_4H_6$), 191($YO_3C_4H_6$), 127(L-Bu), 96($C_6H_8O_2$), 73(OBu), 57(Bu), 41(C_3H_5). **^{1}H NMR:** 5.73 [6H, CH], 2.15 [12H, CH_2], 1.30 [6H, CH], 1.14 [24H, CH_3], 0.99 [12H, CH_3], 0.93 [54H, CH_3]. **$^{13}C\{^1H\}$ NMR:** (t, b designate the terminal and bridging side of the bridging ligand respectively) 200.4 [*t*Bu-CO_b], 198.6 [*t*Bu-CO_t], 194.0 [*i*Bu-CO_b], 192.2 [*i*Bu-CO_t], 97.0 [CH_t], 96.3 [CH_b], 50.2 [CH_b], 50.0 [CH_t], 40.2 [ipso C_b], 39.8 [ipso C_t], 28.1 [($\mathbf{C}H_3)_3C_t$], 27.8 [($\mathbf{C}H_3)_3C_b$], 27.1 [CH_b], 26.3 [CH_t], 22.7 [($\mathbf{C}H_3)_2CH_t$], 22.5 [($\mathbf{C}H_3)_2CH_b$]. **solution IR:**

3618(w), 2948(vs), 2916(s), 2892(m), 2856(m), 1582(vs), 1566(vs), 1544(s), 1528(s), 1524(s), 1504(vs), 1504(vs), 1468(m), 1456(s), 1444(s), 1416(vs), 1396(vs), 1384(s), 1354(s), 1224(m), 1160(m). **UV/VIS:** $\lambda_{max} = 287$, $c = 1.57 \times 10^{-5}$ **M**, $\varepsilon = 1.29 \times 10^{5}$ $\mathbf{M^{-1}}$ cm^{-1}. **TGA: (Figure 4-6).**

Observations on the Attempted Hydration of $[Y(tmod)_3]_2$ with H_2O. Two hundred milligrams of $[Y(tmod)_3]_2$ were dissolved in 10 ml of Fisher Scientific Optima grade acetone. Ten drops of distilled water then were added to the solution causing some precipitation. The solution was stirred until the precipitate dissolved. The solvent was allowed to evaporate over a period of seven days under a N_2 purge leaving a white solid. The IR spectrum of the white solid was identical to that of the starting material, showing no O-H stretch to indicate hydration of the dimer.

Chemical Vapor Deposition. Chemical vapor deposition was performed in a Lindberg Model 55035 furnace with a 20 mm I.D. quartz tube. The temperature profile of the furnace, at thermally equilibrated growth conditions, was mapped out with a movable thermocouple by measuring the actual tube interior temperature at 1 cm intervals from the furnace center (maximum temperature) to the furnace entrance (minimum temperature), a total distance of 18 cm. Glass substrates (microscope slide cover-slips) of dimensions 1.0 cm x 2.0 cm were cleaned by 3 cycles of washings with 6 **M** HNO_3, distilled H_2O, acetone, and hexane followed by oven drying at 130°C for 24 hours prior to use. The precursors were prepared and purified as described above. The evaporator temperature necessary for entrainment of the source compound in the carrier gas stream was ascertained by examination of TGA volatility data for the precursors (**Figure 4-6**).

Onset of weight loss under inert atmosphere conditions occurred at 187°C for $[Y(tmod)_3]_2$, at 198°C for $[Y(tmhd)_3 \cdot H_2O]_2$, and at 170°C for $Y(tmhd)_3$, therefore an evaporator temperature of 220°C was used for each precursor in the CVD experiments. Thin films were deposited using both hydrous and anhydrous carrier gas streams each of reducing, inert and oxidizing composition. For inert conditions, pure N_2 was used. For reducing conditions, a 10% mixture of H_2 in N_2 was used (the individual high purity gases were mixed prior to injection). For oxidizing conditions, a separate, inert carrier gas was used to prevent premature decomposition of the source in the sublimator. Nitrogen (G2 in **Figure 4-12**) was flowed over the evaporator and O_2 was injected at the

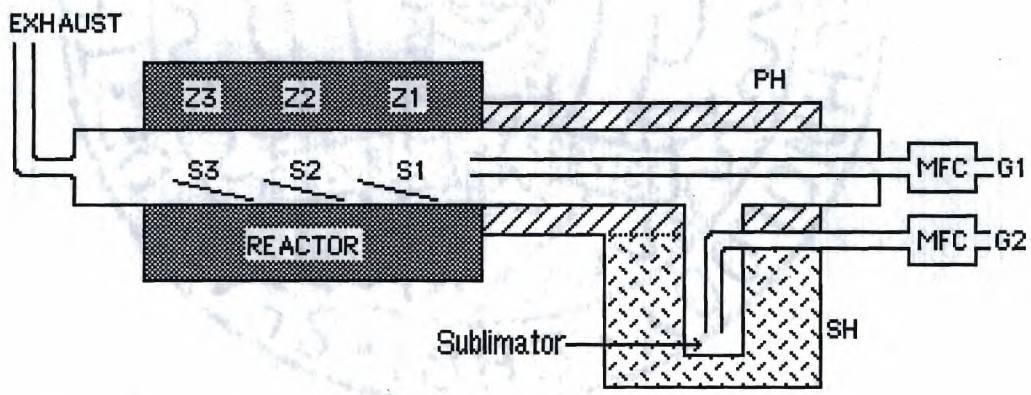

Figure 4-12. Schematic diagram of the hot-walled reactor used to deposit films. Key: Z1 - Z3, independent temperature zones; S1 - S3, substrates to be coated; SH, sublimator heater; PH, pre-heater for deposition gasses; MFC, mass flow controller.

entrance to the reactor (G1 in **Figure 4-12**). Thus, a 50% mixture of O_2 in N_2 was used. Hydrous gas streams were obtained by bubbling the mass flow controlled gas through ambient temperature, distilled H_2O prior to injection into the CVD apparatus. Under

reducing and oxidizing conditions, where gas mixtures were employed, the H_2 and O_2 each were bubbled through H_2O at ambient temperature prior to mixing with the anhydrous N_2. Substrates were placed end-to-end from the reactor center to the reactor entrance. The entire growth system was equilibrated at growth conditions for 30 min prior to introduction of the source material into the vapor phase. In the summary of data presented for $[Y(tmhd)_3 \cdot H_2O]_2$, $Y(tmhd)_3$, and $[Y(tmod)_3]_2$, each reported result represents an average value of data collected from three independent growth runs. The composition of the deposited films and their deposition conditions are given in **Table 4-3** and **Table 4-4** respectively.

Table 4-4. CVD deposition data for $[Y(tmhd)_3 \cdot H_2O]_2$, $Y(tmhd)_3$ and $[Y(tmod)_3]_2$.

Deposition	Flow Rates		Deposition Temperatures		
Atmosphere	G1	G2 (N_2)	$[Y(tmhd)_3 \cdot H_2O]_2$	$[Y(tmod)_3]_2$	$Y(tmhd)_3$
N_2		200	480	540	530
$N_2 + H_2O$		200	580	540	570
O_2	100	100	320	545	540
$O_2 + H_2O$	100	100	395	615	—
H_2	20	180	315	515	540
$H_2 + H_2O$	20	180	460	525	—

Single Crystal X-ray Diffraction. Space group and data collection parameters are given in **Table 4-5**. A Biosym InsightII plot of the solid state structure of $[Y(tmhd)_3 \cdot H_2O]_2$ is shown in **Figure 4-4**. The structure was determined by X-ray diffraction of a single crystal grown from a cooled hexane solution. The structure was

Table 4-5. Space group and data collection parameters.

Crystal Data	**$[Y(tmod)_3]_2$**	**$[Y(tmhd)_3H_2O]_2$**
formula	$C_{66}H_{114}O_{12}Y_2$	$C_{33}H_{59}O_7Y$
space group	$P2_1/n$	P-1
cryst system	monoclinic	triclinic
a, Å	12.993 (3)	11.553 (3)
b, Å	15.400 (7)	14.579 (3)
c, Å	18.349 (6)	14.875 (5)
α, deg	——	6045(2)
β, deg	91.50 (2)	63.10 (2)
γ, deg	——	73.28 (2)
V, $Å^3$	3670 (3)	1937.0 (8)
Z	4	2
cryst dimens, mm	0.3 x 0.3 x 0.3	0.3 x 0.3 x 0.3
cryst color	colorless	colorless
δ(calc), g/cm^3	1.156	1.095
μ(Mo Kα), cm^{-1}	16.3	15.45
temp, °C	23 (1)	23 (1)
diffractometer	CAD - 4	CAD - 4
monochromator	graphite	graphite
scan tecnique	θ - 2θ	θ - 2θ
radiation	Mo K_α	Mo K_α
2θ scan range, deg	2 - 50	1 - 50
scan speed, deg / min	1.0	2.0
rflns collected	6642	7165
indpt reflns	2649	7165
reflns obsd $I_o > 2\sigma I_o$	3 std / 2649	3 std/4923
R, %	10.6	7.0
R_w, %	10.3	8.8
D(r), $e^-Å^{-3}$	0.3	0.6

solved by Patterson and difference Fourier techniques. In the final refinement, anisotropic thermal parameters were used for all nonhydrogen atoms. Hydrogen atom parameters were calculated assuming idealized geometry. Hydrogen atom contributions were included in the structure factor calculations, but their parameters were not refined.

The final discrepancy indices were R = 7.0% and R_w = 8.8% for the 4923 observed reflections. The final difference Fourier map essentially was featureless with no peaks observed near the yttrium atom greater than 0.3 e^-A^{-3}.

A Biosym InsightII plot of the solid state structure of $[Y(tmod)_3]_2$ is shown in **Figure 4-5**. The structure was determined by X-ray diffraction of a single crystal grown from a cooled hexane solution. The structure was solved by Patterson and difference Fourier techniques. In the final refinement, anisotropic thermal parameters were used for all nonhydrogen atoms. Hydrogen atom parameters were calculated assuming idealized geometry. Hydrogen atom contributions were included in the structure factor calculations, but their parameters were not refined. The final discrepancy indices were R = 10.6% and R_w = 10.3% for the 2649 observed reflections. The final difference Fourier map essentially was featureless with no peaks observed near the Y atom greater than 0.3 e^-A^{-3}.

References

1. F.G. Sherif, L.J. Shyu, *J. Amer. Ceram. Soc.* **1991**, *74(2)*, 375.

2. D.C. Hanna, A.C. Large, D.P. Shepherd, A.C. Tropper, I. Chartier, B. Ferrand, D. Pelenc, *Appl. Phys. Lett.* **1993**, *63(1)*, 7.

3. W. van Schaik, G. Blasse, *Chem. Mater.* **1992**, *4*, 410.

4. J.E. Greeden *J. Less Common Metals* ***1985***, *111*, 335.

5. W.S. Rees, Jr., A.R. Barron, *Adv. Mater. Opt. Electr.* **1993**, *2*, 271.

6. W.S. Rees, Jr., A.R. Barron, *Mater. Sci. Forum* **1993**, *137*, 473.

7. B. Han, A. Neuymayer, D.L. Schultz, B.J. Hinds, T.J. Marks, H. Zhang, V.P. Dravid, *Chem. Mater.* **1993**, *5*, 14.

8. G.B. Sringfellow, *Organometallic Vapor-Phase Epitaxy, Theory and Practice*, Academic Press Inc., New York **1989**, 5-14.

9. W.S. Rees, Jr., in *Encyclopedia of Inorganic Chemistry, Vol. 1* (Ed: R.B. King), John Wiley and Sons, New York **1994**, 67-87.

10. W.S. Rees, Jr., "Superconductors: An Overview of the Present and Potential Materials and Markets," *Ceramic Industries International* **1993**, *April*, 22-26.

11. M.I. Faley, U. Poppe, H. Soltner, C.L. Jia, M. Siegel, K. Urban, *Appl. Phys. Lett.* **1993**, *63*, 2138.

12. D. Koelle, A.H. Miklich, E. Dantsker, F. Ludwig, D.T. Nemeth, J. Clarke, W. Ruby, K. Char, *Appl. Phys. Lett.* **1993**, *63*, 3633.

13. tmhd = 2,2,6,6-tetramethylheptane-3,5-dionate; tmod = 2,2,7-trimethyloctane-3,5dionate; hfac = 1,1,1,5,5,5-hexafluoropentane-2,4-dionate; tfac = 1,1,1-trifluoropentane-2,4- dionate; tdfnd = 1,1,1,2,2,3,3,7,7,8,8,9,9,9-tetradecafluorononane-4,6-dionate; dmmod = 2,2-dimethyl-8-methoxyoctane-3,5-dionate; tfdmhd = 1,1,1-trifluoro-5,5-dimethylhexane-2,4-dionate; COD = cycloocta-1,5-diene; o-phen = 1,10-phenanthroline.

14. R.W. Moshier, R.E. Sievers, *Gas Chromatography of Metal Chelates*, Permagnon, Oxford, **1965**.

15. R.C. Mehrotra, R. Bohra, D.P. Gaur, *Metal β-Diketonates and Allied Derivatives*, Academic Press, New York **1978**.

16. N.H. Dryden, J.J. Vittal, R.J. Puddephatt, *Chem. Mater.* **1993**, *5*, 765.

17. A. Bailey, T.S. Corbitt, M.J. Hampden-Smith, E.N. Duesler, T.T. Kodas, *Polyhedron* **1993**, *12(14)*, 1785.

18. K.C. Brooks, S.B. Turnipseed, R.M. Barkley, R.E. Sievers, V. Tulchinsky, A.E. Kaloyeros, *Chem. Mater.* **1992**, *4*, 912.

19. M. Becht, T. Gerfin, K. Dahmen, *Chem. Mater.* **1993**, *5*, 137.

20. G.K. Fukin, A.P. Pisavevskii, A.I. Yanovskii, Yu.T. Struchkov, *Russ. J. Inorg. Chem.* **1993**, *38(7)* 118.

21. W.S. Rees, Jr., C.R. Caballero, *Mater. Res. Soc. Symp. Proc.* **1992**, *250*, 297.

22. W.S. Rees, Jr., C.R. Caballero, *Adv. Mater. Opt. Electr.* **1992**, *1*, 59.

23. W.S. Rees, Jr., M.W. Carris, W. Hesse, *Inorg. Chem.* **1991**, *30*, 4479.

24. W.S. Rees, Jr., C.R. Caballero, W. Hesse, *Angew. Chem. Int. Ed. Eng.* **1992**, *31*, *6*, 735.

25. A.L. Spek, P. van der Sluis, K. Timmer, H.A. Meinema, *Acta Crystallogr. C* **1990**, *46*, 1741.

26. R. Gardiner, D.W. Brown, P.S. Kirlin, A.L. Rheingold, *Chem. Mater.* **1991**, *3*, 1053.

27. S.R. Drake, S.A.S. Miller, M.B. Hursthouse, K.M.A. Malik, *Polyhedron* **1993**, *12(13)*, 1621.

28. J.A.P. Nash, J.C. Barnes, D.J. Cole-Hamilton, B.C. Richards, S.L. Cook, M.L. Hitchman, *Adv. Mater. Opt. Electr.* **1995**, *5*, 1.

29. H.K. Shin, M.J. Hampden-Smith, T.T. Kodas, E.N. Duesler, *Can. J. Chem.* **1992**, *70*, 2954.

30. V.A. Mode, G.S. Smith, *J. Inorg. Nucl. Chem.* **1969**, *31*, 1857.

31. J.P.R. deVilliers, J.C.A. Boeyens, *Acta. Cryst.* **1971**, *B27*, 2335.

32. C.S. Erasmus, J.C.A. Boeyens, *Acta. Cryst.* **1970**, *B26*, 1843.

33. C.S. Erasmus, J.C.A. Boeyens, *J. Cryst. Mol. Struct.* **1971**, *1*, 83.

34. S. Matsuno, F. Urchikawa, K. Yoshizaki, *Jpn. J. Appl. Phys.* **1990**, *29L*, 947.

35. W.S. Rees, Jr., K.A. Dippel, M.W. Carris, C.R. Caballero, D.A. Moreno, W. Hesse, *Mater. Res. Soc. Symp. Proc.* **1992**, *271*, 127.

36. W.S. Rees, Jr., H.A. Luten, M.C. Carris, C.R. Caballero, W. Hesse, V.L. Goedken, *Mater. Res. Soc. Symp. Proc.* **1993**, *310*, 375.

37. W.S. Rees, Jr., H.A. Luten, M.C. Carris, E.J. Doscocil, V.L. Goedken, *Mater. Res. Soc. Symp. Proc.* **1992**, *271*, 141.

38. W.S. Rees, Jr., *Proc. Fourth Florida Microelectronics and Mater. Conf.*, (Ed: R. Rasmussen), University of South Florida Press, Tampa, Florida **1992**, 83.

39. W.S. Rees, Jr., Y.S. Hacisick, L.R. Testardi, *Mater. Res. Soc. Symp. Proc.* **1992**, *271*, 925.

40. W.S. Rees, Jr., M.W. Carris, "Tris(2,2,6,6-tetramethyl-3,5-heptanedionato)yttrium," *Inorg. Synth.* **1995**, accepted for publication.

41. A. Gleizes, D. Medus, S. Sans-Lenain, *Mater. Res. Soc. Symp. Proc.* **1992**, *271*, 919.

42. A. Gleizes, S. Sans-Lenain, D. Medus, N. Hovnanian, P. Miele, J.D. Foulon, *Inorg. Chim. Acta.* **1993**, *209*, 47.

43. J.T. Adams, C.R. Hauser, *J. Am. Chem. Soc.*, **1944**, *66*, 1220.

44. K.J. Eisentraut, R.E. Sievers, *Inorg. Synth.*, *11*, (Ed: W.L. Jolly), McGraw Hill, New York **1968**, 94-98.

45. T.J. Wenzel, E.J. Williams, R.E. Sievers, *Inorg. Synth.*, *23*, (Ed: S. Kirschner), Wiley-Interscience, New York **1985**, 144-149.

46. T. Hashimoto, H. Koinuma, M. Nakabayashi, T. Shiraishi, Y. Suemune, Y.; T. Yamamoto, *J. Mater. Res.* **1992**, *7*, 1336.

47. *Handbook of Chemistry and Physics, 68th. Edition*, (Ed: R.C. Weast), Chemical Rubber Publishing Company, Boca Raton, Florida **1987**, F159.

48. S. Shibata, K. Iijima, T. Inuzuka, *J. Molec. Struct.* **1986**, *144*, 181.

49. G.V. Girichev, N.I. Giricheva, N.V. Belova, A.R. Kaul', N.P. Kuz'mina, O. Yu. Gorbenko, *Russ. J. Inorg. Chem.* **1993**, *38(4)*, 647.

50. M. Tammenmaa, H. Antson, M. Asplund, L. Hiltunen, M. Leskelä, L. Niinistö, E. Ristolainen, *J. Cryst. Growth* **1987**, *84*, 151.

51. G.G. Condorelli, G. Malandrino, F. Ignazio, *Chem. Mater.* **1995**, *6*, 1861.

52. H.A. Meinema, K. Timmer, H.L. Linden, C.I.M.A. Spee, *Mater. Res. Soc. Symp. Proc.*, **1994**, *335*, 193.

53. T. Marks, Work presented at the 2nd International Conference on CVD of Metal Oxides, San Fransisco, CA. April **1994**.

54. C.I.M.A. Spee, H.A. Meinema, K. Tumer, E.A. van der Zouwen and A. Mackor, Materials Research Society Meeting, Late News Papers, Boston, MA. **1989**.

55. D.L. Schultz, T.J. Marks, *Adv. Mater.*, **1994**, *6*, *10*, 719.

CHAPTER V.

OTHER COMPOUNDS

A. Magnesium *bis*[N-(γ-dimethylaminopropyl)trimethylsilylamide]

Introduction

The preparation of blue light-emitting materials has become a heavily researched field in recent years. This interest is caused by the significant number of potential applications for blue light emitters. The two most technologically significant applications of blue light emitting diodes (LED's) are electroluminescent displays and read / write heads for optical data storage. Electroluminescent displays require blue LED devices to be manufactured as a component of an array of red, green and blue (RGB) LED's. Read / write heads for optical data storage require an LED laser. The benefits of the use of blue LED's in these devices are significant. LED displays are flat, bright and energy efficient. A blue LED laser-based optical data storage device, such as a CD-ROM, could store on the order of five times as much data as a standard red LED laser-based CD-ROM. This translates to about 3.25 Gbytes of data for a blue laser based CD, versus 650 Mbytes for the commonly used red laser based CD's. Another less obvious, significant, use of blue (or blue-green) LED's is in traffic signals. Traditional signals utilize a white

incandescent light source with an appropriately colored glass filter. The use of an incandescent source, as well as a filter, yields a very inefficient device. The efficiency and longevity of traffic signals can be enhanced through the use of blue LED's, as well as commonly available red and yellow LED's. The energy cost savings and the lower maintenance requirements, when multiplied by the number of traffic signals in an average city, represent vast cost reductions. This approach is currently in use in Japan.[1]

Gallium nitride (GaN) and zinc selenide (ZnSe) have emerged as strong candidates for blue light-emitting materials; however, ZnSe suffers from short device lifetimes, relative to GaN.[2] The thermodynamically stable phase of GaN at room temperature and atmospheric pressure is the hexagonal wurtzite phase.[3] This material is a direct bandgap semiconductor with a band gap of 3.45 eV.[4] Light emitting diodes require a p-n junction. The fabrication of n-type GaN is not difficult. The fabrication of p-type GaN has presented challenges. Zinc has been used as a p-type dopant for GaN, however its large size and propensity for forming covalent bonds have limited its usefulness. Magnesium has emerged as the dopant of choice for p-type GaN.[5] Commonly utilized magnesium sources in the CVD of GaN:Mg have been organometallic compounds such as magnesium cyclopentadienides. The drawback of these sources is that they create a large carbon impurity (MgC) in the deposited GaN, which destroys the material's electronic usefulness. To counter the formation of MgC, large quantities of H_2 have been injected into the reactor. This, in turn, causes the formation of MgH_2, which also passivates the material. It was, therefore, of interest to prepare a volatile magnesium precursor lacking magnesium-carbon bonds. Since the final material, theoretically, places

magnesium on a gallium site, a source material containing only magnesium-nitrogen bonds would seem most promising. The most commonly prepared magnesium amide is *tetrakis*[*bis*(trimethylsilyl)amido] dimagnesium.[6] This compound is a high molecular weight dimer. A more volatile, monomeric compound would be preferable for CVD applications.

Results and Discussion

Magnesium *bis*[N-(γ-dimethylaminopropyl)trimethylsilylamide], **5-2,** was prepared by the reaction of the free amine, **5-1,** with dibutylmagnesium in hexane. It is a white solid at ambient conditions and has been shown to be a monomer in the solid state by single crystal x-ray diffraction. Compound **5-2** is volatile, as demonstrated by its thermogravimetric trace (**Figure 5-1**), and can be sublimed at 80°C and 0.01 Torr. Compound **5-2**, like most other group 2 element amides, is quite air sensitive.

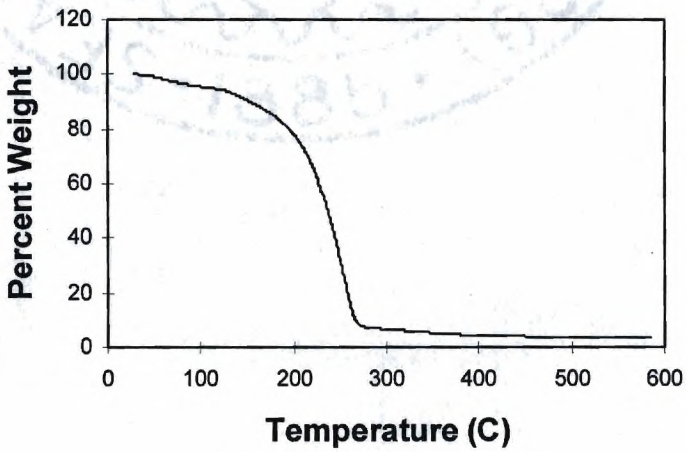

Figure 5-1. Thermogravimetric trace of $Mg[N(TMS)CH_2CH_2CH_2NMe_2]_2$

Single crystals of **5-2** were obtained by slow sublimation. A crystal of suitable quality for x-ray diffraction was selected and mounted in a glass capillary in an inert atmosphere glove box. The unit cell was determined from 25 centered reflections with 2θ values between 20 and 35°. Unit cell data and collection parameters are given in **Table 5-1.** The magnesium atom is tetrahedrally bonded to four nitrogen atoms; two from amide bonds and two from coordinate covalent bonds to tertiary amines (**Figure 5-2**). The amide nitrogen atoms are planar, indicating an sp^2 hybridization, due to dative bonding from the full nitrogen p-orbital to the empty silicon d-orbital, as shown in **Figure 5-3**. Interatomic distance and angle data is given in **Table 5-1**.

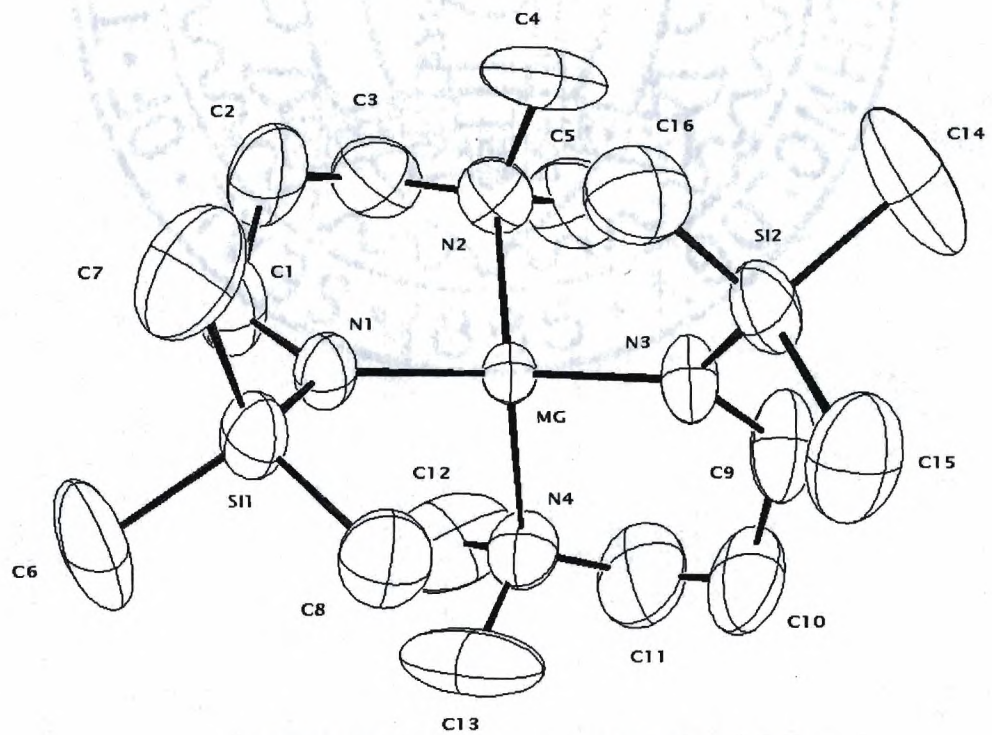

Figure 5-2. ORTEP plot of compound **5-2**.

Table 5-1. Unit cell and data collection parameters for **5-2.**

Empirical Formula	$MgC_{16}H_{42}N_4Si_2$
Formula Weight	371.01 g/mol.
Temperature	293(2) K
Wavelength	0.71073 Å
Crystal System	orthorhombic
Space Group	P21/n
Unit Cell Dimensions	a = 10.188(2) Å
	b = 16.401(5) Å β = 101.79(3)°
	c = 15.208(7) Å
Volume	2487.6(15) $Å^3$
Z	4
Density (calc'd)	0.991 g/cc
Absorption Coefficient	0.17 mm^{-1}
F(000)	824.94
θ Range for Data Collection	2.29° to 25°
Index Ranges	$-12 \leq h \leq 11$, $0 \leq k \leq 19$, $0 \leq l \leq 18$
Reflections Collected	4771
Independent Reflections	4360
Refinement Method	Full-matrix least-squares on F^2
Data / Restraints / Parameters	1793 / 0 / 208
Goodness of Fit on F^2	2.45
Final R Indices [$I>2\sigma(I)$]	$R = 0.079$, $R_w = 0.085$
R Indices (all data)	$R = 0.163$, $R_w = 0.096$
Largest Difference Peak and Hole	0.340 and -0.180 e/$Å^3$

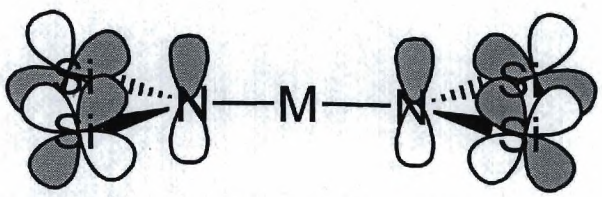

Figure 5-3. Dative p-d bonding in metal silylamides.

Table 5-2. Interatomic distances **5-2.**

Atoms	Distance(Å)	Atoms	Distance(Å)
MG-N1	1.979(7)	N1-C1	1.495(12)
MG-N2	2.189(8)	N2-C3	1.459(17)
MG-N3	1.969(7)	N2-C4	1.482(15)
MG-N4	2.212(8)	N2-C5	1.442(17)
SI1-N1	1.668(7)	N3-C9	1.503(14)
SI1-C6	1.835(12)	N4-C11	1.437(19)
SI1-C7	1.853(12)	N4-C12	1.418(17)
SI1-C8	1.859(10)	N4-C13	1.427(18)
SI2-N3	1.682(7)	C1-C2	1.463(18)
SI2-C14	1.874(11)	C2-C3	1.537(23)
SI2-C15	1.872(12)	C9-C10	1.493(23)
SI2-C16	1.820(12)	C10-C11	1.51(3)

Table 5-3. Interatomic angles for **5-2.**

Atoms	Angle (°)	Atoms	Angle (°)
N1-MG-N2	97.0(3)	MG-N2-C3	113.6(7)
N1-MG-N3	137.6(3)	MG-N2-C4	106.4(6)
N1-MG-N4	105.5(3)	MG-N2-C5	113.0(7)
N2-MG-N3	107.1(3)	C3-N2-C4	115.1(9)
N2-MG-N4	111.8(3)	C3-N2-C5	104.9(10)
N3-MG-N4	97.4(3)	C4-N2-C5	103.5(10)
N1-SI1-C6	112.6(5)	MG-N3-SI2	130.2(4)
N1-SI1-C7	111.3(5)	MG-N3-C9	115.8(6)
N1-SI1-C8	111.1(4)	SI2-N3-C9	114.0(6)
C6-SI1-C7	105.4(6)	MG-N4-C11	114.5(8)
C6-SI1-C8	108.8(6)	MG-N4-C12	114.8(8)
C7-SI1-C8	107.3(5)	MG-N4-C13	105.8(7)
N3-SI2-C14	111.7(4)	C11-N4-C12	106.2(13)
N3-SI2-C15	113.4(5)	C11-N4-C13	112.6(12)
N3-SI2-C16	111.4(4)	C12-N4-C13	102.5(13)
C14-SI2-C15	104.9(6)	N1-C1-C2	116.5(9)
C14-SI2-C16	108.5(6)	C1-C2-C3	115.8(11)
C15-SI2-C16	106.4(5)	N2-C3-C2	112.6(10)
MG-N1-SI1	128.3(4)	N3-C9-C10	116.8(10)
MG-N1-C1	116.9(5)	C9-C10-C11	115.1(12)
SI1-N1-C1	114.8(6)	N4-C11-C10	114.4(13)

Table 5-4. Atomic coordinates for **5-2**.

Atom	x	y	z
MG	0.85598(23)	0.34056(14)	0.19779(15)
SI1	1.08267(25)	0.46996(16)	0.30000(18)
SI2	0.68260(29)	0.32077(17)	0.35870(18)
N1	1.03505(65)	0.39205(39)	0.23031(43)
N2	0.92555(94)	0.21749(46)	0.17523(55)
N3	0.69597(65)	0.32860(44)	0.25060(45)
N4	0.75620(88)	0.39939(58)	0.07076(50)
C1	1.14391(99)	0.35599(72)	0.18994(79)
C2	1.16103(122)	0.26754(86)	0.19764(105)
C3	1.04893(168)	0.21620(73)	0.14057(92)
C4	0.93137(158)	0.17209(69)	0.26023(84)
C5	0.83008(149)	0.17175(71)	0.11077(101)
C6	1.18284(129)	0.54536(76)	0.25351(99)
C7	1.19092(119)	0.43522(93)	0.40649(73)
C8	0.93533(100)	0.52203(58)	0.32934(67)
C9	0.56473(109)	0.32078(88)	0.18474(90)
C10	0.53485(125)	0.38379(109)	0.11251(107)
C11	0.61756(172)	0.37769(112)	0.04093(111)
C12	0.81851(191)	0.38511(122)	-0.00308(90)
C13	0.77494(191)	0.48495(91)	0.08512(94)
C14	0.59022(163)	0.22617(80)	0.37928(80)
C15	0.58646(123)	0.40651(79)	0.39686(81)
C16	0.84655(119)	0.31997(71)	0.43364(66)

Conclusions

A new monomeric magnesium amide has been prepared, containing only magnesium-nitrogen bonds. It has enhanced stability and volatility, relative to currently utilized organomagnesium and magnesium-amide based precursors.

Experimental

N-(γ-dimethylaminopropyl)trimethylsilylamine. 5-1 Under argon, in a 500 ml Schlenk flask containing a magnetic stir bar, 49.38g (0.480 mol) of 3-dimethylaminopropylamine (99%, Aldrich) was added to 120 ml of anhydrous hexanes (distilled from Na). This mixture was stirred and cooled with a constant temperature bath at 10°C. From a dropping funnel, 25g of TMS-Cl (0.230 mol) were added dropwise to the mixture over a

period of two hours. A white precipitate formed, and later redissolved forming a separate layer at the bottom of the flask. Once the TMS-Cl addition was complete, 200 ml of anhydrous ether (distilled from Na/K) was added to the flask. The mixture then was rapidly stirred overnight causing the two layers to merge into a homogeneous solution over a white precipitate. The solution was separated from the white solid by cannulation and distilled at ambient pressure to give TMS-NH-$CH_2CH_2CH_2NMe_2$ at 160°C. Yield: 85%. **Characterization: ^{1}H NMR:** (400 MHz, positive δ downfield referenced to $Si(CH_3)_4$ = 0 ppm utilizing residual $CDCl_3$ = 7.24 ppm in solvent $CDCl_3$) 2.72 [m, 2H, -CH_2NMe_2], 2.24 [m, 2H, TMS-NH-CH_2-], 2.20 [s, 6H, -NCH_3], 1.54 [m, 4H, TMS-NH-CH_2CH_2-], 0.02 [s, 18H, CH_3Si-]. **^{13}C{^{1}H} NMR:** (75 MHz, positive δ downfield referenced to $Si(CH_3)_4$ = 0 ppm utilizing residual C_6D_5H = 128.0 ppm in solvent C_6D_6) 57.45 [-CH_2NMe_2], 45.40 [-NCH_3], 40.00 [TMS-N-CH_2-], 32.66 [TMS-N-CH_2CH_2-], -0.20 [$(CH_3)_3Si$-N-]. **Mass Spectrum:** (EI, 70eV) 174 [TMS-$NHCH_2CH_2CH_2NMe_2$]$^+$, 159 (M - Me), 129, 114, 100, 85, 72, 58.

Magnesium *bis*[N-(γ-dimethylaminopropyl)trimethylsilylamide]. 5-2 In a 100 ml Schlenk flask equipped with a magnetic stir bar and argon purge were combined 4.46g of N-(γ-dimethylaminopropyl)trimethylsilylamine and 10 ml of anhydrous THF (twice distilled from Na). The contents of the flask were stirred and cooled to -10°C, then 12 ml of $MgBu_2$ (1M solution in heptane) were added slowly by syringe over a period of two minutes. The solution was allowed to warm to room temperature and then was heated to reflux for 5 hours. The flask was allowed to cool to room temperature. The THF was

removed under vacuum leaving an off-white solid. The solid was sublimed at 80°C and 10^{-4} mm Hg to yield purified $Mg(N\{TMS\}CH_2CH_2CH_2NMe_2)_2$ as a crystalline, white solid. Yield: 52%. **Characterization: TGA: (Figure 5-1**) Onset of weight loss, 200°C; 3.5% residue at 600°C. **$^{29}Si\{^1H\}$ NMR:** (79.5 MHz, in C_6D_6, positive δ downfield referenced to $Si(CH_3)_4$ = 0 ppm) -8.16 [$SiMe_3$]. **^1H NMR:** (400 MHz, positive δ downfield referenced to $Si(CH_3)_4$ = 0 ppm utilizing residual C_6D_5H = 7.15 ppm in solvent C_6D_6) 3.41 [m, 2H, -$CH_{2(a)}NMe_2$], 3.03 [m, 2H, -$CH_{2(b)}NMe_2$], 2.15 [s, 6H, -$NCH_{3(a)}$], 2.05 [m, 4H, TMS-N-CH_2CH_2-], 1.71 [s, 6H, -$NCH_{3(b)}$], 1.57 [m, 2H, TMS-N-$CH_{2(a)}$-], 1.28 [m, 2H, TMS-N-$CH_{2(b)}$-], 0.49 [s, 18H, $(CH_3)_3Si$-]. **$^{13}C\{^1H\}$ NMR:** (100 MHz, positive δ downfield referenced to $Si(CH_3)_4$ = 0 ppm utilizing residual C_6D_5H = 128.0 ppm in solvent C_6D_6) 62.91 [-CH_2NMe_2], 49.11 [TMS-N-CH_2-], 47.78 [-$NCH_{3(a)}$], 45.82 [-$NCH_{3(b)}$], 32.70 [TMS-N-CH_2CH_2-], 2.37 [$(CH_3)_3Si$-N-]. **Mass Spectrum:** (EI, 70eV) 370.3 $[Mg(N\{TMS\}CH_2CH_2CH_2NMe_2)_2]^+$, 353.2, 324.4, 306.3, 277.3, 250.3, 196.2, 174.2, 159.2, 146.1, 129.1, 114.1, 100.1, 85.1, 73.1, 58.1. **Elemental Analysis:** Calculated: C 51.9%, H 11.4%, N 15.1%; Found: C 52.0%, H 12.5%, N15.2%.

References

1. R.A. Metzger, *Compound Semiconductor*, **1996**, *1(1)*, 26.

2. *ibid*, 34.

3. D.A. Neumayer and J.G. Ekerdt, *Chem. Mater.*, **1996**, *8*, 9.

4. A. Miehr, O. Ambacher, W. Rieger, T. Metzger, E. Born and R. Fischer, *Chem. Vap. Deposition*, **1996**, *2(2)*, 51.

5. C. Wang and R.F. Davis, *Appl. Phys. Lett.*, **1993**, *63(7)*, 990.

6. W.S. Rees, *Alkaline Earth Metals: Inorganic Chemistry*, in *Encyclopedia of Inorganic Chemistry II.*, Vol. 1, Editor in chief: R.B. King, John Wiley and Sons, New York, **1994**, 67 - 87.

B. Preparation and Characterization of a Novel Organo-P_2S_5 Cluster

Introduction

Various methods for general conversion of ketones to thiones are known.[1] Simple ketones can be coverted to thiones by the acid catalyzed addition of H_2S, eliminating H_2O.[2] Reaction of ketones with P_4S_{10} has been shown to give thiones in certain instances.[3] β-Diketones can be converted to their corresponding β-ketothiones by reaction with H_2S and HCl in alcohol at low temperature,[4] however, this route does not give the β-dithione in more than trace quantities.

Results and Discussion

It was of interest to prepare 2,2,6,6-tetramethylheptane-3,5-dithione (**Figure 5-4**). In an attempt to prepare this compound, 2,2,6,6-tetramethylheptane-3,5-dione (Htmhd) was reacted in 1:1 stoichiometry with P_4S_{10} in refluxing toluene.

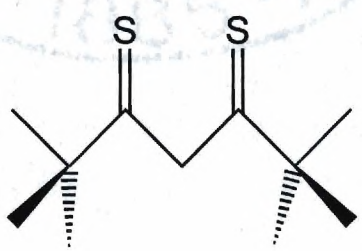

Figure 5-4. 2,2,6,6-tetramethylheptane-3,5-dithione.

The Htmhd was consumed completely. A crystalline product was isolated in low yield by CS_2 extraction and was characterized by standard methods. The product was determined by single crystal x-ray diffraction to be $C_{11}H_{20}P_2S_5$ (**Figure 5-5**). Unit cell data and collection parameters are given in **Table 5-5**. Atomic coordinates and interatomic distances and angles are given in **Table 5-6**.

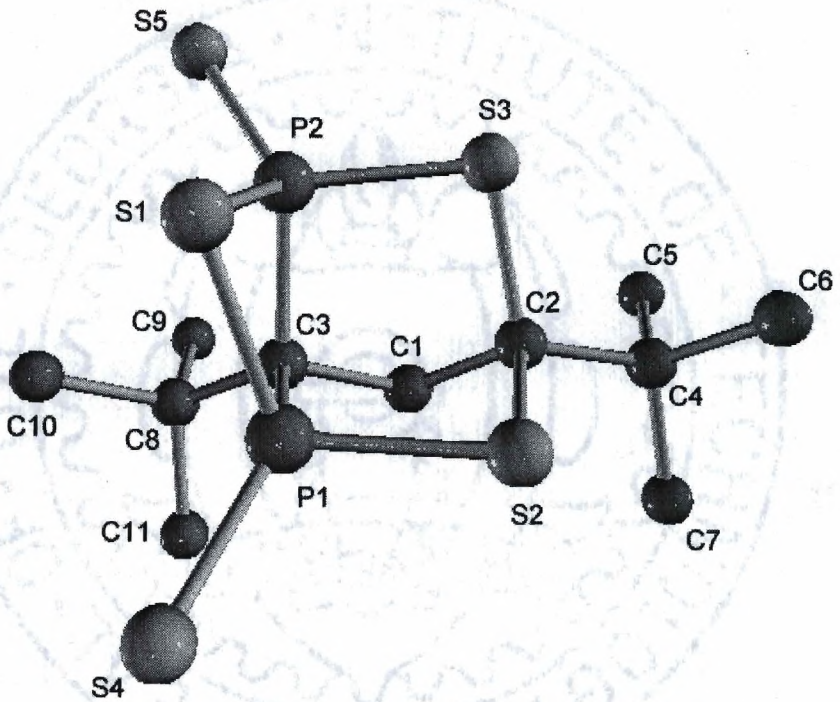

Figure 5-5. Molecular structure of $C_{11}H_{20}P_2S_5$.

Due to the mirror symmetry and rigid structure of this molecule, interesting coupling is seen between the methylene protons (residing on C1) and the two phosphorus atoms both in the ^{1}H- (**Figure 5-6**) and ^{31}P-NMR (**Figure 5-7**) spectra. The mirror symmetry at the

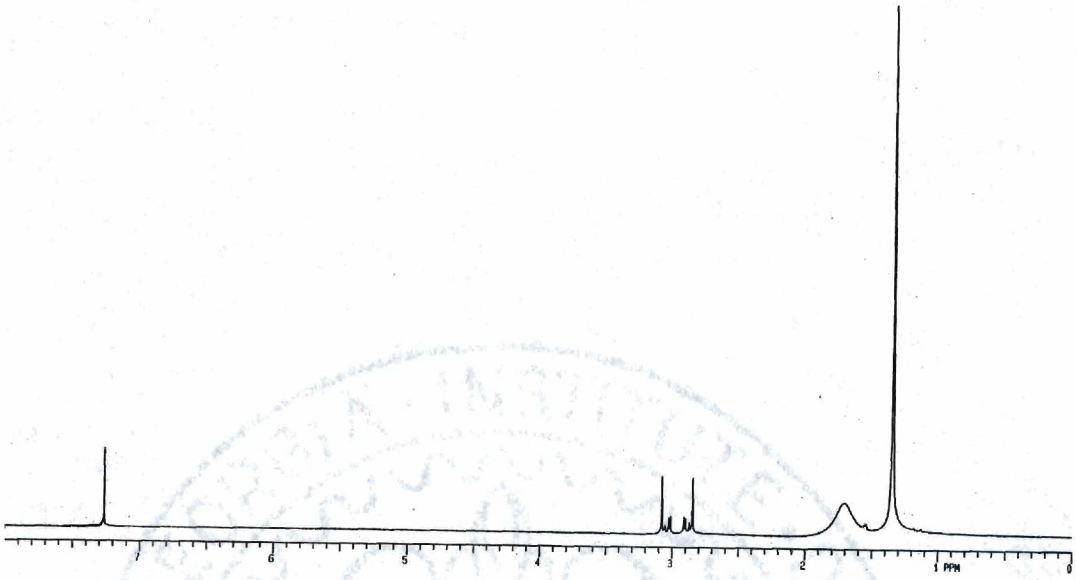

Figure 5-6. ^{1}H-NMR spectrum of $C_{11}H_{20}P_2S_5$ ($CDCl_3$).

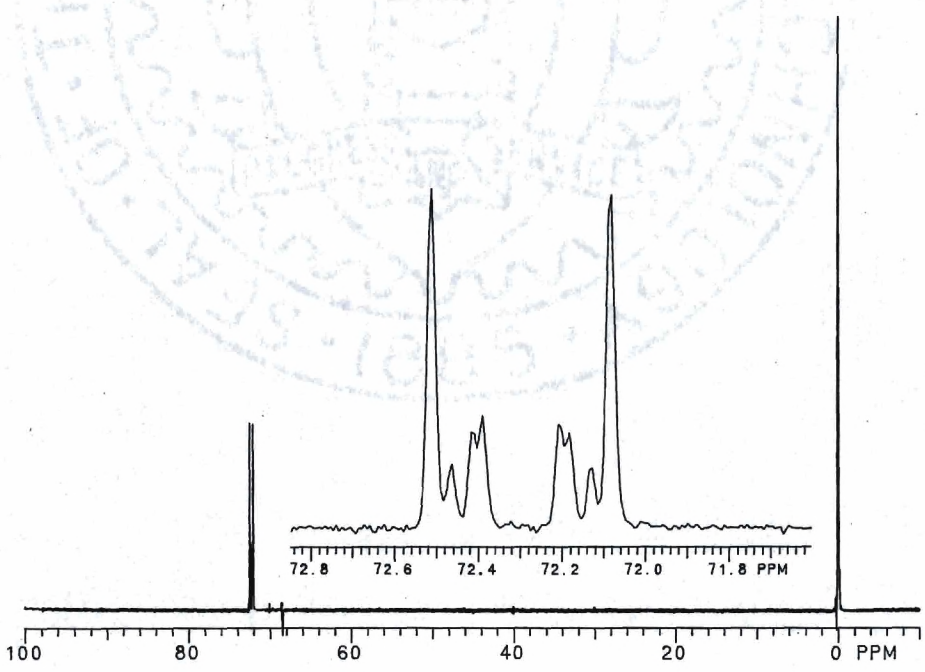

Figure 5-7. ^{31}P-NMR spectrum of $C_{11}H_{20}P_2S_5$ (vs. H_3PO_4).

carbon backbone is indicated by the clean triplet signals in the $^{13}C\{^1H\}$-NMR for four of the five backbone carbons, due to splitting by two equivalent spin ½ phosphorus atoms.

Table 5-5. Unit cell data and collection parameters for $C_{11}H_{20}P_2S_5$.

Empirical Formula	$C_{11}H_{20}P_2S_5$
Formula Weight	374.51 g/mol.
Temperature	293(2) K
Wavelength	0.71073 Å
Crystal System	orthorhombic
Space Group	Pbca
Unit Cell Dimensions	a = 11.9320(10) Å
	b = 16.045(2) Å $\alpha=\beta=\gamma = 90°$
	c = 17.802(4) Å
Volume	3408.2(9) $Å^3$
Z	8
Density (calc'd)	1.460 g/cc
Absorption Coefficient	0.849 mm^{-1}
F(000)	1568
θ Range for Data Collection	2.29° to 22.5°
Index Ranges	$-1\leq h\leq 12$, $-1\leq k\leq 17$, $-1\leq l\leq 25$
Reflections Collected	2939
Independent Reflections	2238 [R(int) = 0.0326]
Refinement Method	Full-matrix least-squares on F^2
Data / Restraints / Parameters	2238 / 0 / 163
Goodness of Fit on F^2	1.018
Final R Indices [$I>2\sigma(I)$]	$R = 0.0377$, $R_w = 0.0905$
R Indices (all data)	$R = 0.0524$, $R_w = 0.0981$
Largest Difference Peak and Hole	0.203 and -0.235 e/$Å^3$

The coupling observed in the ^{31}P-NMR spectrum can be reproduced in an H, H', P, P' spin system modeled with higher order coupling. The predicted spectrum is shown in **Figure 5-8**. The coupling constants employed in this model are given in **Table 5-9**.

Table 5-6. Interatomic distances for $C_{11}H_{20}P_2S_5$.

Atoms	Distance (Å)	Atoms	Distance (Å)
P1-S1	2.099	C1-C2	1.531
P1-S2	2.073	C1-C3	1.525
P1-S4	1.922	C2-C4	1.558
P1-C3	1.888	C3-C8	1.564
P2-S1	2.101	C4-C5	1.530
P2-S3	2.081	C4-C6	1.527
P2-S5	1.924	C4-C7	1.540
P2-C3	1.896	C8-C9	1.532
S2-C2	1.861	C8-C10	1.541
S3-C2	1.861	C8-C11	1.528

Table 5-7. Interatomic angles for $C_{11}H_{20}P_2S_5$.

Atoms	Angle (°)	Atoms	Angle (°)
S1-P1-S2	109.2	S3-C2-C4	109.7
S1-P1-S4	114.4	C1-C2-C4	116.7
S1-P1-C3	91.3	P1-C3-P2	91.5
S2-P1-S4	113.0	P1-C3-C1	106.6
S2-P1-C3	96.9	P1-C3-C8	116.6
S4-P1-C3	128.9	P2-C3-C1	106.8
S1-P2-S3	108.5	P2-C3-C8	117.3
S1-P2-S5	114.1	C1-C3-C8	115.2
S1-P2-C3	91.0	C2-C4-C5	110.1
S3-P2-S5	113.9	C2-C4-C6	110.0
S3-P2-C3	96.6	C2-C4-C7	109.7
S5-P2-C3	129.3	C5-C4-C6	109.3
P1-S1-P2	80.4	C5-C4-C7	108.4
P1-S2-C2	94.5	C6-C4-C7	109.3
P2-S3-C2	94.6	C3-C8-C9	109.8
C2-C1-C3	108.3	C3-C8-C10	111.2
S2-C2-S3	111.3	C3-C8-C11	109.5
S2-C2-C1	104.6	C9-C8-C10	108.9
S2-C2-C4	109.2	C9-C8-C11	108.4
S3-C2-C1	105.2	C10-C8-C11	108.9

Table 5-8. Atomic coordinates for $C_{11}H_{20}P_2S_5$.

Name	x	y	z
P1	0.13340	0.62300	0.59040
P2	0.24850	0.48550	0.54720
S1	0.09400	0.49630	0.60300
S2	0.09260	0.66060	0.48240
S3	0.22220	0.50450	0.43290
S4	0.07120	0.69410	0.66660
S5	0.32910	0.38480	0.57000
C1	0.31540	0.64030	0.49740
C2	0.22420	0.62020	0.43970
C3	0.28510	0.59740	0.57110
C4	0.23870	0.65860	0.35990
C5	0.34430	0.62390	0.32250
C6	0.13690	0.63790	0.31140
C7	0.25070	0.75390	0.36610
C8	0.36940	0.61200	0.63710
C9	0.48540	0.57900	0.61520
C10	0.33050	0.56740	0.70920
C11	0.37920	0.70530	0.65290

$P_2S_5C_{11}H_{20}$ decomposes at 250°C to give a single volatile product that has been identified by GC-high resolution-MS as $C_{11}H_{20}P_2$. One potential structure of this product is shown in **Figure 5-9**. This compound was isolated in a separate experiment as an orange oil that decomposes rapidly at room temperature to give a mixture of phosphorus-containing species.

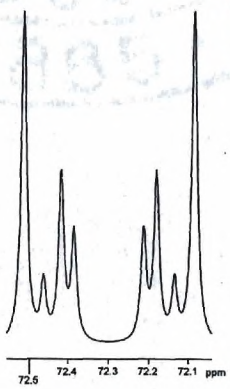

Figure 5-8. The predicted coupling for the modeled spin system in $C_{11}H_{20}P_2S_5$.

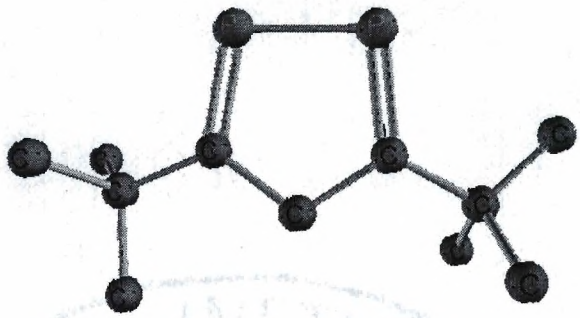

Figure 5-9. The proposed structure of $C_{11}H_{20}P_2$, the thermal decomposition product of $C_{11}H_{20}P_2S_5$.

Table 5-9. Coupling constants used in the system modeled in **Figure 5-8.**

Couple	J (Hz)
PP'	-4.70
HP	11.55
HP'	40.60
H'P	40.60
H'P'	40.60
H'H	4.70

Conclusions

A novel organo-P_2S_5 cluster compound has been prepared. This compound has a structure that may lead to interesting coordination chemistry. The positioning of the three bridging sulfur atoms leaves one lone pair of each bridging sulfur well placed for coordination to a metal. Currently, this compound has been coordinated to $Hg(NO_3)_2$ to form $[HgL_2]^{2+}$ 2 NO_3^-. This mercury complex has been identified by FAB-MS.

Experimental

$C_{11}H_{20}P_2S_5$. 13.33 g (0.0300 mol) of P_4S_{10} and 100 ml of toluene (distilled from Na) were combined in a 250 ml Schlenk flask under argon purge. A magnetic stir bar was added followed by 5.00 g (0.0272 mol) of 2,2,6,6-tetramethylheptane-3,5-dione (H-tmhd). The flask was fitted with a reflux condenser. The mixture was stirred and brought to reflux for 2 hours, giving a yellow solution over a small quantity of orange oil. The solution was then cooled to 0°C for 1 hour, yielding a colorless solution over a yellow, wax-like solid. The toluene was decanted and 100 ml of CS_2 (distilled from P_4O_{10}) were added to the flask. This mixture was heated to reflux for 1 hour and then cooled to 0°C. The resulting slightly colored solution was decanted into another flask and the CS_2 was removed by evacuation. This yielded a small quantity of slightly colored solution which contained residual toluene. The solution was allowed to stand in a sealed flask under argon for 2 weeks, producing large, colorless, cubic crystals of pure $C_{11}H_{20}P_2S_5$. Yield: 10% based on initial charge of H-tmhd. **Characterization: mp:** 194 - 198°C. **^{1}H-NMR: (Figure 3).** **^{31}P-NMR: (Figure 4).** **^{13}C{^{1}H}-NMR:** 100.07 [t, C3], 91.30 [s, C2], 52.44 [t, C1], 40.33 [t, C8], 38.46 [t, C4], 28.47 [broad, C9, C10, C11], 27.13 [s, C5, C6, C7]. **Mass Spectrum:** (EI, 70 eV) 374.0 (M^+), 342.0, 309.0, 279.0, 246.1, 231.0, 214.1, 199.1, 183.1. **TGA:** Onset of weight loss: 245°C, Residue at 550°C: 10%. **High Resolution Mass Spectroscopy of Decomposition Product:** Exact Mass $C_{11}H_{20}P_2$ = 214.1040, Found 214.1067.

References

1. E. Campaigne, *Thioketones*, in *The Chemistry of the Functional Groups*, Ed. S. Patai, Interscience Publishers, New York, **1966**, 917 - 959.

2. E. Campaigne, in *Organic Sulfur Compounds*, Ed. N. Kharasch, Permagnon Press, Oxford, **1961**, 134 - 145.

3. Scheeren, Ooms, and Nivard, *Synthesis*, **1973**, 149.

4. S.H.H Chaston, S.E. Livingstone, T.N. Lockyer, V.A. Pickles and J.S. Shannon, *Aust. J. Chem.*, **1965**, *18*, 673.

CHAPTER VI.

SOLID STATE MOLECULAR STRUCTURES DETERMINED BY SINGLE CRYSTAL X-RAY DIFFRACTION

The contents of this chapter represent solid state molecular structures determined through single crystal x-ray diffraction by this researcher. All data sets were collected on an Enraf-Nonius CAD4 single crystal diffractometer equipped with a copper K_α source utilizing a graphite monochromater. Single crystals were mounted with epoxy on the tip of a glass fiber, attached to a brass pin. Unit cell parameters were determined from 25 centered reflections ranging from 15 to 35 degrees 2θ. Data sets were collected in ω-2θ scan mode at room temperature. Three intensity standards and three orientation standards were selected from the 25 centered reflections of each set. Data treatment and structure solution were performed with the NRCVAX for DOS structural solution package.[1] Data sets were scaled to the intensity standards and corrected for absorption, when necessary. Patterson maps were used to determine heavy atom positions whenever possible and the SHELXS for DOS direct methods software was used for the initial phase solution when Patterson techniques were not successful. Refinement was performed in all cases with the NRCVAX software. Structural plots were obtained with the PLUTO and ORTEP programs built into NRCVAX.

Barium *bis*(1,3-diphenylpropane-1,3-dionate) tetraglyme.

Prepared by: David Otway

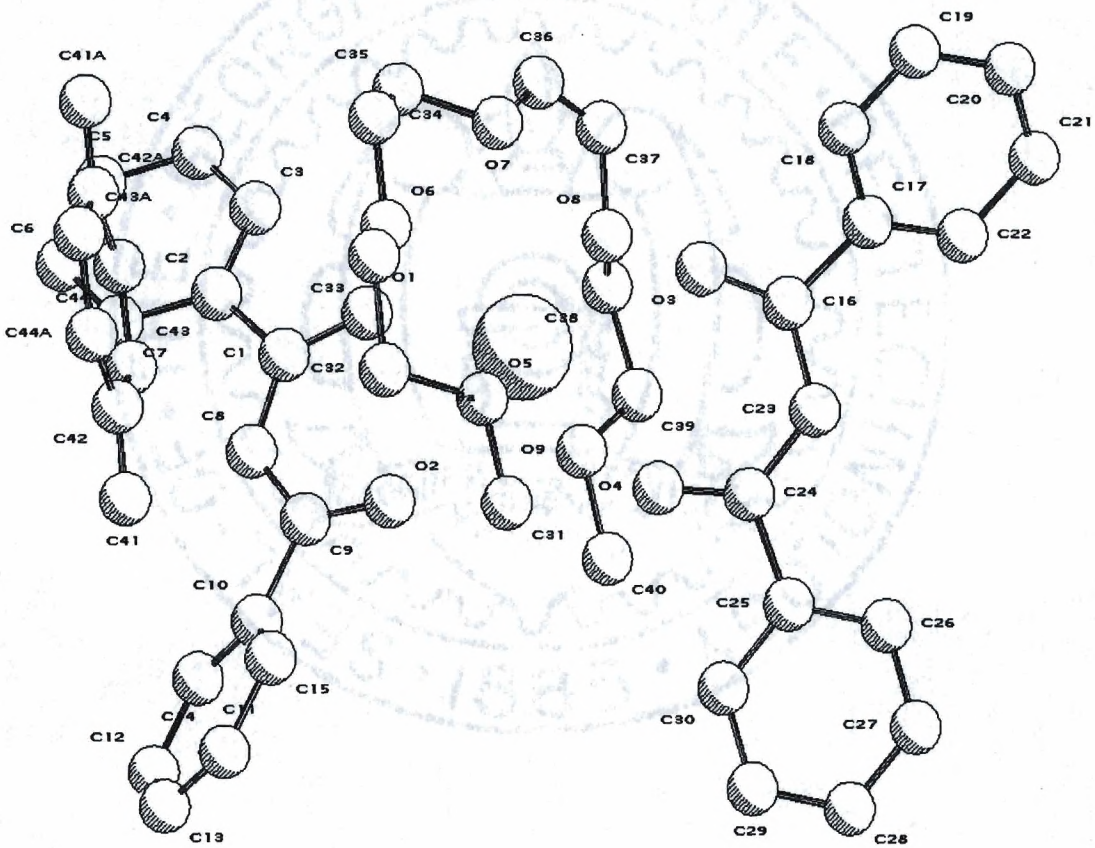

Figure 6-1. PLUTO plot of $Ba(dppd)_2$•tetraglyme cocrystallized with one disordered molecule of toluene.

Table 6-1. Unit cell and data collection parameters for $BaO_9C_{40}H_{44}$.

Empirical Formula	$BaO_9C_{40}H_{44}$
Formula Weight	851.67 g/mol.
Temperature	293(2) K
Wavelength	0.71073 Å
Crystal System	monoclinic
Space Group	$P2_1/a$
Unit Cell Dimensions	a = 12.3792(13) Å
	b = 27.505(3) Å β = 112.793(9)°
	c = 13.1866(18) Å
Volume	4139.3(8) $Å^3$
Z	4
Density (calc'd)	1.367 g/cc
Absorption Coefficient	8.02 mm^{-1}
F(000)	1747.92
θ Range for Data Collection	2.29° to 71.8°
Index Ranges	$-15 \leq h \leq 14$, $0 \leq k \leq 33$, $0 \leq l \leq 16$
Reflections Collected	9607
Independent Reflections	8127
Refinement Method	Full-matrix least-squares on F^2
Data / Restraints / Parameters	6814 / 0 / 487
Goodness of Fit on F^2	3.38
Final R Indices [$I>2\sigma(I)$]	$R = 0.037$, $R_w = 0.030$
R Indices (all data)	$R = 0.044$, $R_w = 0.030$
Largest Difference Peak and Hole	0.840 and -1.180 e/$Å^3$

Table 6-2. Atomic coordinates for $BaO_9C_{40}H_{44}$.

	x	y	z	Biso (Å^2)
Ba	0.969958(18)	0.631994(8)	0.092608(18)	3.299(10)
O1	0.95501 (22)	0.68244 (10)	0.26388 (22)	4.93 (15)
O2	0.78096 (22)	0.61220 (10)	0.13386 (24)	5.41 (17)
O3	1.09509 (21)	0.62512 (11)	-0.03692 (21)	4.78 (15)
O4	0.84889 (21)	0.61103 (11)	-0.11526 (22)	5.11 (16)
O5	0.9508 (3)	0.52880 (11)	0.0923 (3)	6.41 (21)
O6	1.1035 (3)	0.57385 (13)	0.2815 (3)	6.17 (19)
O7	1.20490 (24)	0.65488 (13)	0.2398 (3)	6.89 (21)
O8	1.0693 (3)	0.72392 (12)	0.0812 (3)	7.45 (23)
O9	0.8282 (3)	0.71471 (13)	-0.0118 (3)	7.48 (22)
C16	1.0725 (3)	0.62781 (13)	-0.1380 (3)	3.61 (18)
C17	1.1760 (3)	0.63359 (14)	-0.1695 (3)	3.69 (18)
C12	0.4414 (4)	0.59407 (22)	0.2099 (4)	6.5 (3)
C23	0.9611 (3)	0.62261 (14)	-0.2217 (3)	3.94 (19)
C11	0.5424 (3)	0.61980 (16)	0.2208 (4)	5.14 (25)
C1	0.8933 (3)	0.68124 (14)	0.3204 (3)	3.89 (19)
C9	0.7401 (3)	0.62255 (14)	0.2053 (3)	4.07 (20)
C25	0.7506 (3)	0.59634 (14)	-0.3047 (3)	3.85 (19)
C10	0.6279 (3)	0.59711 (16)	0.1936 (3)	4.05 (20)
C24	0.8591 (3)	0.61125 (14)	-0.2062 (3)	3.91 (19)
C18	1.2840 (4)	0.61495 (14)	-0.0985 (4)	4.59 (22)
C8	0.7910 (3)	0.65366 (14)	0.2958 (3)	4.09 (20)
C7	0.8833 (4)	0.71362 (17)	0.4983 (4)	5.6 (3)
C15	0.6103 (4)	0.55093 (18)	0.1560 (4)	6.1 (3)
C2	0.9333 (3)	0.71425 (15)	0.4206 (3)	4.10 (19)
C26	0.7485 (4)	0.59039 (17)	-0.4097 (4)	5.15 (25)
C22	1.1687 (4)	0.65672 (16)	-0.2651 (4)	5.05 (24)
C30	0.6490 (4)	0.58591 (18)	-0.2883 (4)	6.0 (3)
C19	1.3824 (4)	0.61893 (17)	-0.1238 (5)	6.1 (3)
C4	1.0568 (4)	0.77972 (21)	0.5207 (5)	7.6 (3)
C21	1.2677 (4)	0.66074 (19)	-0.2906 (4)	6.8 (3)
C27	0.6485 (4)	0.57407 (20)	-0.4939 (4)	6.6 (3)
C3	1.0208 (4)	0.74751 (18)	0.4332 (4)	5.9 (3)
C33	1.0915 (6)	0.52189 (24)	0.2719 (5)	8.3 (4)
C31	0.8484 (5)	0.50793 (17)	0.0104 (5)	7.6 (4)
C20	1.3716 (4)	0.64124 (20)	-0.2209 (5)	7.1 (4)
C5	1.0058 (5)	0.77924 (21)	0.5967 (5)	7.4 (3)
C29	0.5497 (4)	0.56940 (22)	-0.3721 (5)	7.4 (3)
C14	0.5082 (5)	0.52515 (19)	0.1471 (5)	7.8 (4)
C6	0.9215 (5)	0.74625 (21)	0.5856 (4)	7.4 (3)
C34	1.2164 (5)	0.5879 (3)	0.3533 (5)	8.9 (4)
C35	1.2288 (5)	0.6407 (3)	0.3511 (6)	9.7 (5)
C13	0.4258 (4)	0.54742 (24)	0.1763 (5)	7.4 (4)
C28	0.5485 (4)	0.56366 (20)	-0.4763 (4)	7.0 (3)
C32	0.9723 (6)	0.51035 (19)	0.1994 (6)	8.5 (5)
C39	0.8841 (7)	0.75480 (25)	-0.0302 (6)	10.0 (5)
C43	0.9163 (11)	0.5322 (5)	0.4430 (9)	12.7 (9)
C41	0.7971 (12)	0.4674 (7)	0.3707 (12)	10.7 (11)
C40	0.7163 (5)	0.70829 (24)	-0.0953 (5)	11.8 (5)
C44	0.9817 (12)	0.4502 (4)	0.4896 (10)	13.0 (8)
C37	1.1873 (8)	0.7276 (3)	0.1454 (7)	14.8 (7)
C38	0.9955 (8)	0.76233 (23)	0.0573 (8)	12.4 (7)
C36	1.2362 (7)	0.7032 (3)	0.2273 (9)	15.9 (7)
C42	0.8925 (9)	0.4807 (6)	0.4295 (7)	12.4 (9)

Table 6-3. Interatomic distances for $BaO_9C_{40}H_{44}$.

Atoms	Dist. (Å)	Atoms	Dist. (Å)
Ba-O1	2.717(3)	C1-C2	1.520(6)
Ba-O2	2.656(3)	C9-C10	1.510(5)
Ba-O3	2.7207(25)	C9-C8	1.403(6)
Ba-O4	2.629(3)	C25-C24	1.520(5)
Ba-O5	2.848(3)	C25-C26	1.385(6)
Ba-O6	2.882(3)	C25-C30	1.386(6)
Ba-O7	2.872(3)	C10-C15	1.350(6)
Ba-O8	2.841(3)	C18-C19	1.386(6)
Ba-O9	2.877(3)	C7-C2	1.387(6)
O1-C1	1.257(5)	C7-C6	1.390(7)
O2-C9	1.263(5)	C15-C14	1.413(7)
O3-C16	1.254(5)	C2-C3	1.377(6)
O4-C24	1.253(5)	C26-C27	1.380(6)
O5-C31	1.429(6)	C22-C21	1.396(7)
O5-C32	1.425(7)	C30-C29	1.373(6)
O6-C33	1.438(8)	C19-C20	1.379(8)
O6-C34	1.405(7)	C4-C3	1.384(7)
O7-C35	1.434(9)	C4-C5	1.377(9)
O7-C36	1.412(9)	C21-C20	1.368(8)
O8-C37	1.380(9)	C27-C28	1.376(8)
O8-C38	1.352(9)	C33-C32	1.449(10)
O9-C39	1.373(9)	C5-C6	1.347(9)
O9-C40	1.408(7)	C29-C28	1.378(8)
C16-C17	1.501(5)	C14-C13	1.368(8)
C16-C23	1.400(5)	C34-C35	1.462(11)
C17-C18	1.399(6)	C39-C38	1.430(12)
C17-C22	1.383(6)	C43-C44a	1.323(21)
C12-C11	1.395(7)	C43-C42	1.442(22)
C12-C13	1.346(9)	C41-C42	1.192(17)
C23-C24	1.390(5)	C44-C43a	1.323(21)
C11-C10	1.389(6)	C44-C42	1.368(18)
C1-C8	1.402(6)	C37-C36	1.215(13)

Table 6-4. Interatomic angles for $BaO_9C_{40}H_{44}$.

Atoms	Angle (°)	Atoms	Angle (°)
O1-Ba-O2	65.50(8)	C17-C16-C23	118.6(3)
O1-Ba-O3	142.74(8)	C16-C17-C18	118.2(4)
O1-Ba-O4	141.61(8)	C16-C17-C22	122.6(3)
O1-Ba-O5	118.52(9)	C18-C17-C22	119.2(4)
O1-Ba-O6	76.46(9)	C11-C12-C13	121.8(4)
O1-Ba-O7	72.75(9)	C16-C23-C24	125.5(4)
O1-Ba-O8	76.11(10)	C12-C11-C10	119.1(4)
O1-Ba-O9	76.62(10)	O1-C1-C8	125.4(4)
O2-Ba-O3	151.09(8)	O1-C1-C2	115.5(3)
O2-Ba-O4	88.68(8)	C8-C1-C2	119.0(4)
O2-Ba-O5	73.52(9)	O2-C9-C10	116.0(4)
O2-Ba-O6	88.00(9)	O2-C9-C8	126.5(3)
O2-Ba-O7	130.41(10)	C10-C9-C8	117.5(4)
O2-Ba-O8	128.83(10)	C24-C25-C26	123.7(4)
O2-Ba-O9	80.65(10)	C24-C25-C30	118.5(4)
O3-Ba-O4	64.11(8)	C26-C25-C30	117.7(4)
O3-Ba-O5	89.85(9)	C11-C10-C9	121.9(4)
O3-Ba-O6	103.21(8)	C11-C10-C15	119.1(4)
O3-Ba-O7	76.46(10)	C9-C10-C15	119.0(4)
O3-Ba-O8	70.44(10)	O4-C24-C23	125.2(3)
O3-Ba-O9	98.32(10)	O4-C24-C25	115.7(3)
O4-Ba-O5	76.49(10)	C23-C24-C25	119.1(4)
O4-Ba-O6	133.16(10)	C17-C18-C19	120.7(4)
O4-Ba-O7	140.53(10)	C1-C8-C9	126.4(4)
O4-Ba-O8	102.92(10)	C2-C7-C6	119.8(4)
O4-Ba-O9	71.27(10)	C10-C15-C14	120.9(4)
O5-Ba-O6	57.85(11)	C1-C2-C7	123.1(4)
O5-Ba-O7	106.35(10)	C1-C2-C3	118.6(4)
O5-Ba-O8	157.59(10)	C7-C2-C3	118.3(4)
O5-Ba-O9	138.78(11)	C25-C26-C27	120.4(4)
O6-Ba-O7	56.34(11)	C17-C22-C21	120.1(4)
O6-Ba-O8	115.13(11)	C25-C30-C29	121.8(4)
O6-Ba-O9	153.08(10)	C18-C19-C20	118.7(4)
O7-Ba-O8	59.68(11)	C3-C4-C5	120.7(5)
O7-Ba-O9	114.86(10)	C22-C21-C20	119.5(4)
O8-Ba-O9	57.80(11)	C26-C27-C28	121.2(4)
Ba-O1-C1	137.03(24)	C2-C3-C4	120.7(5)
Ba-O2-C9	138.25(24)	O6-C33-C32	108.7(4)
Ba-O3-C16	135.76(23)	C19-C20-C21	121.8(4)
Ba-O4-C24	140.19(23)	C4-C5-C6	118.8(5)
Ba-O5-C31	116.8(3)	C30-C29-C28	120.0(4)
Ba-O5-C32	111.7(3)	C15-C14-C13	119.5(5)
C31-O5-C32	112.1(4)	C7-C6-C5	121.7(5)
Ba-O6-C33	118.1(3)	O6-C34-C35	110.1(4)
Ba-O6-C34	121.2(3)	O7-C35-C34	108.0(5)
C33-O6-C34	112.0(4)	C12-C13-C14	119.4(4)
Ba-O7-C35	112.7(3)	C27-C28-C29	118.8(4)
Ba-O7-C36	112.3(4)	O5-C32-C33	109.1(5)
C35-O7-C36	114.8(6)	O9-C39-C38	111.6(5)
Ba-O8-C37	114.2(4)	C44a-C43-C42	122.6(9)
Ba-O8-C38	116.2(3)	C43a-C44-C42	120.7(12)
C37-O8-C38	123.0(6)	O8-C37-C36	123.3(7)
Ba-O9-C39	117.7(3)	O8-C38-C39	115.3(6)
Ba-O9-C40	120.5(3)	O7-C36-C37	124.0(7)
C39-O9-C40	111.9(5)	C43-C42-C41	119.1(14)
O3-C16-C17	115.9(3)	C43-C42-C44	116.7(10)
O3-C16-C23	125.3(3)	C41-C42-C44	124.2(16)

Barium *bis*(2,2-dimethylhexane-3,5-dionate) tetraglyme

Prepared by: Henry Luten

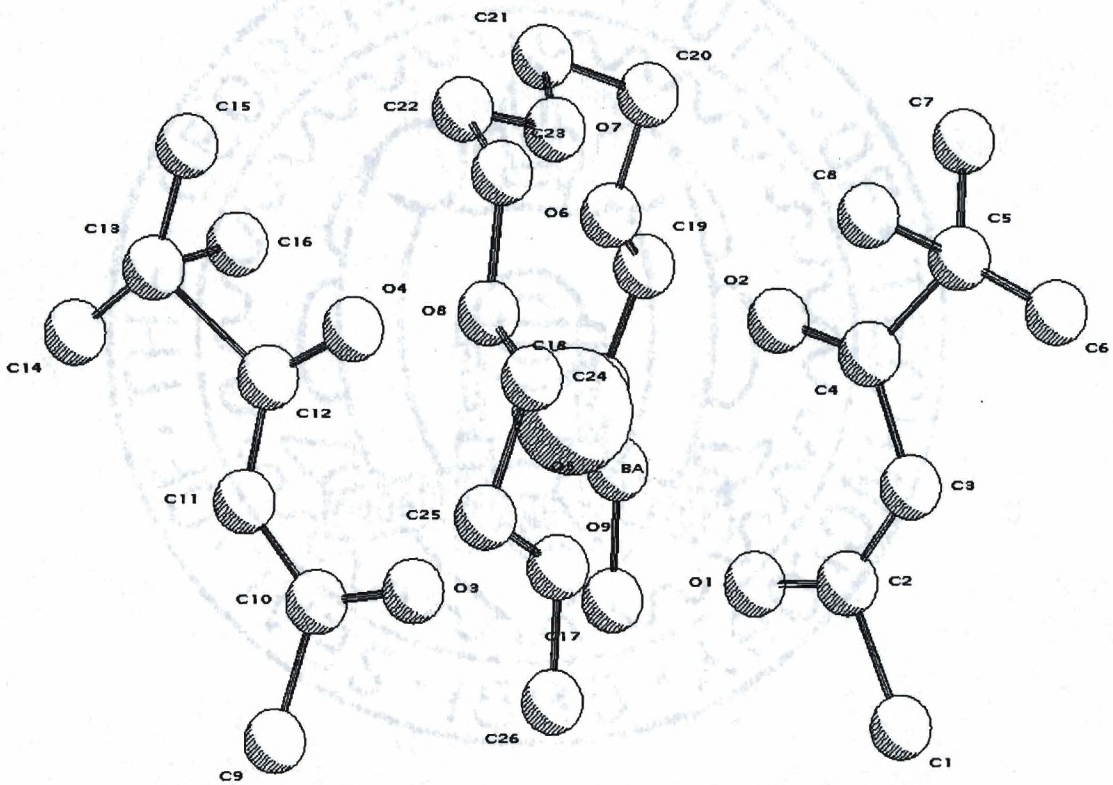

Figure 6-2. PLUTO plot of $Ba(dmhd)_2$•tetraglyme*.

*Note: Due to crystal decompostition in the beam, insufficient data was collected to perform anisotropic refinement; therefore isotropic refinement only was used.

Table 6-5. Unit cell and data collection parameters for $BaO_9C_{26}H_{48}$.

Empirical Formula	$BaO_9C_{26}H_{48}$
Formula Weight	593.60 g/mol.
Temperature	293(2) K
Wavelength	0.71073 Å
Crystal System	monoclinic
Space Group	C2/c
Unit Cell Dimensions	a = 48.821(13) Å
	b = 7.8662(22) Å β = 109.764(3)°
	c = 17.923(4) Å
Volume	6478(3) $Å^3$
Z	8
Density (calc'd)	1.217 g/cc
Absorption Coefficient	10.06 mm^{-1}
F(000)	2273.46
θ Range for Data Collection	2.29° to 72.0°
Index Ranges	$-60 \leq h \leq 56$, $0 \leq k \leq 9$, $0 \leq l \leq 22$
Reflections Collected	4353
Independent Reflections	3136
Refinement Method	Full-matrix least-squares on F^2
Data / Restraints / Parameters	2301 / 0 / 145
Goodness of Fit on F^2	10.13
Final R Indices [$I>2\sigma(I)$]	$R = 0.101$, $R_w = 0.090$
R Indices (all data)	$R = 0.101$, $R_w = 0.090$
Largest Difference Peak and Hole	1.950 and -1.590 e/$Å^3$

Table 6-6. Atomic coordinates for $BaO_9C_{26}H_{48}$.

	x	y	z	Biso (Å^2)
BA	0.37232(3)	0.0788(3)	0.40012(9)	3.82(4)
O1	0.3404 (3)	-0.074 (3)	0.2612 (8)	3.6 (3)
O2	0.3241 (3)	-0.060 (3)	0.3997 (8)	4.2 (4)
O3	0.4096 (3)	0.203 (3)	0.3363 (9)	5.8 (5)
O4	0.4217 (3)	0.212 (3)	0.5020 (9)	4.7 (4)
O5	0.4051 (3)	-0.214 (3)	0.3894 (11)	6.3 (5)
O6	0.3968 (4)	-0.185 (3)	0.5302 (12)	7.7 (6)
O7	0.3654 (3)	0.118 (4)	0.5596 (10)	6.4 (5)
O8	0.3486 (3)	0.391 (3)	0.4440 (10)	6.6 (5)
O9	0.3397 (4)	0.341 (3)	0.2845 (12)	7.1 (6)
C1	0.3032 (4)	-0.121 (4)	0.1384 (14)	5.2 (7)
C2	0.3130 (5)	-0.093 (4)	0.2335 (13)	4.4 (6)
C3	0.2919 (4)	-0.107 (4)	0.2681 (13)	3.8 (5)
C4	0.2987 (5)	-0.084 (5)	0.3538 (14)	4.9 (6)
C5	0.2722 (6)	-0.118 (5)	0.3820 (19)	7.2 (9)
C6	0.2444 (6)	-0.135 (5)	0.3216 (18)	9.0 (10)
C7	0.2815 (6)	-0.203 (5)	0.4570 (22)	11.2 (12)
C8	0.2707 (6)	0.075 (5)	0.4120 (18)	8.9 (10)
C9	0.4495 (5)	0.262 (4)	0.2907 (14)	5.3 (7)
C10	0.4363 (5)	0.237 (4)	0.3579 (15)	5.3 (7)
C11	0.4564 (5)	0.244 (4)	0.4374 (14)	4.6 (6)
C12	0.4475 (5)	0.232 (4)	0.5008 (14)	4.3 (6)
C13	0.4724 (6)	0.295 (5)	0.5918 (18)	7.3 (9)
C14	0.4995 (6)	0.296 (5)	0.5815 (18)	9.6 (11)
C15	0.4578 (6)	0.300 (5)	0.6489 (20)	10.7 (12)
C16	0.4776 (6)	0.085 (6)	0.6040 (19)	11.4 (12)
C17	0.4150 (5)	-0.245 (5)	0.3210 (16)	7.1 (9)
C18	0.4235 (6)	-0.305 (5)	0.4534 (19)	7.9 (10)
C19	0.4080 (7)	-0.319 (6)	0.5069 (21)	10.5 (13)
C20	0.3796 (7)	-0.173 (6)	0.5843 (22)	10.1 (12)
C21	0.3853 (6)	0.006 (5)	0.6184 (18)	7.7 (10)
C22	0.3656 (6)	0.305 (6)	0.5780 (20)	9.3 (13)
C23	0.3407 (6)	0.391 (5)	0.5182 (17)	7.1 (8)
C24	0.3243 (5)	0.463 (5)	0.3840 (17)	7.0 (8)
C25	0.3385 (7)	0.492 (5)	0.3177 (21)	10.0 (13)
C26	0.3464 (5)	0.330 (4)	0.2121 (17)	7.2 (9)

Table 6-7. Interatomic distances for $BaO_9C_{26}H_{48}$.

Atoms	Dist. (Å)	Atoms	Dist. (Å)
BA-O1	2.729(15)	O9-C25	1.34(5)
BA-O2	2.594(15)	O9-C26	1.44(4)
BA-O3	2.641(16)	C1-C2	1.62(3)
BA-O4	2.694(15)	C2-C3	1.38(3)
BA-O5	2.846(21)	C3-C4	1.47(3)
BA-O6	3.050(21)	C4-C5	1.56(4)
BA-O7	3.005(18)	C5-C6	1.43(4)
BA-O8	2.932(22)	C5-C7	1.43(5)
BA-O9	2.975(21)	C5-C8	1.62(6)
O1-C2	1.270(24)	C9-C10	1.56(3)
O2-C4	1.25(3)	C10-C11	1.43(3)
O3-C10	1.26(3)	C11-C12	1.35(3)
O4-C12	1.28(3)	C12-C13	1.74(4)
O5-C17	1.48(3)	C13-C14	1.39(4)
O5-C18	1.39(4)	C13-C15	1.43(5)
O6-C19	1.31(5)	C13-C16	1.67(6)
O6-C20	1.49(4)	C18-C19	1.41(5)
O7-C21	1.46(4)	C20-C21	1.52(6)
O7-C22	1.51(6)	C22-C23	1.48(5)
O8-C23	1.50(3)	C24-C25	1.58(4)
O8-C24	1.42(3)		

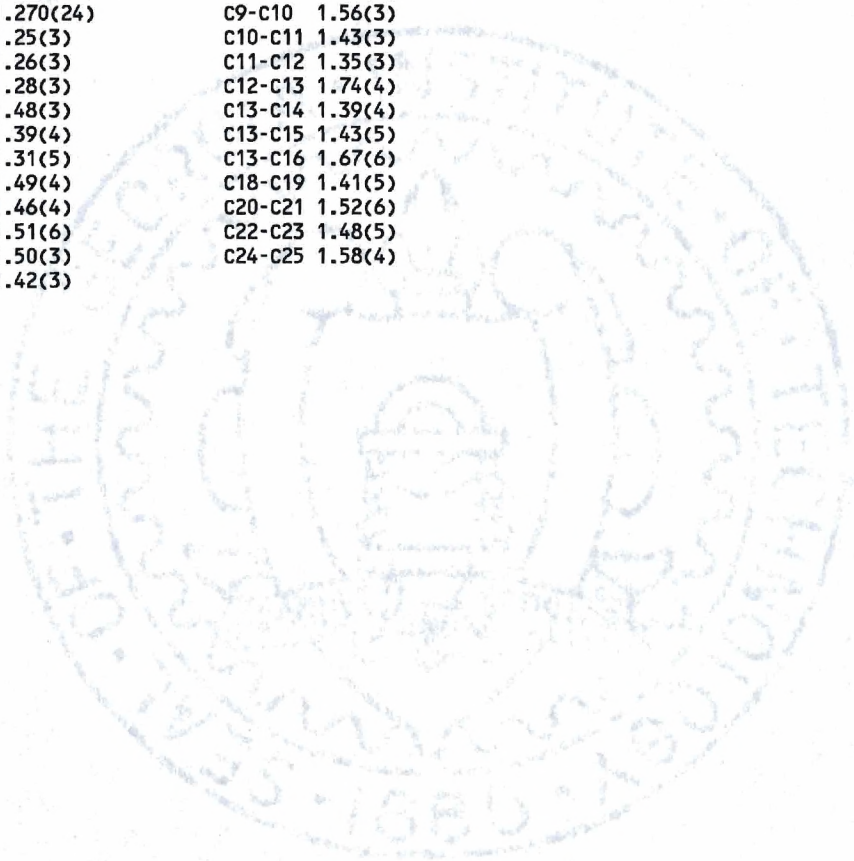

Table 6-8. Interatomic angles for $BaO_9C_{26}H_{48}$.

Atoms	Angle (°)	Atoms	Angle (°)
O1-BA-O2	64.8(4)	C19-O6-C20	130(3)
O1-BA-O3	91.8(5)	BA-O7-C21	111.3(16)
O1-BA-O4	153.3(4)	BA-O7-C22	108.3(16)
O1-BA-O5	75.1(5)	C21-O7-C22	118.5(23)
O1-BA-O6	110.6(6)	BA-O8-C23	118.8(18)
O1-BA-O7	134.4(5)	BA-O8-C24	115.9(16)
O1-BA-O8	117.2(5)	C23-O8-C24	105.7(19)
O1-BA-O9	70.3(6)	BA-O9-C25	113.4(18)
O2-BA-O3	155.8(5)	BA-O9-C26	110.7(17)
O2-BA-O4	140.2(4)	C25-O9-C26	120(3)
O2-BA-O5	101.0(6)	O1-C2-C1	108.9(17)
O2-BA-O6	80.6(5)	O1-C2-C3	133.2(20)
O2-BA-O7	69.6(5)	C1-C2-C3	117.7(18)
O2-BA-O8	84.9(6)	C2-C3-C4	121.6(19)
O2-BA-O9	91.0(5)	O2-C4-C3	122.1(20)
O3-BA-O4	64.0(5)	O2-C4-C5	124.0(22)
O3-BA-O5	77.6(6)	C3-C4-C5	113.4(21)
O3-BA-O6	115.7(5)	C4-C5-C6	116(3)
O3-BA-O7	133.6(6)	C4-C5-C7	110.4(24)
O3-BA-O8	101.5(6)	C4-C5-C8	94(3)
O3-BA-O9	74.1(5)	C6-C5-C7	125(3)
O4-BA-O5	88.0(5)	C6-C5-C8	101(3)
O4-BA-O6	73.6(6)	C7-C5-C8	99(3)
O4-BA-O7	71.2(5)	O3-C10-C9	116.4(21)
O4-BA-O8	80.7(5)	O3-C10-C11	127.3(23)
O4-BA-O9	110.4(6)	C9-C10-C11	116.1(19)
O5-BA-O6	54.3(6)	C10-C11-C12	121.8(20)
O5-BA-O7	113.2(7)	O4-C12-C11	128.5(21)
O5-BA-O8	167.6(5)	O4-C12-C13	113.6(20)
O5-BA-O9	133.9(6)	C11-C12-C13	116.5(21)
O6-BA-O7	58.9(7)	C12-C13-C14	105.8(24)
O6-BA-O8	117.0(6)	C12-C13-C15	108.4(22)
O6-BA-O9	169.8(6)	C12-C13-C16	82.6(22)
O7-BA-O8	58.5(7)	C14-C13-C15	144(3)
O7-BA-O9	112.7(7)	C14-C13-C16	85(3)
O8-BA-O9	56.0(6)	C15-C13-C16	91(3)
BA-O1-C2	127.6(14)	O5-C18-C19	104.7(25)
BA-O2-C4	139.9(16)	O6-C19-C18	121(3)
BA-O3-C10	137.7(16)	O6-C20-C21	105(3)
BA-O4-C12	134.3(15)	O7-C21-C20	106(3)
BA-O5-C17	122.6(17)	O7-C22-C23	110(3)
BA-O5-C18	125.6(17)	O8-C23-C22	104.2(22)
C17-O5-C18	107.2(21)	O8-C24-C25	99.3(20)
BA-O6-C19	113.6(19)	O9-C25-C24	107(3)
BA-O6-C20	106.9(18)		

Dicalcium *tetrakis*(tetraphenyldiphosphaiminate)•H_2O

Prepared by: Debrah A. Moreno

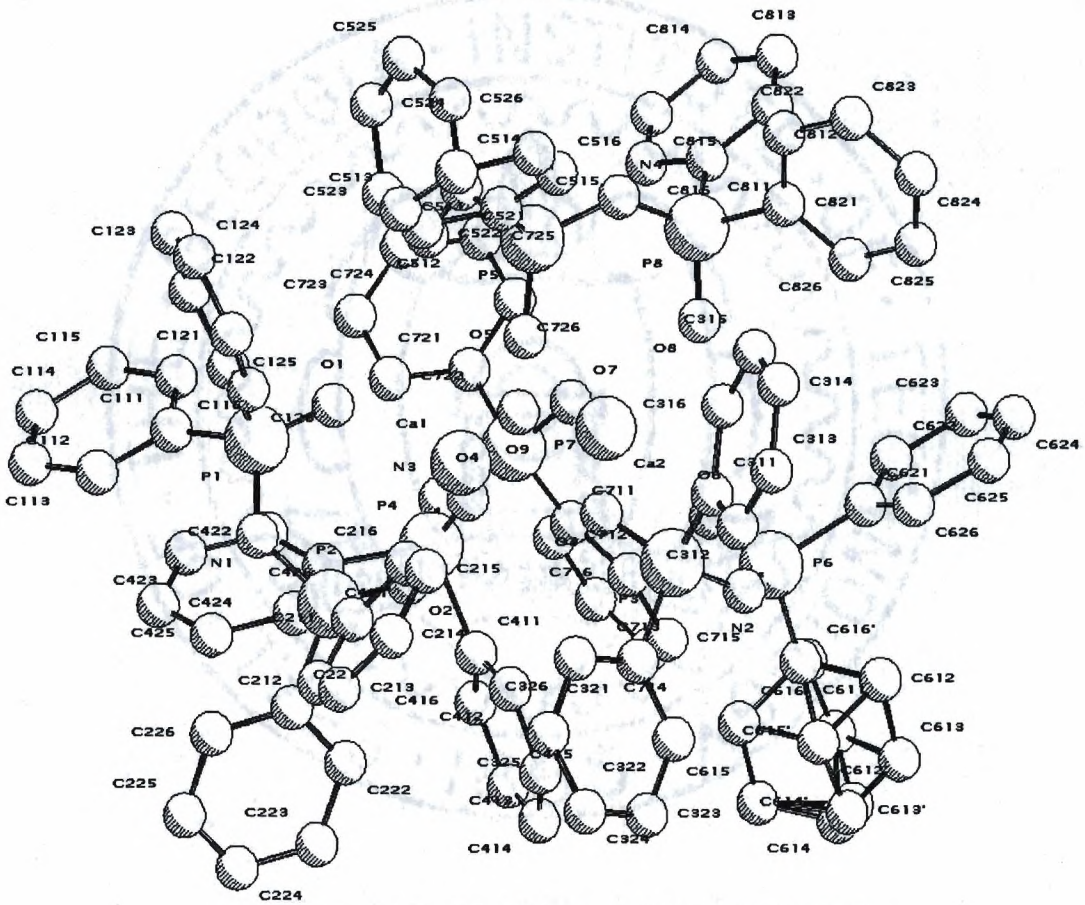

Figure 6-3. PLUTO plot of $Ca_2(tpdtpi)_4•H_2O$

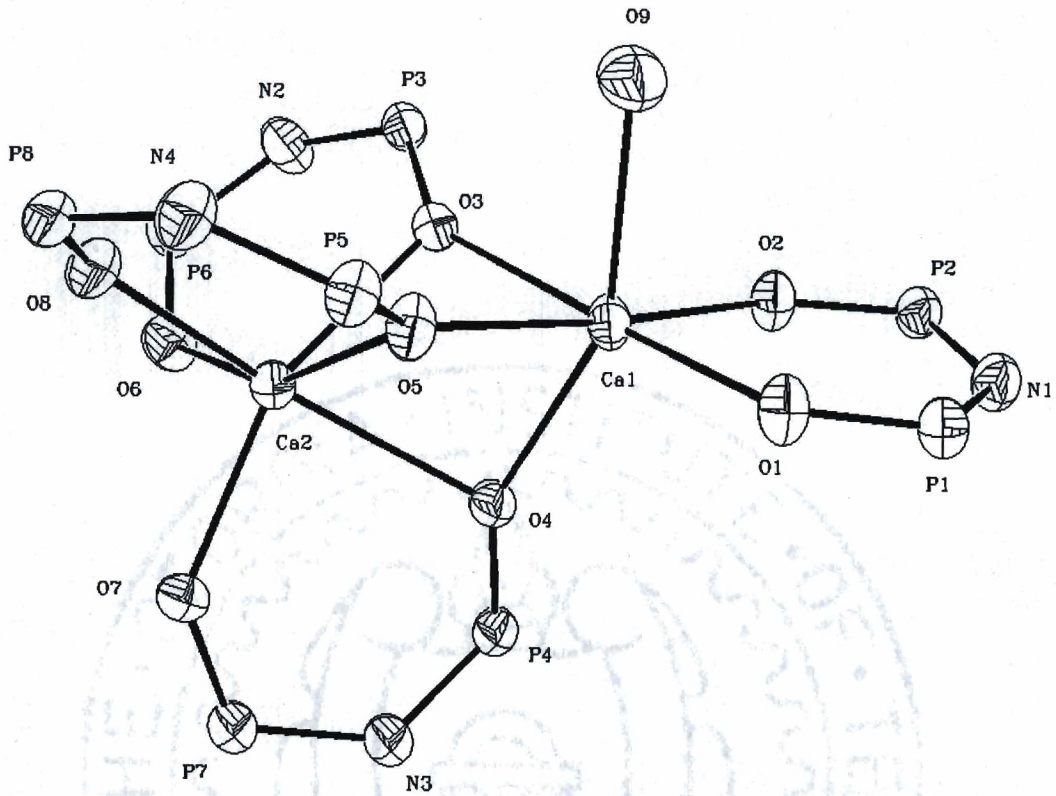

Figure 6-4. ORTEP plot of the Ca_2O_9 core of $Ca_2(tpdtpi)_4 \cdot H_2O$.

Table 6-9. Unit cell and data collection parameters for $Ca_2C_{96}H_{82}N_4O_9P_8$.

Empirical Formula	$Ca_2C_{96}H_{82}N_4O_9P_8$
Formula Weight	851.67 g/mol.
Temperature	293(2) K
Wavelength	0.71073 Å
Crystal System	monoclinic
Space Group	$P2_1/n$
Unit Cell Dimensions	a = 13.598(3) Å
	b = 26.712(4) Å β = 90.818(13)°
	c = 24.635(3) Å
Volume	8947.5(24) $Å^3$
Z	8
Density (calc'd)	1.308 g/cc
Absorption Coefficient	2.95 mm^{-1}
F(000)	3685.00
θ Range for Data Collection	2.29° to74.8°
Index Ranges	$-17 \leq h \leq 17$, $0 \leq k \leq 33$, $0 \leq l \leq 30$
Reflections Collected	21691
Independent Reflections	18382
Refinement Method	Full-matrix least-squares on F^2
Data / Restraints / Parameters	10816 / 0 / 1106
Goodness of Fit on F^2	1.71
Final R Indices [$I>2\sigma(I)$]	$R = 0.050$, $R_w = 0.058$
R Indices (all data)	$R = 0.094$, $R_w = 0.064$
Largest Difference Peak and Hole	0.330 and -0.280 e/$Å^3$

Table 6-10. Atomic coordinates for $Ca_2C_{96}H_{82}N_4O_9P_8$.

	x	y	z	Biso (Å^2)
Ca1	0.23702(8)	0.17281(4)	0.33133(4)	3.55(4)
Ca2	0.20803(6)	0.06804(3)	0.25403(3)	3.10(3)
P1	0.22616(9)	0.22952(4)	0.45957(4)	3.79(4)
P2	0.38986(9)	0.26030(4)	0.39573(4)	3.66(4)
P3	0.31629(9)	0.17023(4)	0.18396(4)	3.64(4)
P4	0.37353(9)	0.05684(4)	0.36602(4)	3.63(4)
P5	-0.01222(8)	0.12037(4)	0.30585(4)	3.73(4)
P6	0.33445(10)	0.07199(4)	0.13425(4)	3.92(4)
P7	0.27788(10)	-0.03378(4)	0.33214(5)	4.08(5)
P8	-0.03459(8)	0.06554(4)	0.20545(4)	3.48(4)
O1	0.18626(23)	0.19454(11)	0.41634(11)	4.43(13)
O2	0.36481(23)	0.22386(11)	0.35101(11)	4.23(12)
O3	0.27816(22)	0.15123(9)	0.23779(10)	3.56(12)
O4	0.30266(20)	0.09316(9)	0.33813(10)	3.42(11)
O5	0.09931(21)	0.12310(11)	0.30444(11)	4.02(12)
O6	0.29925(24)	0.04365(11)	0.18287(11)	4.29(13)
O7	0.20916(24)	-0.00912(10)	0.29202(11)	4.23(13)
O8	0.07373(21)	0.05748(11)	0.19949(11)	3.88(12)
O9	0.1485 (3)	0.24052(13)	0.28436(15)	6.16(18)
N1	0.3252 (3)	0.25816(13)	0.44850(13)	3.95(15)
N2	0.3488 (3)	0.13059(13)	0.14071(14)	5.05(19)
N3	0.3371 (3)	0.00127(12)	0.37268(14)	4.48(17)
N4	-0.0680 (3)	0.10082(14)	0.25349(13)	4.17(15)
C111	0.2398 (4)	0.19562(17)	0.52240(17)	4.34(20)
C112	0.2931 (4)	0.21638(20)	0.56556(19)	5.27(24)
C113	0.3018 (5)	0.1913 (3)	0.61466(21)	6.8 (3)
C114	0.2576 (7)	0.1465 (3)	0.6211 (3)	8.9 (4)
C115	0.2027 (7)	0.1258 (3)	0.5800 (3)	10.0 (5)
C116	0.1938 (5)	0.15023(22)	0.53011(23)	7.3 (3)
C121	0.1335 (4)	0.27636(20)	0.47464(19)	4.87(22)
C122	0.0550 (5)	0.2665 (3)	0.5064 (3)	8.3 (4)
C123	-0.0187 (6)	0.3029 (4)	0.5155 (3)	9.8 (5)
C124	-0.0102 (8)	0.3479 (4)	0.4916 (5)	11.9 (7)
C125	0.0688 (7)	0.3587 (3)	0.4604 (5)	12.5 (7)
C126	0.1403 (5)	0.32352(24)	0.4519 (3)	7.9 (4)
C211	0.3837 (4)	0.32348(16)	0.36894(17)	4.43(20)
C212	0.4489 (5)	0.36025(21)	0.3813 (3)	7.5 (3)
C213	0.4376 (7)	0.40788(24)	0.3591 (4)	9.9 (5)
C214	0.3649 (8)	0.41884(25)	0.3256 (3)	9.4 (5)
C215	0.2975 (8)	0.3829 (3)	0.3125 (3)	10.3 (5)
C216	0.3073 (6)	0.33552(23)	0.3342 (3)	8.3 (4)
C221	0.5162 (4)	0.25222(18)	0.41606(20)	4.73(21)
C222	0.5785 (5)	0.22665(24)	0.38150(25)	6.5 (3)
C223	0.6780 (5)	0.2189 (3)	0.3972 (4)	8.9 (4)
C224	0.7113 (5)	0.2386 (4)	0.4455 (4)	9.8 (5)
C225	0.6514 (6)	0.2649 (3)	0.4791 (3)	8.5 (4)
C226	0.5530 (4)	0.27111(23)	0.46484(22)	6.2 (3)
C311	0.2198 (4)	0.20875(15)	0.15475(16)	4.01(19)
C312	0.2375 (4)	0.25332(19)	0.12820(23)	5.9 (3)
C313	0.1603 (6)	0.27976(23)	0.1041 (3)	7.7 (4)
C314	0.0669 (5)	0.26275(24)	0.1075 (3)	7.3 (3)
C315	0.0476 (4)	0.21842(22)	0.13316(24)	6.3 (3)
C316	0.1237 (4)	0.19167(19)	0.15582(21)	5.26(23)
C321	0.4204 (4)	0.21116(17)	0.19429(17)	4.17(19)
C322	0.5051 (5)	0.20457(23)	0.1668 (3)	7.5 (3)
C323	0.5853 (5)	0.2366 (3)	0.1750 (4)	9.5 (5)
C324	0.5782 (5)	0.2753 (3)	0.2099 (3)	8.0 (4)
C325	0.4937 (5)	0.28374(24)	0.23778(23)	7.2 (3)
C326	0.4144 (5)	0.25149(22)	0.22944(20)	6.3 (3)
C411	0.4869 (4)	0.05999(20)	0.32883(18)	4.72(21)
C412	0.5085 (5)	0.1003 (3)	0.29717(24)	7.6 (3)

C413	0.5973 (6)	0.1038 (4)	0.2715 (3)	11.8 (6)
C414	0.6644 (6)	0.0654 (5)	0.2760 (3)	10.6 (6)
C415	0.6433 (5)	0.0246 (3)	0.3057 (4)	9.3 (5)
C416	0.5557 (5)	0.02146(24)	0.3330 (3)	7.2 (3)
C421	0.4069 (4)	0.07705(16)	0.43338(17)	4.36(20)
C422	0.3894 (8)	0.04839(24)	0.47763(23)	10.6 (5)
C423	0.4202 (10)	0.0623 (3)	0.52827(24)	14.1 (8)
C424	0.4695 (7)	0.1051 (3)	0.53621(23)	8.7 (4)
C425	0.4851 (6)	0.1345 (3)	0.4939 (3)	8.9 (4)
C426	0.4519 (6)	0.12094(23)	0.44273(22)	8.2 (4)
C511	-0.0612 (3)	0.18202(17)	0.31807(19)	4.32(19)
C512	-0.0367 (4)	0.20837(21)	0.36518(22)	5.9 (3)
C513	-0.0687 (5)	0.25732(24)	0.3726 (3)	7.0 (3)
C514	-0.1274 (6)	0.27911(23)	0.3338 (3)	8.5 (4)
C515	-0.1530 (6)	0.25392(25)	0.2870 (3)	8.1 (4)
C516	-0.1186 (5)	0.20541(21)	0.27912(22)	6.1 (3)
C521	-0.0457 (4)	0.08219(20)	0.36299(18)	4.97(23)
C522	0.0236 (6)	0.0518 (3)	0.38781(23)	8.8 (4)
C523	-0.0051 (10)	0.0167 (4)	0.4259 (3)	12.4 (7)
C524	-0.1028 (11)	0.0129 (4)	0.4398 (3)	12.4 (8)
C525	-0.1703 (7)	0.0434 (4)	0.4161 (3)	10.3 (5)
C526	-0.1422 (5)	0.0773 (3)	0.37682(23)	7.1 (3)
C621	0.2543 (4)	0.06030(19)	0.07671(19)	4.85(22)
C622	0.2130 (5)	0.01269(23)	0.07012(23)	6.7 (3)
C623	0.1547 (6)	0.0030 (3)	0.0243 (3)	9.2 (4)
C624	0.1380 (6)	0.0388 (4)	-0.0138 (3)	9.7 (6)
C625	0.1761 (6)	0.0847 (4)	-0.0075 (3)	8.6 (4)
C626	0.2348 (5)	0.09640(24)	0.03817(21)	6.4 (3)
C711	0.3657 (4)	-0.07107(18)	0.29555(21)	5.24(24)
C712	0.3995 (6)	-0.1163 (3)	0.3137 (3)	9.4 (4)
C713	0.4714 (9)	-0.1421 (4)	0.2865 (5)	13.1 (7)
C714	0.5138 (9)	-0.1215 (4)	0.2441 (5)	14.2 (8)
C715	0.4843 (9)	-0.0764 (4)	0.2250 (4)	13.4 (7)
C716	0.4087 (6)	-0.05167(24)	0.2506 (3)	8.6 (4)
C721	0.2109 (4)	-0.07675(16)	0.37366(19)	4.99(23)
C722	0.2365 (6)	-0.08412(20)	0.42760(22)	7.0 (3)
C723	0.1813 (8)	-0.1165 (3)	0.4600 (3)	9.2 (5)
C724	0.1034 (7)	-0.1418 (3)	0.4378 (4)	9.6 (5)
C725	0.0782 (6)	-0.1355 (3)	0.3841 (3)	8.5 (4)
C726	0.1322 (5)	-0.10289(22)	0.35179(25)	6.8 (3)
C811	-0.0940 (3)	0.00542(17)	0.21305(17)	4.13(18)
C812	-0.1589 (5)	-0.01401(21)	0.17550(22)	6.3 (3)
C813	-0.2012 (6)	-0.06059(24)	0.1834 (3)	8.8 (4)
C814	-0.1760 (6)	-0.08841(24)	0.2281 (3)	8.3 (4)
C815	-0.1120 (6)	-0.06946(24)	0.2656 (3)	7.7 (3)
C816	-0.0705 (5)	-0.02327(20)	0.25852(20)	6.0 (3)
C821	-0.0843 (3)	0.09272(15)	0.14365(16)	3.73(17)
C822	-0.1733 (4)	0.11815(20)	0.14336(19)	4.99(22)
C823	-0.2083 (4)	0.14072(22)	0.09573(24)	6.3 (3)
C824	-0.1550 (5)	0.13777(21)	0.04926(22)	6.2 (3)
C825	-0.0673 (5)	0.11276(21)	0.04964(19)	5.7 (3)
C826	-0.0315 (4)	0.08992(18)	0.09664(17)	4.53(21)

Figure 6-11. Interatomic distances for $Ca_2C_{96}H_{82}N_4O_9P_8$.

Atoms	Dist. (Å)	Atoms	Dist. (Å)
Ca1-Ca2	3.4049(12)	C324-C325	1.367(11)
Ca1-O1	2.289(3)	C325-C326	1.393(8)
Ca1-O2	2.256(3)	C411-C412	1.364(9)
Ca1-O3	2.448(3)	C411-C416	1.393(8)
Ca1-O4	2.312(3)	C412-C413	1.374(10)
Ca1-O5	2.382(3)	C413-C414	1.376(15)
Ca1-O9	2.454(4)	C414-C415	1.345(16)
Ca2-O3	2.453(3)	C415-C416	1.379(11)
Ca2-O4	2.514(3)	C421-C422	1.356(7)
Ca2-O5	2.438(3)	C421-C426	1.341(7)
Ca2-O6	2.258(3)	C422-C423	1.361(9)
Ca2-O7	2.264(3)	C423-C424	1.340(12)
Ca2-O8	2.269(3)	C424-C425	1.325(10)
P1-O1	1.512(3)	C425-C426	1.381(8)
P1-N1	1.576(4)	C511-C512	1.394(7)
P1-C111	1.800(5)	C511-C516	1.378(8)
P1-C121	1.818(5)	C512-C513	1.391(8)
P2-O2	1.506(3)	C513-C514	1.366(12)
P2-N1	1.581(4)	C514-C515	1.376(11)
P2-C211	1.813(4)	C515-C516	1.393(9)
P2-C221	1.795(5)	C521-C522	1.380(9)
P3-O3	1.518(3)	C521-C526	1.368(8)
P3-N2	1.570(4)	C522-C523	1.387(12)
P3-C311	1.809(5)	C523-C524	1.379(19)
P3-C321	1.804(5)	C524-C525	1.354(17)
P4-O4	1.524(3)	C525-C526	1.383(10)
P4-N3	1.574(4)	C621-C622	1.399(8)
P4-C411	1.807(5)	C621-C626	1.376(8)
P4-C421	1.797(4)	C622-C623	1.395(10)
P5-O5	1.519(3)	C623-C624	1.356(15)
P5-N4	1.576(4)	C624-C625	1.341(15)
P5-C511	1.803(5)	C625-C626	1.405(9)
P5-C521	1.802(5)	C711-C712	1.365(9)
P6-O6	1.501(3)	C711-C716	1.363(10)
P6-N2	1.585(4)	C712-C713	1.378(13)
P6-C621	1.803(5)	C713-C714	1.320(18)
P6-C611	1.772(4)	C714-C715	1.354(16)
P7-O7	1.502(3)	C715-C716	1.382(12)
P7-N3	1.581(4)	C721-C722	1.383(7)
P7-C711	1.806(5)	C721-C726	1.381(8)
P7-C721	1.795(5)	C722-C723	1.401(10)
P8-O8	1.498(3)	C723-C724	1.364(14)
P8-N4	1.585(4)	C724-C725	1.372(13)
P8-C811	1.809(5)	C725-C726	1.396(10)
P8-C821	1.809(4)	C811-C812	1.371(7)
C111-C112	1.394(7)	C811-C816	1.391(6)
C111-C116	1.378(7)	C812-C813	1.386(8)
C112-C113	1.386(7)	C813-C814	1.368(10)
C113-C114	1.350(11)	C814-C815	1.358(10)
C114-C115	1.366(13)	C815-C816	1.369(8)
C115-C116	1.395(9)	C821-C822	1.388(7)
C121-C122	1.358(8)	C821-C826	1.373(6)
C121-C126	1.383(9)	C822-C823	1.397(7)
C122-C123	1.416(11)	C823-C824	1.366(9)
C123-C124	1.343(17)	C824-C825	1.367(9)
C124-C125	1.361(17)	C825-C826	1.391(7)
C125-C126	1.372(11)	C612'-C613'	1.379(18)
C211-C212	1.356(8)	C612'-C611	1.349(11)
C211-C216	1.374(8)	C612'-C612	1.640(12)
C212-C213	1.393(9)	C612'-C616	1.486(12)
C213-C214	1.312(14)	C613'-C614'	1.32(4)

C214-C215	1.362(14)	C613'-C613	1.385(21)
C215-C216	1.380(9)	C613'-C614	0.958(21)
C221-C222	1.389(8)	C613'-C615	1.563(18)
C221-C226	1.390(7)	C614'-C615'	1.31(3)
C222-C223	1.418(10)	C614'-C613	1.179(18)
C223-C224	1.371(14)	C614'-C614	0.51(4)
C224-C225	1.364(14)	C614'-C615	1.73(3)
C225-C226	1.389(9)	C615'-C616'	1.400(17)
C311-C312	1.381(6)	C615'-C613	1.672(18)
C311-C316	1.385(7)	C615'-C614	1.707(19)
C312-C313	1.390(9)	C616'-C611	1.510(12)
C313-C314	1.353(11)	C616'-C612	1.673(13)
C314-C315	1.369(9)	C611-C612	1.395(6)
C315-C316	1.369(8)	C611-C616	1.395(7)
C321-C322	1.355(8)	C612-C613	1.395(10)
C321-C326	1.385(7)	C613-C614	1.395(10)
C322-C323	1.399(10)	C614-C615	1.395(14)
C323-C324	1.348(11)	C615-C616	1.395(9)

Figure 6-12. Interatomic angles for $Ca_2C_{96}H_{82}N_4O_9P_8$.

Atoms	Angle (°)	Atoms	Angle (°)
Ca2-Ca1-O1	133.31(9)	C324-C325-C326	118.6(6)
Ca2-Ca1-O2	134.40(8)	C321-C326-C325	121.4(5)
Ca2-Ca1-O3	46.06(6)	P4-C411-C412	121.2(4)
Ca2-Ca1-O4	47.60(7)	P4-C411-C416	120.3(4)
Ca2-Ca1-O5	45.73(7)	C412-C411-C416	118.4(5)
Ca2-Ca1-O9	106.86(9)	C411-C412-C413	120.9(7)
O1-Ca1-O2	83.78(11)	C412-C413-C414	119.9(8)
O1-Ca1-O3	175.45(12)	C413-C414-C415	120.1(7)
O1-Ca1-O4	106.75(11)	C414-C415-C416	120.5(7)
O1-Ca1-O5	98.60(11)	C411-C416-C415	120.1(7)
O1-Ca1-O9	95.29(12)	P4-C421-C422	121.9(4)
O2-Ca1-O3	99.15(10)	P4-C421-C426	122.0(4)
O2-Ca1-O4	104.20(11)	C422-C421-C426	116.1(5)
O2-Ca1-O5	175.40(11)	C421-C422-C423	121.9(6)
O2-Ca1-O9	91.56(12)	C422-C423-C424	120.9(6)
O3-Ca1-O4	76.02(9)	C423-C424-C425	118.5(5)
O3-Ca1-O5	78.24(10)	C424-C425-C426	120.6(6)
O3-Ca1-O9	81.19(11)	C421-C426-C425	122.0(5)
O4-Ca1-O5	78.95(10)	P5-C511-C512	121.0(4)
O4-Ca1-O9	153.99(11)	P5-C511-C516	120.3(4)
O5-Ca1-O9	84.33(12)	C512-C511-C516	118.5(5)
Ca1-Ca2-O3	45.93(6)	C511-C512-C513	120.8(5)
Ca1-Ca2-O4	42.78(6)	C512-C513-C514	119.3(5)
Ca1-Ca2-O5	44.39(7)	C513-C514-C515	121.1(6)
Ca1-Ca2-O6	127.65(8)	C514-C515-C516	119.4(6)
Ca1-Ca2-O7	121.14(8)	C511-C516-C515	120.8(5)
Ca1-Ca2-O8	121.27(8)	P5-C521-C522	120.1(5)
O3-Ca2-O4	72.37(8)	P5-C521-C526	120.2(4)
O3-Ca2-O5	77.08(10)	C522-C521-C526	119.0(5)
O3-Ca2-O6	85.16(10)	C521-C522-C523	120.0(8)
O3-Ca2-O7	153.11(11)	C522-C523-C524	119.9(9)
O3-Ca2-O8	109.11(10)	C523-C524-C525	120.0(8)
O4-Ca2-O5	74.11(9)	C524-C525-C526	120.2(8)
O4-Ca2-O6	115.87(11)	C521-C526-C525	120.8(7)
O4-Ca2-O7	84.37(9)	P6-C621-C622	119.1(4)
O4-Ca2-O8	156.79(10)	P6-C621-C626	122.0(4)
O5-Ca2-O6	155.98(11)	C622-C621-C626	118.9(5)
O5-Ca2-O7	109.84(11)	C621-C622-C623	119.1(6)
O5-Ca2-O8	83.56(10)	C622-C623-C624	121.0(7)
O6-Ca2-O7	93.31(11)	C623-C624-C625	120.4(7)
O6-Ca2-O8	87.18(11)	C624-C625-C626	120.6(7)
O7-Ca2-O8	97.61(11)	C621-C626-C625	119.9(6)
O1-P1-N1	118.49(18)	P7-C711-C712	123.1(5)
O1-P1-C111	109.04(20)	P7-C711-C716	119.4(4)
O1-P1-C121	109.04(20)	C712-C711-C716	117.2(6)
N1-P1-C111	108.38(21)	C711-C712-C713	121.5(8)
N1-P1-C121	107.34(22)	C712-C713-C714	119.7(9)
C111-P1-C121	103.51(22)	C713-C714-C715	121.1(9)
O2-P2-N1	117.11(18)	C714-C715-C716	119.0(9)
O2-P2-C211	109.07(19)	C711-C716-C715	121.3(7)
O2-P2-C221	109.39(21)	P7-C721-C722	121.1(4)
N1-P2-C211	108.04(20)	P7-C721-C726	119.9(4)
N1-P2-C221	107.89(21)	C722-C721-C726	119.1(5)
C211-P2-C221	104.63(23)	C721-C722-C723	120.3(6)
O3-P3-N2	118.05(17)	C722-C723-C724	119.8(6)
O3-P3-C311	106.43(19)	C723-C724-C725	120.5(6)
O3-P3-C321	110.89(18)	C724-C725-C726	120.0(7)
N2-P3-C311	108.88(21)	C721-C726-C725	120.3(6)
N2-P3-C321	106.03(23)	P8-C811-C812	123.4(4)
C311-P3-C321	105.95(21)	P8-C811-C816	118.4(4)
O4-P4-N3	116.71(19)	C812-C811-C816	118.2(4)

O4-P4-C411	106.29(20)	C811-C812-C813	120.6(5)
O4-P4-C421	112.00(18)	C812-C813-C814	120.1(6)
N3-P4-C411	111.64(23)	C813-C814-C815	119.7(5)
N3-P4-C421	105.23(20)	C814-C815-C816	120.7(5)
C411-P4-C421	104.37(23)	C811-C816-C815	120.6(5)
O5-P5-N4	117.80(18)	P8-C821-C822	121.1(3)
O5-P5-C511	109.33(19)	P8-C821-C826	119.6(4)
O5-P5-C521	107.96(22)	C822-C821-C826	119.3(4)
N4-P5-C511	105.33(21)	C821-C822-C823	120.1(5)
N4-P5-C521	109.14(22)	C822-C823-C824	120.0(5)
C511-P5-C521	106.77(23)	C823-C824-C825	119.7(5)
O6-P6-N2	117.26(17)	C824-C825-C826	121.0(5)
O6-P6-C621	110.12(21)	C821-C826-C825	119.8(5)
O6-P6-C611	108.90(19)	C613'-C612'-C611	127.1(11)
N2-P6-C621	108.80(24)	C613'-C612'-C612	88.1(10)
N2-P6-C611	108.10(22)	C613'-C612'-C616	102.1(10)
C621-P6-C611	102.64(20)	C611-C612'-C612	54.6(5)
O7-P7-N3	117.54(18)	C611-C612'-C616	58.7(5)
O7-P7-C711	108.84(21)	C612-C612'-C616	101.1(7)
O7-P7-C721	109.84(23)	C612'-C613'-C614'	118.5(15)
N3-P7-C711	107.88(24)	C612'-C613'-C613	91.9(11)
N3-P7-C721	106.08(22)	C612'-C613'-C614	125.0(15)
C711-P7-C721	106.05(24)	C612'-C613'-C615	78.2(9)
O8-P8-N4	116.86(18)	C614'-C613'-C613	51.6(12)
O8-P8-C811	108.91(20)	C614'-C613'-C614	18.8(11)
O8-P8-C821	109.34(19)	C614'-C613'-C615	73.3(12)
N4-P8-C811	108.49(20)	C613-C613'-C614	70.4(13)
N4-P8-C821	106.40(20)	C613-C613'-C615	109.9(12)
C811-P8-C821	106.34(19)	C614-C613'-C615	61.8(11)
Ca1-O1-P1	133.73(18)	C613'-C614'-C615'	123.8(14)
Ca1-O2-P2	135.53(18)	C613'-C614'-C613	67.1(15)
Ca1-O3-Ca2	88.01(9)	C613'-C614'-C614	36.9(21)
Ca1-O3-P3	146.00(15)	C613'-C614'-C615	59.8(14)
Ca2-O3-P3	125.71(14)	C615'-C614'-C613	84.0(16)
Ca1-O4-Ca2	89.62(9)	C615'-C614'-C614	132(3)
Ca1-O4-P4	149.23(16)	C615'-C614'-C615	91.0(11)
Ca2-O4-P4	120.96(14)	C613-C614'-C614	103(3)
Ca1-O5-Ca2	89.88(10)	C613-C614'-C615	110.7(16)
Ca1-O5-P5	143.28(17)	C614-C614'-C615	42.2(19)
Ca2-O5-P5	126.54(15)	C614'-C615'-C616'	118.3(15)
Ca2-O6-P6	131.22(17)	C614'-C615'-C613	44.5(9)
Ca2-O7-P7	132.20(18)	C614'-C615'-C614	12.8(12)
Ca2-O8-P8	135.09(16)	C616'-C615'-C613	91.4(9)
P1-N1-P2	130.28(22)	C616'-C615'-C614	108.8(10)
P3-N2-P6	134.31(25)	C613-C615'-C614	48.8(6)
P4-N3-P7	130.59(23)	C615'-C616'-C611	121.9(10)
P5-N4-P8	131.94(25)	C615'-C616'-C612	87.7(9)
P1-C111-C112	120.1(4)	C611-C616'-C612	51.7(4)
P1-C111-C116	121.3(4)	P6-C611-C612'	131.2(5)
C112-C111-C116	118.5(4)	P6-C611-C616'	118.9(5)
C111-C112-C113	120.7(5)	P6-C611-C612	123.8(4)
C112-C113-C114	119.9(6)	P6-C611-C616	116.1(4)
C113-C114-C115	120.8(6)	C612'-C611-C616'	109.8(7)
C114-C115-C116	120.2(6)	C612'-C611-C612	73.4(5)
C111-C116-C115	120.0(6)	C612'-C611-C616	65.5(6)
P1-C121-C122	122.5(5)	C616'-C611-C612	70.2(6)
P1-C121-C126	119.6(4)	C616'-C611-C616	84.5(6)
C122-C121-C126	117.9(6)	C612-C611-C616	120.0(5)
C121-C122-C123	121.4(7)	C612'-C612-C616'	89.9(6)
C122-C123-C124	118.7(8)	C612'-C612-C611	52.0(4)
C123-C124-C125	120.8(8)	C612'-C612-C613	81.4(6)
C124-C125-C126	120.5(9)	C616'-C612-C611	58.1(5)
C121-C126-C125	120.7(7)	C616'-C612-C613	91.5(6)
P2-C211-C212	124.5(4)	C611-C612-C613	120.0(5)
P2-C211-C216	118.4(4)	C613'-C613-C614'	61.3(18)
C212-C211-C216	117.2(5)	C613'-C613-C615'	98.5(9)
C211-C212-C213	120.3(6)	C613'-C613-C612	98.6(9)

C212-C213-C214	122.0(7)	C613'-C613-C614	40.3(9)
C213-C214-C215	119.3(6)	C614'-C613-C615'	51.5(15)
C214-C215-C216	119.6(7)	C614'-C613-C612	125.6(10)
C211-C216-C215	121.6(6)	C614'-C613-C614	21.0(17)
P2-C221-C222	118.5(4)	C615'-C613-C612	88.0(6)
P2-C221-C226	121.9(4)	C615'-C613-C614	66.9(7)
C222-C221-C226	119.6(5)	C612-C613-C614	120.0(7)
C221-C222-C223	119.5(6)	C613'-C614-C614'	124.3(25)
C222-C223-C224	118.9(7)	C613'-C614-C615'	118.7(12)
C223-C224-C225	122.1(7)	C613'-C614-C613	69.3(13)
C224-C225-C226	119.4(6)	C613'-C614-C615	80.9(14)
C221-C226-C225	120.6(6)	C614'-C614-C615'	34.5(21)
P3-C311-C312	123.3(4)	C614'-C614-C613	55.1(21)
P3-C311-C316	119.0(3)	C614'-C614-C615	123.4(24)
C312-C311-C316	117.6(5)	C615'-C614-C613	64.3(7)
C311-C312-C313	120.3(5)	C615'-C614-C615	89.4(7)
C312-C313-C314	120.4(5)	C613-C614-C615	120.0(6)
C313-C314-C315	120.3(6)	C613'-C615-C614'	46.8(11)
C314-C315-C316	119.4(6)	C613'-C615-C614	37.3(8)
C311-C316-C315	121.9(5)	C613'-C615-C616	97.6(8)
P3-C321-C322	121.4(4)	C614'-C615-C614	14.4(10)
P3-C321-C326	120.4(4)	C614'-C615-C616	113.3(8)
C322-C321-C326	118.1(5)	C614-C615-C616	120.0(6)
C321-C322-C323	121.0(6)	C612'-C616-C611	55.7(5)
C322-C323-C324	119.9(6)	C612'-C616-C615	80.4(6)
C323-C324-C325	121.0(6)	C611-C616-C615	120.0(6)

Distrontium *tetrakis*(tetraphenyldiphosphaiminate)•H_2O

Prepared by: Debrah A. Moreno

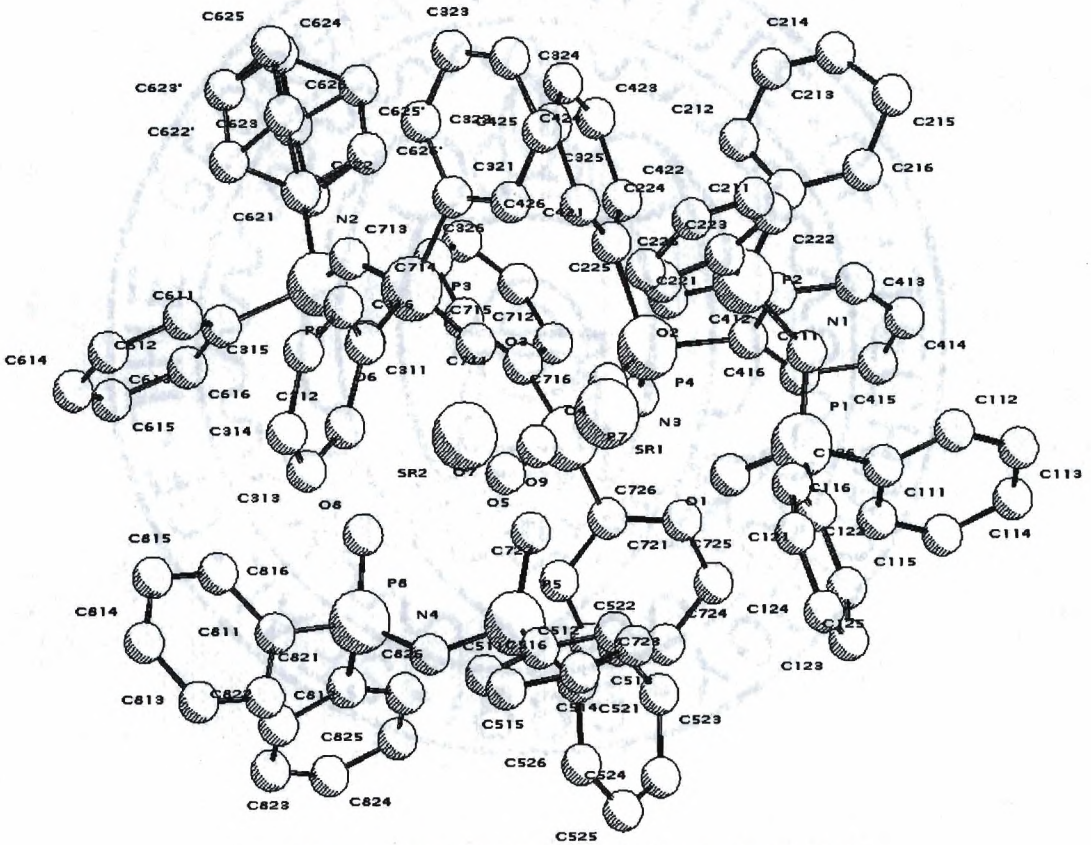

Figure 6-5. PLUTO plot of $Sr_2(tpdpi)_4•H_2O$.

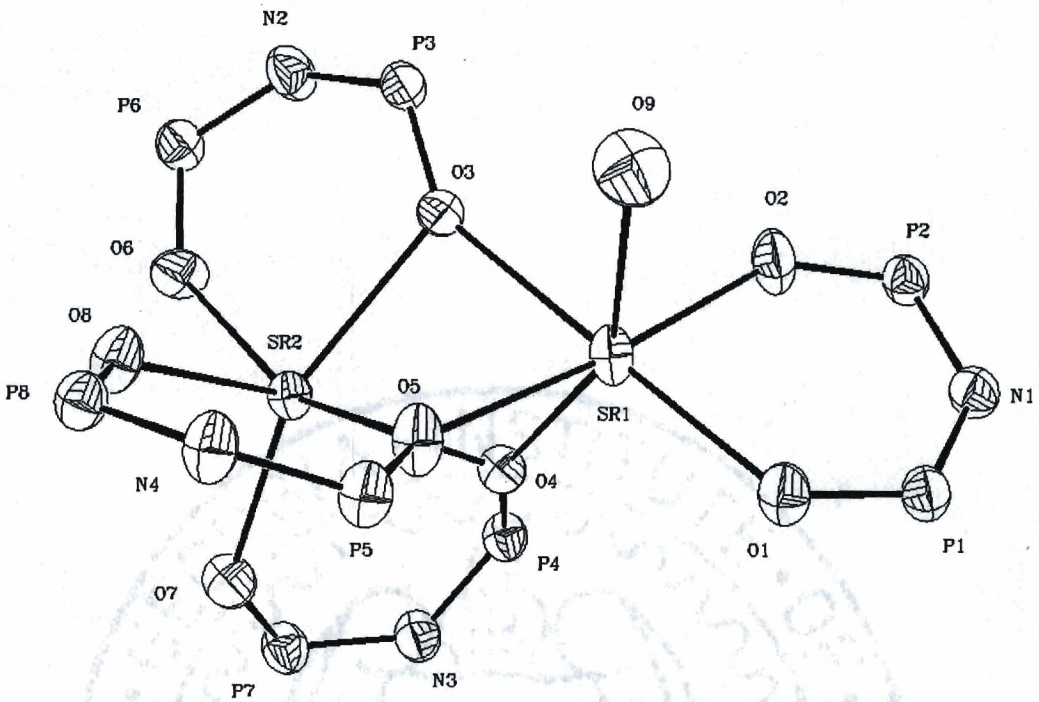

Figure 6-6. ORTEP plot of Sr_2O_9 core of $Sr_2(tpdpi)_4 \cdot H_2O$.

Table 6-13. Unit cell and data collection parameters for $Sr_2O_9N_4P_8C_{96}H_{82}$.

Empirical Formula	$Sr_2O_9N_4P_8C_{96}H_{82}$
Formula Weight	1858.24 g/mol.
Temperature	293(2) K
Wavelength	0.71073 Å
Crystal System	monoclinic
Space Group	$P2_1/n$
Unit Cell Dimensions	a = 13.6947(13) Å
	b = 26.6629(16) Å β = 90.224(11)°
	c = 25.0800(21) Å
Volume	9157.7(11) $Å^3$
Z	4
Density (calc'd)	1.348 g/cc
Absorption Coefficient	3.35 mm^{-1}
F(000)	3828.58
θ Range for Data Collection	2.29° to 74.9°
Index Ranges	$-17 \leq h \leq 17$, $0 \leq k \leq 33$, $0 \leq l \leq 31$
Reflections Collected	21303
Independent Reflections	18241
Refinement Method	Full-matrix least-squares on F^2
Data / Restraints / Parameters	12022 / 0 / 1109
Goodness of Fit on F^2	3.03
Final R Indices [$I>2\sigma(I)$]	$R = 0.056$, $R_w = 0.044$
R Indices (all data)	$R = 0.056$, $R_w = 0.044$
Largest Difference Peak and Hole	0.780 and -1.110 e/$Å^3$

Table 6-14. Atomic coordinates for $Sr_2O_9N_4P_8C_{96}H_{82}$.

	x	y	z	Biso (Å^2)
SR1	0.77172(4)	0.172374(21)	0.667188(23)	4.127(25)
SR2	0.79695(4)	0.059452(19)	0.746560(20)	3.278(21)
O1	0.8152 (3)	0.19654 (14)	0.57753 (14)	4.61 (19)
O2	0.6394 (3)	0.22865 (15)	0.64814 (15)	5.46 (21)
O3	0.7203 (3)	0.14712 (13)	0.76263 (13)	3.75 (17)
O4	0.7029 (3)	0.08704 (13)	0.65919 (14)	3.79 (17)
O5	0.9132 (3)	0.11745 (15)	0.69572 (15)	4.71 (20)
O6	0.7067 (3)	0.03548 (14)	0.82389 (15)	4.70 (20)
O7	0.7960 (3)	-0.02022 (14)	0.70333 (15)	4.82 (20)
O8	0.9405 (3)	0.05158 (15)	0.80128 (14)	4.44 (19)
O9	0.8594 (4)	0.24307 (18)	0.71969 (18)	8.2 (3)
P1	0.77344(12)	0.23328 (6)	0.53742 (6)	4.15 (7)
P2	0.61118(12)	0.26266 (6)	0.60325 (7)	4.01 (7)
P3	0.68189(12)	0.16445 (6)	0.81619 (6)	3.82 (7)
P4	0.63330(12)	0.05014 (6)	0.63251 (6)	3.92 (7)
P5	1.02405(11)	0.11495 (6)	0.69408 (7)	4.12 (7)
P6	0.66605(12)	0.06643 (6)	0.86824 (7)	4.16 (7)
P7	0.72705(13)	-0.04270 (6)	0.66279 (7)	4.47 (8)
P8	1.04817(11)	0.06089 (6)	0.79319 (6)	3.74 (7)
N1	0.6734 (3)	0.26119 (17)	0.55007 (17)	4.23 (23)
N2	0.6493 (4)	0.12374 (17)	0.85758 (19)	5.0 (3)
N3	0.6708 (4)	-0.00512 (17)	0.62461 (18)	4.71 (25)
N4	1.0795 (3)	0.09645 (17)	0.74559 (17)	4.18 (22)
C111	0.7603 (5)	0.20273 (23)	0.47501 (25)	4.6 (3)
C112	0.7058 (5)	0.22406 (25)	0.4342 (3)	5.2 (3)
C113	0.6967 (6)	0.2002 (3)	0.3849 (3)	6.9 (5)
C114	0.7402 (7)	0.1547 (4)	0.3763 (4)	8.8 (6)
C115	0.7962 (7)	0.1329 (3)	0.4163 (4)	9.2 (6)
C116	0.8060 (6)	0.1568 (3)	0.4662 (3)	6.9 (4)
C121	0.8650 (5)	0.2819 (3)	0.5248 (3)	5.0 (3)
C122	0.9311 (8)	0.3636 (4)	0.5468 (5)	11.7 (8)
C123	1.0193 (8)	0.3100 (4)	0.4887 (4)	10.2 (7)
C124	1.0101 (9)	0.3530 (4)	0.5151 (5)	11.1 (8)
C125	0.9442 (6)	0.2730 (3)	0.4924 (3)	8.4 (5)
C126	0.8591 (6)	0.3269 (3)	0.5506 (3)	7.8 (5)
C211	0.4848 (5)	0.2495 (3)	0.5851 (3)	5.8 (4)
C212	0.4290 (6)	0.2232 (4)	0.6202 (4)	9.1 (6)
C213	0.3316 (16)	0.2137 (13)	0.6068 (11)	21.7 (22)
C214	0.2961 (18)	0.2222 (15)	0.5664 (13)	21.4 (22)
C215	0.3426 (8)	0.2562 (5)	0.5264 (5)	13.1 (9)
C216	0.4442 (6)	0.2685 (3)	0.5377 (4)	8.7 (5)
C221	0.6103 (5)	0.32576 (24)	0.62778 (25)	4.5 (3)
C222	0.5615 (7)	0.3630 (3)	0.6058 (4)	11.9 (7)
C223	0.5685 (9)	0.4111 (4)	0.6265 (6)	15.2 (10)
C224	0.6168 (10)	0.4229 (4)	0.6677 (6)	11.9 (9)
C225	0.6772 (12)	0.3874 (5)	0.6880 (5)	16.0 (12)
C226	0.6665 (9)	0.3387 (3)	0.6691 (4)	13.0 (8)
C311	0.7763 (5)	0.20352 (22)	0.84576 (25)	4.6 (3)
C312	0.8731 (5)	0.18567 (24)	0.8457 (3)	5.8 (4)
C313	0.9468 (5)	0.2124 (3)	0.8692 (3)	7.6 (5)
C314	0.9260 (7)	0.2557 (4)	0.8935 (4)	10.1 (6)
C315	0.8323 (7)	0.2743 (3)	0.8956 (4)	11.5 (7)
C316	0.7577 (6)	0.2475 (3)	0.8710 (3)	7.9 (5)
C321	0.5774 (5)	0.20547 (23)	0.80619 (25)	4.4 (3)
C322	0.4960 (6)	0.2002 (3)	0.8374 (4)	9.0 (5)
C323	0.4161 (7)	0.2329 (4)	0.8305 (5)	11.4 (8)
C324	0.4209 (7)	0.2685 (4)	0.7943 (4)	9.9 (7)
C325	0.5007 (7)	0.2757 (4)	0.7633 (3)	10.3 (6)
C326	0.5807 (6)	0.2428 (3)	0.7708 (3)	8.6 (5)
C411	0.5996 (5)	0.07217 (22)	0.56765 (23)	4.2 (3)
C412	0.5566 (7)	0.1169 (3)	0.5600 (3)	8.5 (5)
C413	0.5277 (7)	0.1333 (3)	0.5103 (3)	9.0 (6)

C414	0.5416	(8)	0.1046	(4)	0.4677	(3)	8.5	(6)
C415	0.5852	(10)	0.0600	(4)	0.4742	(3)	13.1	(9)
C416	0.6152	(8)	0.0445	(3)	0.5241	(3)	10.4	(6)
C421	0.5215	(5)	0.0523	(3)	0.67161	(25)	4.9	(3)
C422	0.4530	(6)	0.0142	(3)	0.6651	(3)	7.4	(5)
C423	0.3646	(7)	0.0155	(4)	0.6945	(4)	9.7	(7)
C424	0.3489	(8)	0.0544	(5)	0.7268	(4)	11.7	(9)
C425	0.4152	(7)	0.0914	(5)	0.7334	(4)	14.4	(9)
C426	0.5023	(6)	0.0915	(4)	0.7032	(3)	8.4	(5)
C511	1.0710	(4)	0.17792	(24)	0.6821	(3)	4.7	(3)
C512	1.0396	(5)	0.2039	(3)	0.6363	(3)	5.9	(4)
C513	1.0690	(6)	0.2524	(3)	0.6271	(3)	7.3	(5)
C514	1.1267	(7)	0.2754	(3)	0.6641	(4)	8.7	(6)
C515	1.1586	(7)	0.2505	(3)	0.7088	(4)	8.9	(6)
C516	1.1294	(6)	0.2013	(3)	0.7187	(3)	6.3	(4)
C521	1.0594	(5)	0.0769	(3)	0.6385	(3)	5.3	(4)
C522	0.9914	(7)	0.0473	(4)	0.6123	(3)	9.0	(6)
C523	1.0230	(9)	0.0128	(5)	0.5727	(4)	12.0	(8)
C524	1.1204	(10)	0.0115	(5)	0.5603	(5)	11.5	(9)
C525	1.1834	(8)	0.0412	(5)	0.5855	(5)	11.3	(8)
C526	1.1534	(6)	0.0719	(3)	0.6241	(3)	7.4	(5)
C611	0.7429	(5)	0.0608	(3)	0.9273	(3)	5.3	(3)
C612	0.7611	(6)	0.1009	(3)	0.9594	(3)	7.3	(5)
C613	0.8203	(8)	0.0935	(5)	1.0045	(5)	10.6	(8)
C614	0.8586	(10)	0.0498	(6)	1.0170	(5)	12.2	(12)
C615	0.8422	(9)	0.0096	(5)	0.9849	(5)	11.7	(8)
C616	0.7821	(6)	0.0138	(3)	0.9385	(3)	8.4	(5)
C621	0.5498	(5)	0.0387	(3)	0.8885	(3)	4.4	(3)
C622	0.5327	(12)	-0.0112	(6)	0.8751	(7)	7.7	(10)
C623	0.4450	(14)	-0.0365	(6)	0.8934	(9)	8.4	(12)
C624	0.3761	(7)	-0.0055	(5)	0.9169	(5)	8.6	(7)
C625	0.3893	(14)	0.0412	(8)	0.9291	(9)	7.6	(11)
C626	0.4763	(11)	0.0654	(6)	0.9138	(6)	6.0	(8)
C622'	0.5326	(11)	0.0264	(7)	0.9397	(6)	7.0	(9)
C623'	0.4407	(13)	0.0047	(8)	0.9499	(6)	7.6	(10)
C625'	0.3971	(14)	0.0123	(12)	0.8605	(7)	13.8	(18)
C626'	0.4843	(11)	0.0368	(9)	0.8486	(7)	9.0	(12)
C711	0.6379	(5)	-0.0803	(3)	0.6986	(3)	5.6	(4)
C712	0.6095	(9)	-0.0653	(4)	0.7468	(4)	13.7	(8)
C713	0.5380	(12)	-0.0924	(6)	0.7724	(6)	19.6	(12)
C714	0.4922	(12)	-0.1302	(6)	0.7503	(6)	14.7	(11)
C715	0.5202	(11)	-0.1445	(6)	0.7047	(6)	15.4	(11)
C716	0.5899	(8)	-0.1177	(4)	0.6760	(4)	12.7	(8)
C721	0.7923	(5)	-0.08435	(22)	0.6194	(3)	4.9	(3)
C722	0.8695	(6)	-0.1125	(3)	0.6402	(3)	7.1	(4)
C723	0.9213	(7)	-0.1441	(4)	0.6071	(4)	9.0	(6)
C724	0.8975	(8)	-0.1482	(4)	0.5545	(4)	10.2	(7)
C725	0.8210	(8)	-0.1214	(3)	0.5331	(4)	10.3	(7)
C726	0.7691	(6)	-0.0896	(3)	0.5670	(3)	7.4	(5)
C811	1.0981	(4)	0.08749	(21)	0.85258	(23)	4.0	(3)
C812	1.1870	(5)	0.1124	(3)	0.8543	(3)	6.1	(4)
C813	1.2213	(6)	0.1339	(3)	0.9012	(3)	7.7	(5)
C814	1.1668	(7)	0.1334	(3)	0.9459	(3)	7.2	(5)
C815	1.0776	(6)	0.1087	(3)	0.9456	(3)	6.6	(5)
C816	1.0442	(5)	0.08649	(24)	0.8993	(3)	5.2	(3)
C821	1.1051	(4)	-0.00034	(22)	0.78535	(25)	4.3	(3)
C822	1.1622	(6)	-0.0217	(3)	0.8238	(3)	7.3	(4)
C823	1.1989	(7)	-0.0698	(3)	0.8170	(4)	10.4	(6)
C824	1.1766	(7)	-0.0963	(3)	0.7728	(4)	9.4	(6)
C825	1.1203	(7)	-0.0756	(3)	0.7341	(3)	8.5	(5)
C826	1.0839	(6)	-0.0280	(3)	0.7412	(3)	6.5	(4)

Table 6-15. Interatomic distances for $Sr_2O_9N_4P_8C_{96}H_{82}$.

Atoms	Dist. (Å)	Atoms	Dist. (Å)
SR1-SR2	3.6252(7)	C322-C323	1.410(12)
SR1-O1	2.416(4)	C323-C324	1.316(15)
SR1-O2	2.399(4)	C324-C325	1.358(15)
SR1-O3	2.587(3)	C325-C326	1.416(11)
SR1-O4	2.471(4)	C411-C412	1.345(10)
SR1-O5	2.530(4)	C411-C416	1.336(10)
SR1-O9	2.591(5)	C412-C413	1.375(11)
SR2-O3	2.595(3)	C413-C414	1.329(13)
SR2-O4	2.642(3)	C414-C415	1.340(14)
SR2-O5	2.563(4)	C415-C416	1.378(12)
SR2-O6	2.391(4)	C421-C422	1.390(11)
SR2-O7	2.385(4)	C421-C426	1.338(11)
SR2-O8	2.402(3)	C422-C423	1.420(13)
O1-P1	1.515(4)	C423-C424	1.334(17)
O2-P2	1.495(4)	C424-C425	1.351(17)
O3-P3	1.516(4)	C425-C426	1.416(12)
O4-P4	1.523(4)	C511-C512	1.407(10)
O5-P5	1.520(4)	C511-C516	1.365(10)
O6-P6	1.494(4)	C512-C513	1.375(11)
O7-P7	1.509(4)	C513-C514	1.362(14)
O8-P8	1.510(4)	C514-C515	1.374(14)
P1-N1	1.592(5)	C515-C516	1.395(11)
P1-C111	1.773(6)	C521-C522	1.384(12)
P1-C121	1.832(7)	C521-C526	1.345(11)
P2-N1	1.586(5)	C522-C523	1.421(15)
P2-C211	1.823(7)	C523-C524	1.372(18)
P2-C221	1.792(6)	C524-C525	1.328(18)
P3-N2	1.568(5)	C525-C526	1.334(14)
P3-C311	1.816(7)	C611-C612	1.360(12)
P3-C321	1.817(6)	C611-C616	1.392(12)
P4-N3	1.573(5)	C612-C613	1.405(14)
P4-C411	1.788(6)	C613-C614	1.314(21)
P4-C421	1.823(7)	C614-C615	1.359(21)
P5-N4	1.575(5)	C615-C616	1.427(15)
P5-C511	1.823(6)	C621-C622	1.391(18)
P5-C521	1.793(7)	C621-C626	1.389(16)
P6-N2	1.568(5)	C621-C622'	1.349(16)
P6-C611	1.820(7)	C621-C626'	1.342(17)
P6-C621	1.829(6)	C622-C623	1.453(24)
P7-N3	1.584(5)	C622-C626'	1.59(3)
P7-C711	1.820(7)	C623-C624	1.387(24)
P7-C721	1.796(7)	C623-C623'	1.79(3)
P8-N4	1.585(5)	C623-C625'	1.67(3)
P8-C811	1.783(6)	C624-C625	1.29(3)
P8-C821	1.820(6)	C624-C623'	1.240(22)
C111-C112	1.387(9)	C624-C625'	1.520(22)
C111-C116	1.394(10)	C625-C626	1.410(24)
C112-C113	1.395(11)	C625-C623'	1.31(3)
C113-C114	1.370(13)	C626-C622'	1.448(24)
C114-C115	1.388(14)	C626-C626'	1.808(25)
C115-C116	1.410(12)	C622'-C623'	1.409(22)
C121-C125	1.378(11)	C625'-C626'	1.40(3)
C121-C126	1.367(11)	C711-C712	1.333(13)
C122-C124	1.375(16)	C711-C716	1.322(13)
C122-C126	1.392(12)	C712-C713	1.377(16)
C123-C124	1.331(17)	C713-C714	1.310(20)
C123-C125	1.428(13)	C714-C715	1.266(20)
C211-C212	1.361(12)	C715-C716	1.396(17)
C211-C216	1.406(12)	C721-C722	1.396(11)
C212-C213	1.397(21)	C721-C726	1.356(10)
C213-C214	1.14(5)	C722-C723	1.380(13)

C214-C215	1.50(4)	C723-C724	1.362(15)
C215-C216	1.456(14)	C724-C725	1.376(16)
C221-C222	1.316(11)	C725-C726	1.396(13)
C221-C226	1.334(12)	C811-C812	1.388(9)
C222-C223	1.388(13)	C811-C816	1.387(9)
C223-C224	1.263(18)	C812-C813	1.388(10)
C224-C225	1.356(20)	C813-C814	1.350(12)
C225-C226	1.388(15)	C814-C815	1.388(12)
C311-C312	1.409(10)	C815-C816	1.380(10)
C311-C316	1.357(9)	C821-C822	1.363(10)
C312-C313	1.368(10)	C821-C826	1.360(9)
C313-C314	1.336(12)	C822-C823	1.389(11)
C314-C315	1.377(14)	C823-C824	1.348(13)
C315-C316	1.391(12)	C824-C825	1.356(13)
C321-C322	1.372(11)	C825-C826	1.375(11)
C321-C326	1.335(10)		

Table 6-16. Interatomic angles for $Sr_2O_9N_4P_8C_{96}H_{82}$.

Atoms	Angle (°)	Atoms	Angle (°)
SR2-SR1-O1	135.18(9)	P3-C311-C312	118.3(5)
SR2-SR1-O2	134.35(9)	P3-C311-C316	123.4(5)
SR2-SR1-O3	45.69(8)	C312-C311-C316	118.1(6)
SR2-SR1-O4	46.79(8)	C311-C312-C313	121.0(6)
SR2-SR1-O5	44.98(8)	C312-C313-C314	119.3(7)
SR2-SR1-O9	106.39(11)	C313-C314-C315	122.0(8)
O1-SR1-O2	80.60(13)	C314-C315-C316	118.7(7)
O1-SR1-O3	178.46(12)	C311-C316-C315	120.8(7)
O1-SR1-O4	105.40(12)	P3-C321-C322	120.0(5)
O1-SR1-O5	103.07(12)	P3-C321-C326	120.8(5)
O1-SR1-O9	99.41(14)	C322-C321-C326	119.1(6)
O2-SR1-O3	97.98(12)	C321-C322-C323	119.9(7)
O2-SR1-O4	105.78(13)	C322-C323-C324	119.4(8)
O2-SR1-O5	174.48(14)	C323-C324-C325	122.6(8)
O2-SR1-O9	89.67(15)	C324-C325-C326	117.5(8)
O3-SR1-O4	74.35(11)	C321-C326-C325	121.5(7)
O3-SR1-O5	78.38(11)	P4-C411-C412	122.2(5)
O3-SR1-O9	81.17(13)	P4-C411-C416	121.4(5)
O4-SR1-O5	77.38(12)	C412-C411-C416	116.3(6)
O4-SR1-O9	152.49(13)	C411-C412-C413	122.4(7)
O5-SR1-O9	85.68(14)	C412-C413-C414	120.2(8)
SR1-SR2-O3	45.52(7)	C413-C414-C415	118.6(7)
SR1-SR2-O4	42.96(8)	C414-C415-C416	120.4(8)
SR1-SR2-O5	44.24(8)	C411-C416-C415	122.0(8)
SR1-SR2-O6	128.24(9)	P4-C421-C422	118.8(6)
SR1-SR2-O7	119.33(9)	P4-C421-C426	120.6(6)
SR1-SR2-O8	117.53(9)	C422-C421-C426	120.4(7)
O3-SR2-O4	71.44(10)	C421-C422-C423	119.8(8)
O3-SR2-O5	77.65(12)	C422-C423-C424	118.3(9)
O3-SR2-O6	84.49(12)	C423-C424-C425	122.2(9)
O3-SR2-O7	150.64(12)	C424-C425-C426	120.1(9)
O3-SR2-O8	108.71(12)	C421-C426-C425	119.0(8)
O4-SR2-O5	73.81(11)	P5-C511-C512	118.7(5)
O4-SR2-O6	119.68(12)	P5-C511-C516	121.1(5)
O4-SR2-O7	82.49(12)	C512-C511-C516	120.0(6)
O4-SR2-O8	153.31(12)	C511-C512-C513	120.8(7)
O5-SR2-O6	152.76(13)	C512-C513-C514	118.6(8)
O5-SR2-O7	108.27(13)	C513-C514-C515	121.4(8)
O5-SR2-O8	80.12(12)	C514-C515-C516	120.6(8)
O6-SR2-O7	97.40(13)	C511-C516-C515	118.6(7)
O6-SR2-O8	86.44(13)	P5-C521-C522	120.6(6)
O7-SR2-O8	100.65(13)	P5-C521-C526	121.8(6)
SR1-O1-P1	134.15(22)	C522-C521-C526	117.3(7)
SR1-O2-P2	136.22(23)	C521-C522-C523	119.6(8)
SR1-O3-SR2	88.79(11)	C522-C523-C524	118.2(10)
SR1-O3-P3	146.80(20)	C523-C524-C525	120.5(11)
SR2-O3-P3	123.65(18)	C524-C525-C526	120.6(11)
SR1-O4-SR2	90.25(11)	C521-C526-C525	123.6(9)
SR1-O4-P4	150.31(21)	P6-C611-C612	121.3(6)
SR2-O4-P4	119.12(19)	P6-C611-C616	117.4(6)
SR1-O5-SR2	90.78(11)	C612-C611-C616	121.3(7)
SR1-O5-P5	141.40(22)	C611-C612-C613	118.0(9)
SR2-O5-P5	127.53(20)	C612-C613-C614	123.1(12)
SR2-O6-P6	130.64(22)	C613-C614-C615	119.5(11)
SR2-O7-P7	131.47(22)	C614-C615-C616	121.0(11)
SR2-O8-P8	134.95(21)	C611-C616-C615	117.1(9)
O1-P1-N1	119.56(23)	P6-C621-C622	117.8(7)
O1-P1-C111	109.0(3)	P6-C621-C626	123.6(8)
O1-P1-C121	108.4(3)	P6-C621-C622'	121.2(7)
N1-P1-C111	107.8(3)	P6-C621-C626'	112.8(8)
N1-P1-C121	107.1(3)	C622-C621-C626	118.6(10)

C111-P1-C121	103.9(3)	C622-C621-C622'	88.1(11)
O2-P2-N1	118.69(24)	C622-C621-C626'	71.0(13)
O2-P2-C211	108.3(3)	C626-C621-C622'	63.9(10)
O2-P2-C221	108.2(3)	C626-C621-C626'	82.9(11)
N1-P2-C211	107.4(3)	C622'-C621-C626'	125.7(10)
N1-P2-C221	108.4(3)	C621-C622-C623	120.4(13)
C211-P2-C221	105.0(3)	C621-C622-C626'	53.1(10)
O3-P3-N2	118.41(23)	C623-C622-C626'	99.4(14)
O3-P3-C311	106.7(3)	C622-C623-C624	114.9(13)
O3-P3-C321	109.66(25)	C622-C623-C623'	89.7(12)
N2-P3-C311	109.3(3)	C622-C623-C625'	78.9(13)
N2-P3-C321	106.4(3)	C624-C623-C623'	43.6(10)
C311-P3-C321	105.7(3)	C624-C623-C625'	58.7(12)
O4-P4-N3	117.17(24)	C623'-C623-C625'	84.3(13)
O4-P4-C411	110.25(25)	C623-C624-C625	125.4(12)
O4-P4-C421	105.6(3)	C623-C624-C623'	86.0(14)
N3-P4-C411	106.0(3)	C623-C624-C625'	70.1(15)
N3-P4-C421	111.8(3)	C625-C624-C623'	62.1(15)
C411-P4-C421	105.4(3)	C625-C624-C625'	83.9(16)
O5-P5-N4	118.01(23)	C623'-C624-C625'	114.6(12)
O5-P5-C511	108.5(3)	C624-C625-C626	119.5(15)
O5-P5-C521	108.6(3)	C624-C625-C623'	56.9(13)
N4-P5-C511	104.7(3)	C626-C625-C623'	89.7(15)
N4-P5-C521	109.3(3)	C621-C626-C625	120.4(14)
C511-P5-C521	107.3(3)	C621-C626-C622'	56.7(9)
O6-P6-N2	117.77(24)	C621-C626-C626'	47.4(8)
O6-P6-C611	110.2(3)	C625-C626-C622'	89.9(13)
O6-P6-C621	108.1(3)	C625-C626-C626'	96.2(14)
N2-P6-C611	107.6(3)	C622'-C626-C626'	94.0(12)
N2-P6-C621	108.4(3)	C621-C622'-C626	59.4(9)
C611-P6-C621	104.0(3)	C621-C622'-C623'	115.6(12)
O7-P7-N3	117.25(24)	C626-C622'-C623'	84.3(13)
O7-P7-C711	107.8(3)	C623-C623'-C624	50.5(11)
O7-P7-C721	110.0(3)	C623-C623'-C625	99.2(16)
N3-P7-C711	108.7(3)	C623-C623'-C622'	94.3(13)
N3-P7-C721	105.5(3)	C624-C623'-C625	61.0(15)
C711-P7-C721	107.2(3)	C624-C623'-C622'	127.2(14)
O8-P8-N4	117.82(22)	C625-C623'-C622'	95.9(17)
O8-P8-C811	108.9(3)	C623-C625'-C624	51.2(12)
O8-P8-C821	106.6(3)	C623-C625'-C626'	97.8(16)
N4-P8-C811	106.7(3)	C624-C625'-C626'	120.7(13)
N4-P8-C821	109.7(3)	C621-C626'-C622	55.9(9)
C811-P8-C821	106.5(3)	C621-C626'-C626	49.7(8)
P1-N1-P2	130.1(3)	C621-C626'-C625'	115.3(14)
P3-N2-P6	138.2(3)	C622-C626'-C626	89.2(11)
P4-N3-P7	132.4(3)	C622-C626'-C625'	83.6(16)
P5-N4-P8	132.4(3)	C626-C626'-C625'	87.0(14)
P1-C111-C112	121.1(5)	P7-C711-C712	118.8(6)
P1-C111-C116	120.0(5)	P7-C711-C716	122.5(7)
C112-C111-C116	118.9(6)	C712-C711-C716	118.0(8)
C111-C112-C113	120.9(6)	C711-C712-C713	118.5(10)
C112-C113-C114	120.4(7)	C712-C713-C714	123.0(12)
C113-C114-C115	119.9(8)	C713-C714-C715	118.0(13)
C114-C115-C116	120.1(8)	C714-C715-C716	121.4(12)
C111-C116-C115	119.8(7)	C711-C716-C715	120.3(10)
P1-C121-C125	121.4(6)	P7-C721-C722	119.0(5)
P1-C121-C126	119.9(6)	P7-C721-C726	122.4(6)
C125-C121-C126	118.5(7)	C722-C721-C726	118.7(7)
C124-C122-C126	117.0(9)	C721-C722-C723	119.6(7)
C124-C123-C125	119.5(9)	C722-C723-C724	120.5(9)
C122-C124-C123	122.8(9)	C723-C724-C725	121.1(9)
C121-C125-C123	119.3(8)	C724-C725-C726	117.7(8)
C121-C126-C122	122.8(8)	C721-C726-C725	122.4(8)
P2-C211-C212	118.3(7)	P8-C811-C812	123.3(5)
P2-C211-C216	120.8(6)	P8-C811-C816	119.6(5)
C212-C211-C216	120.8(7)	C812-C811-C816	117.0(6)
C211-C212-C213	118.4(17)	C811-C812-C813	121.2(6)

C212-C213-C214	125(3)	C812-C813-C814	120.9(7)
C213-C214-C215	122.2(21)	C813-C814-C815	119.3(6)
C214-C215-C216	114.4(13)	C814-C815-C816	119.9(7)
C211-C216-C215	117.2(9)	C811-C816-C815	121.7(6)
P2-C221-C222	124.6(6)	P8-C821-C822	122.9(5)
P2-C221-C226	120.4(6)	P8-C821-C826	118.9(5)
C222-C221-C226	114.9(7)	C822-C821-C826	118.0(6)
C221-C222-C223	120.4(8)	C821-C822-C823	120.4(7)
C222-C223-C224	124.8(11)	C822-C823-C824	120.3(7)
C223-C224-C225	116.8(9)	C823-C824-C825	120.0(7)
C224-C225-C226	117.4(11)	C824-C825-C826	119.3(7)
C221-C226-C225	124.6(9)	C821-C826-C825	121.9(7)

Dizinc *tetrakis*(2,2,5,5-tetramethyl-1-aza-2,5-disilacyclopentyl)

Prepared by: Oliver Just

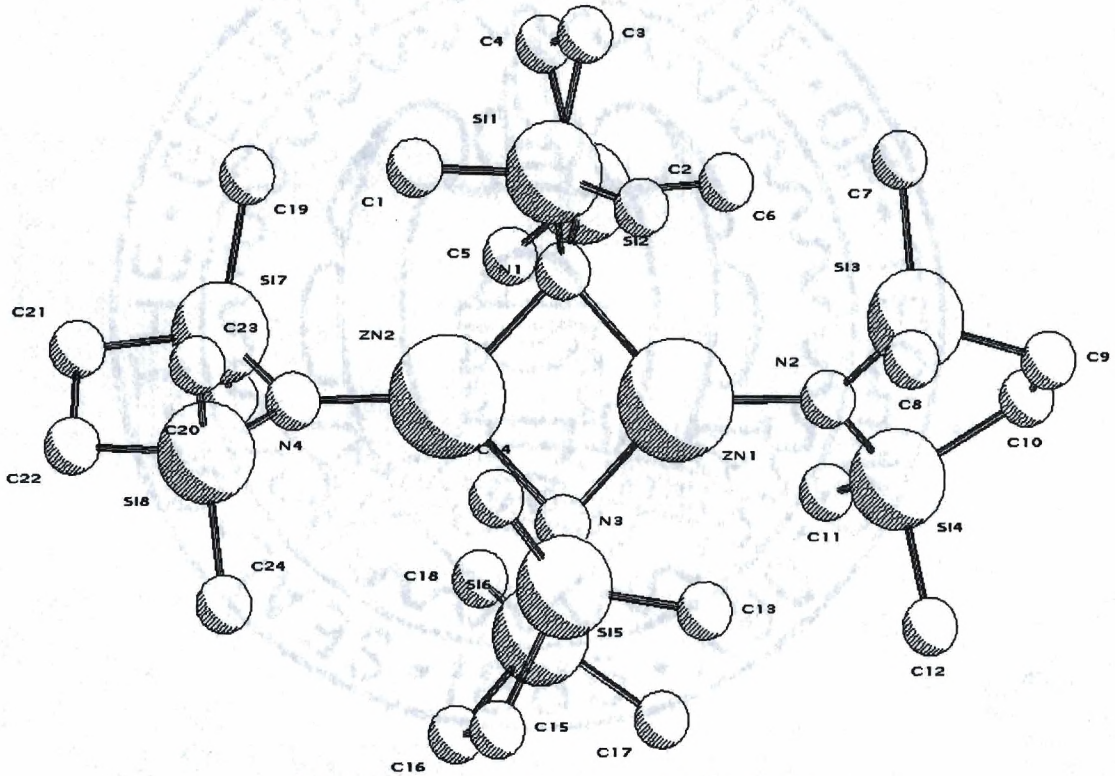

Figure 6-7. PLUTO plot of $Zn_2(tmadscp)_4$.

Table 6-17. Unit cell and data collection parameters for $Zn_2Si_8N_4C_{24}H_{64}$.

Empirical Formula	$Zn_2Si_8N_4C_{24}H_{64}$
Formula Weight	764.23 g/mol.
Temperature	293(2) K
Wavelength	0.71073 Å
Crystal System	monoclinic
Space Group	$P2_1/c$
Unit Cell Dimensions	a = 11.5227(14) Å
	b = 16.881(22) Å β = 99.356(10)°
	c = 21.192(3) Å
Volume	4067.5(9) $Å^3$
Z	4
Density (calc'd)	1.248 g/cc
Absorption Coefficient	3.94 mm^{-1}
F(000)	1629.20
θ Range for Data Collection	2.29° to 74.8°
Index Ranges	$-12 \leq h \leq 12$, $0 \leq k \leq 21$, $0 \leq l \leq 26$
Reflections Collected	9916
Independent Reflections	8031
Refinement Method	Full-matrix least-squares on F^2
Data / Restraints / Parameters	5078 / 0 / 344
Goodness of Fit on F^2	4.20
Final R Indices [$I>2\sigma(I)$]	$R = 0.062$, $R_w = 0.048$
R Indices (all data)	$R = 0.062$, $R_w = 0.048$
Largest Difference Peak and Hole	0.580 and -0.980 e/$Å^3$

Table 6-18. Atomic coordinates for $Zn_2Si_8N_4C_{24}H_{64}$.

	x	y	z	Biso (Å^2)
ZN1	0.64675(9)	0.66127(5)	0.23016(4)	3.67(4)
ZN2	0.86136(9)	0.69204(5)	0.31503(4)	3.80(5)
N1	0.7006 (5)	0.6466 (3)	0.32820(21)	3.9 (3)
N2	0.5049 (5)	0.6351 (3)	0.17499(22)	3.7 (3)
N3	0.8030 (5)	0.7107 (3)	0.21676(20)	4.0 (3)
N4	1.0093 (5)	0.7128 (3)	0.36917(22)	4.2 (3)
SI1	0.63133(22)	0.71413(15)	0.37634(9)	5.15(12)
SI2	0.68023(22)	0.55171(13)	0.35417(10)	4.85(11)
SI3	0.36385(21)	0.66499(14)	0.17881(10)	4.72(11)
SI4	0.50412(22)	0.56916(14)	0.11318(10)	4.91(11)
SI5	0.90392(20)	0.65904(14)	0.17489(9)	4.34(11)
SI6	0.79334(22)	0.80624(13)	0.18932(9)	4.67(11)
SI7	1.07550(23)	0.64493(15)	0.42471(10)	5.41(13)
SI8	1.08505(24)	0.80031(15)	0.37833(10)	6.05(13)
C1	0.7425 (8)	0.7749 (5)	0.4294 (3)	8.1 (6)
C2	0.5309 (7)	0.7856 (5)	0.3298 (3)	6.1 (5)
C3	0.5582 (8)	0.6454 (6)	0.4253 (4)	7.1 (5)
C4	0.6364 (8)	0.5707 (6)	0.4353 (3)	7.3 (6)
C5	0.8127 (7)	0.4884 (4)	0.3521 (3)	6.0 (5)
C6	0.5537 (8)	0.4987 (5)	0.3064 (4)	6.5 (5)
C7	0.3097 (6)	0.6378 (5)	0.2552 (3)	5.5 (4)
C8	0.3431 (7)	0.7719 (4)	0.1643 (3)	5.8 (4)
C9	0.2763 (7)	0.6056 (5)	0.1121 (3)	6.1 (5)
C10	0.3490 (8)	0.5305 (5)	0.1023 (3)	6.3 (5)
C11	0.6160 (7)	0.4880 (4)	0.1321 (3)	6.3 (5)
C12	0.5248 (7)	0.6212 (5)	0.0367 (3)	6.7 (5)
C13	0.6585 (7)	0.8211 (5)	0.1281 (3)	6.4 (5)
C14	0.7853 (7)	0.8792 (4)	0.2542 (3)	6.3 (5)
C15	0.9296 (8)	0.8165 (5)	0.1505 (3)	6.4 (5)
C16	1.0055 (7)	0.7409 (5)	0.1623 (3)	5.7 (5)
C17	0.8407 (7)	0.6240 (5)	0.0926 (3)	6.5 (5)
C18	0.9719 (8)	0.5732 (4)	0.2205 (3)	6.1 (5)
C19	0.9819 (8)	0.6122 (5)	0.4843 (3)	7.6 (6)
C20	1.1364 (7)	0.5543 (5)	0.3910 (3)	6.0 (5)
C21	1.2008 (9)	0.7030 (6)	0.4695 (4)	10.1 (7)
C22	1.2275 (9)	0.7689 (7)	0.4291 (4)	9.8 (7)
C23	1.0158 (9)	0.8792 (5)	0.4218 (4)	9.3 (6)
C24	1.1247 (7)	0.8487 (5)	0.3052 (3)	7.0 (5)

Table 6-19. Atomic distances for $Zn_2Si_8N_4C_{24}H_{64}$.

Atoms	Dist. (Å)	Atoms	Dist. (Å)
ZN1-N1	2.084(4)	SI3-C8	1.839(8)
ZN1-N2	1.900(5)	SI3-C9	1.886(8)
ZN1-N3	2.045(6)	SI4-C10	1.881(9)
ZN2-N1	2.065(6)	SI4-C11	1.879(8)
ZN2-N3	2.106(4)	SI4-C12	1.892(8)
ZN2-N4	1.926(5)	SI5-C16	1.858(8)
N1-SI1	1.801(6)	SI5-C17	1.873(7)
N1-SI2	1.722(5)	SI5-C18	1.845(8)
N2-SI3	1.717(6)	SI6-C13	1.873(7)
N2-SI4	1.718(5)	SI6-C14	1.860(8)
N3-SI5	1.799(6)	SI6-C15	1.896(9)
N3-SI6	1.712(6)	SI7-C19	1.872(9)
N4-SI7	1.729(6)	SI7-C20	1.872(8)
N4-SI8	1.710(6)	SI7-C21	1.871(10)
SI1-C1	1.868(8)	SI8-C22	1.886(10)
SI1-C2	1.843(8)	SI8-C23	1.870(9)
SI1-C3	1.849(9)	SI8-C24	1.873(8)
SI2-C4	1.897(8)	C3-C4	1.544(14)
SI2-C5	1.869(9)	C9-C10	1.552(13)
SI2-C6	1.864(8)	C15-C16	1.543(12)
SI3-C7	1.884(7)	C21-C22	1.467(15)

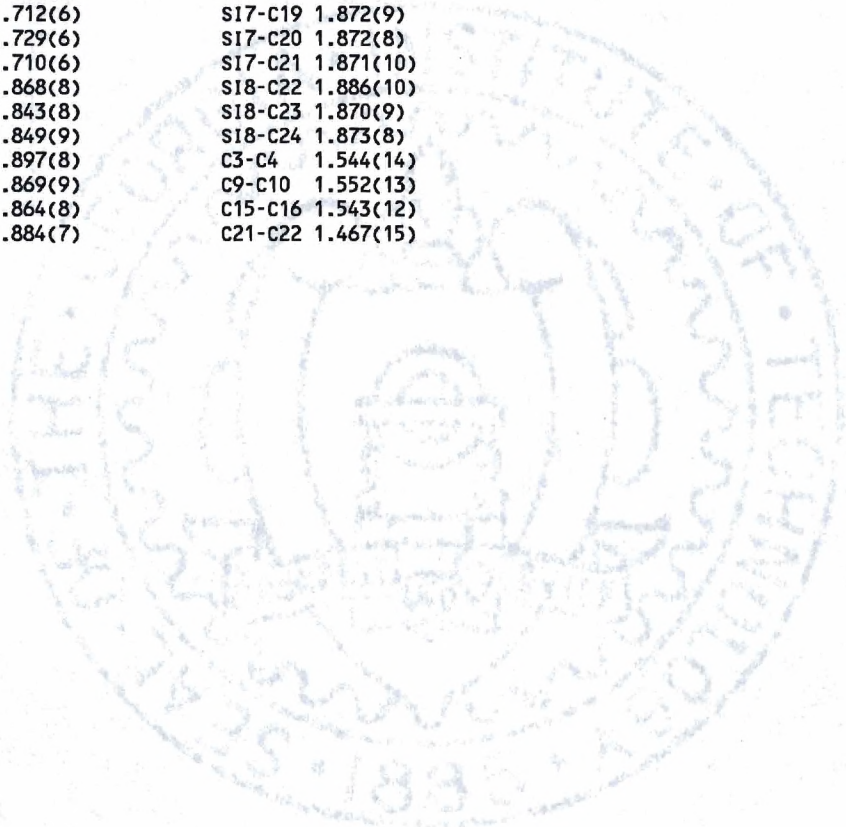

Table 6-20. Atomic angles for $Zn_2Si_8N_4C_{24}H_{64}$.

Atoms	Angle (°)	Atoms	Angle (°)
N1-ZN1-N2	132.27(22)	C7-SI3-C9	107.7(4)
N1-ZN1-N3	93.49(20)	C8-SI3-C9	110.9(4)
N2-ZN1-N3	134.22(20)	N2-SI4-C10	101.9(3)
N1-ZN2-N3	92.29(20)	N2-SI4-C11	113.0(3)
N1-ZN2-N4	135.52(20)	N2-SI4-C12	111.5(3)
N3-ZN2-N4	132.18(23)	C10-SI4-C11	112.2(4)
ZN1-N1-ZN2	87.10(19)	C10-SI4-C12	107.8(4)
ZN1-N1-SI1	113.7(3)	C11-SI4-C12	110.1(4)
ZN1-N1-SI2	113.3(3)	N3-SI5-C16	100.5(3)
ZN2-N1-SI1	109.3(3)	N3-SI5-C17	115.3(3)
ZN2-N1-SI2	124.1(3)	N3-SI5-C18	112.1(3)
SI1-N1-SI2	108.2(3)	C16-SI5-C17	105.1(3)
ZN1-N2-SI3	129.0(3)	C16-SI5-C18	115.9(4)
ZN1-N2-SI4	121.2(3)	C17-SI5-C18	107.9(4)
SI3-N2-SI4	109.8(3)	N3-SI6-C13	111.3(3)
ZN1-N3-ZN2	87.04(19)	N3-SI6-C14	112.4(3)
ZN1-N3-SI5	121.7(3)	N3-SI6-C15	102.7(3)
ZN1-N3-SI6	114.9(3)	C13-SI6-C14	106.8(4)
ZN2-N3-SI5	106.7(3)	C13-SI6-C15	109.8(3)
ZN2-N3-SI6	118.0(3)	C14-SI6-C15	113.9(4)
SI5-N3-SI6	107.5(3)	N4-SI7-C19	114.6(3)
ZN2-N4-SI7	122.3(3)	N4-SI7-C20	115.6(3)
ZN2-N4-SI8	127.7(3)	N4-SI7-C21	102.5(4)
SI7-N4-SI8	109.5(3)	C19-SI7-C20	108.0(4)
N1-SI1-C1	111.4(3)	C19-SI7-C21	107.1(4)
N1-SI1-C2	114.2(3)	C20-SI7-C21	108.4(4)
N1-SI1-C3	101.8(3)	N4-SI8-C22	101.7(4)
C1-SI1-C2	105.8(4)	N4-SI8-C23	114.8(4)
C1-SI1-C3	109.7(4)	N4-SI8-C24	118.1(3)
C2-SI1-C3	114.0(4)	C22-SI8-C23	108.7(4)
N1-SI2-C4	101.7(3)	C22-SI8-C24	106.7(4)
N1-SI2-C5	111.7(3)	C23-SI8-C24	106.1(4)
N1-SI2-C6	114.1(3)	SI1-C3-C4	106.3(6)
C4-SI2-C5	117.2(4)	SI2-C4-C3	104.4(5)
C4-SI2-C6	105.9(4)	SI3-C9-C10	107.5(5)
C5-SI2-C6	106.4(4)	SI4-C10-C9	102.9(5)
N2-SI3-C7	114.7(3)	SI6-C15-C16	110.0(5)
N2-SI3-C8	112.3(3)	SI5-C16-C15	106.5(5)
N2-SI3-C9	101.7(3)	SI7-C21-C22	108.6(6)
C7-SI3-C8	109.3(4)	SI8-C22-C21	107.5(7)

Diindium *tetrakis*(2-methoxy-5-methylthiophenoxide)

Prepared by: Rod Schluter

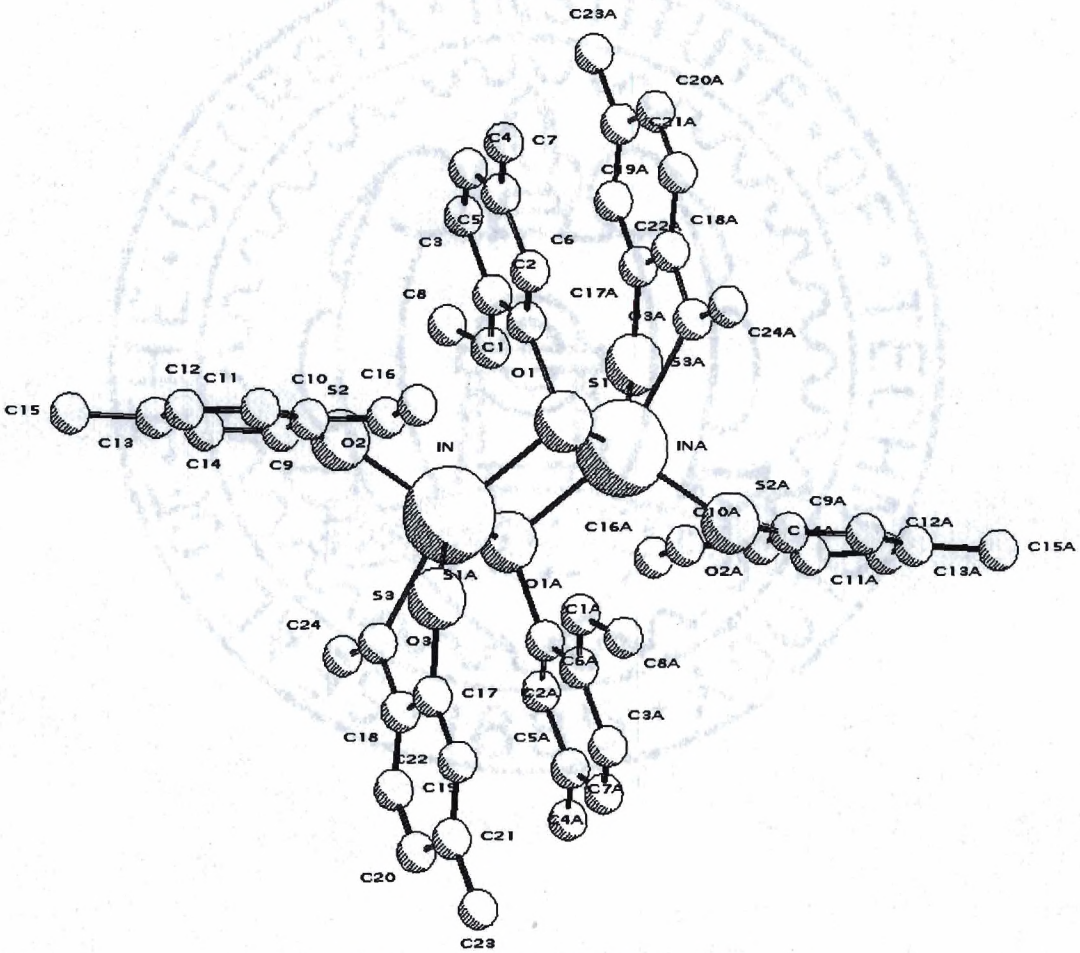

Figure 6-8. PLUTO plot of $In_2(momtp)_4$.

Table 6-21. Unit cell and data collection parameters for $In_2C_{48}H_{54}O_3S_3$.

Empirical Formula	$In_2C_{48}H_{54}O_3S_3$
Formula Weight	574.47 g/mol.
Temperature	293(2) K
Wavelength	0.71073 Å
Crystal System	monoclinic
Space Group	$P2_1/n$
Unit Cell Dimensions	a = 8.3228(24) Å
	b = 24.970(4) Å β = 104.317(19)°
	c = 12.4656(22) Å
Volume	2510.1(9) $Å^3$
Z	4
Density (calc'd)	1.520 g/cc
Absorption Coefficient	10.18 mm^{-1}
F(000)	1174.67
θ Range for Data Collection	2.29° to 74.8°
Index Ranges	$-10 \leq h \leq 10$, $0 \leq k \leq 31$, $0 \leq l \leq 15$
Reflections Collected	6520
Independent Reflections	5173
Refinement Method	Full-matrix least-squares on F^2
Data / Restraints / Parameters	4555 / 0 / 280
Goodness of Fit on F^2	9.59
Final R Indices [$I>2\sigma(I)$]	$R = 0.082$, $R_w = 0.078$
R Indices (all data)	$R = 0.082$, $R_w = 0.078$
Largest Difference Peak and Hole	1.880 and -2.830 e/$Å^3$

Table 6-22. Atomic coordinates for $In_2C_{48}H_{54}O_3S_3$.

	x	y	z	Biso (Å^2)
IN	0.07675(9)	0.06780(3)	0.05931(5)	4.68(3)
S1	-0.1759 (3)	0.00678(10)	0.05766(18)	4.49(10)
S2	0.2983 (4)	0.05461(13)	0.22638(23)	6.47(14)
S3	-0.0347 (4)	0.15713(12)	0.01209(24)	6.12(14)
O1	0.1062 (8)	-0.0593 (3)	0.1675 (5)	5.6 (3)
O2	-0.0095 (11)	0.1084 (3)	0.2489 (7)	6.6 (4)
O3	0.2869 (10)	0.1211 (3)	-0.0186 (6)	6.2 (4)
C1	-0.1375 (12)	-0.0198 (4)	0.1942 (7)	4.3 (4)
C2	0.0025 (13)	-0.0502 (4)	0.2364 (8)	4.9 (4)
C3	0.0300 (14)	-0.0710 (5)	0.3446 (9)	6.3 (6)
C4	-0.0805 (16)	-0.0596 (5)	0.4063 (8)	6.8 (7)
C5	-0.2209 (14)	-0.0294 (5)	0.3664 (8)	5.7 (5)
C6	-0.2470 (12)	-0.0101 (4)	0.2592 (7)	5.0 (5)
C7	-0.3362 (15)	-0.0166 (6)	0.4350 (9)	7.5 (7)
C8	0.2640 (13)	-0.0851 (5)	0.2142 (10)	6.4 (6)
C9	0.2830 (15)	0.1087 (4)	0.3113 (8)	5.4 (5)
C10	0.1280 (17)	0.1315 (5)	0.3164 (8)	6.0 (6)
C11	0.1208 (19)	0.1733 (5)	0.3882 (10)	7.4 (8)
C12	0.2641 (25)	0.1928 (6)	0.4538 (11)	9.1 (10)
C13	0.4155 (22)	0.1701 (5)	0.4532 (12)	8.8 (9)
C14	0.4230 (17)	0.1292 (5)	0.3801 (9)	7.0 (6)
C15	0.5750 (22)	0.1901 (5)	0.5325 (11)	11.4 (10)
C16	-0.1709 (17)	0.1299 (6)	0.2520 (12)	8.2 (8)
C17	0.0563 (15)	0.1763 (5)	-0.0951 (9)	6.0 (6)
C18	0.2139 (16)	0.1583 (5)	-0.1001 (9)	5.9 (6)
C19	0.2827 (18)	0.1785 (6)	-0.1815 (11)	7.8 (8)
C20	0.2016 (24)	0.2160 (7)	-0.2550 (11)	9.2 (10)
C21	0.0428 (21)	0.2321 (6)	-0.2565 (12)	7.7 (8)
C22	-0.0232 (16)	0.2123 (5)	-0.1759 (10)	6.4 (6)
C23	-0.0409 (20)	0.2708 (6)	-0.3433 (11)	9.3 (9)
C24	0.4504 (14)	0.1031 (5)	-0.0179 (10)	7.0 (7)

Table 6-23. Interatomic distances for $In_2C_{48}H_{54}O_3S_3$.

Atoms	Dist. (Å)	Atoms	Dist. (Å)
IN-S1	2.593(3)	C4-C5	1.376(17)
IN-S1a	2.621(3)	C5-C6	1.385(14)
IN-S2	2.439(3)	C5-C7	1.470(17)
IN-S3	2.431(3)	C9-C10	1.425(19)
S1-INa	2.621(3)	C9-C14	1.364(15)
S1-C1	1.780(9)	C10-C11	1.387(17)
S2-C9	1.741(11)	C11-C12	1.359(22)
S3-C17	1.758(13)	C12-C13	1.38(3)
O1-C2	1.379(13)	C13-C14	1.380(20)
O1-C8	1.450(12)	C13-C15	1.531(20)
O2-C10	1.368(14)	C17-C18	1.403(18)
O2-C16	1.456(17)	C17-C22	1.390(17)
O3-C18	1.399(15)	C18-C19	1.378(19)
O3-C24	1.431(15)	C19-C20	1.365(23)
C1-C2	1.381(14)	C20-C21	1.38(3)
C1-C6	1.383(14)	C21-C22	1.352(21)
C2-C3	1.411(14)	C21-C23	1.490(20)
C3-C4	1.366(18)		

Table 6-24. Interatomic angles for $In_2C_{48}H_{54}O_3S_3$.

Atoms	Angle (°)	Atoms	Angle (°)
S1-IN-S1a	86.82(8)	C1-C6-C5	122.4(9)
S1-IN-S2	111.59(10)	S2-C9-C10	122.6(8)
S1-IN-S3	106.08(10)	S2-C9-C14	119.6(10)
S1a-IN-S2	95.93(9)	C10-C9-C14	117.7(11)
S1a-IN-S3	132.13(9)	O2-C10-C9	115.7(10)
S2-IN-S3	119.56(11)	O2-C10-C11	123.4(13)
IN-S1-INa	93.18(8)	C9-C10-C11	120.8(11)
IN-S1-C1	105.0(3)	C10-C11-C12	119.1(14)
INa-S1-C1	105.1(3)	C11-C12-C13	121.0(12)
IN-S2-C9	105.1(4)	C12-C13-C14	119.8(13)
IN-S3-C17	102.9(4)	C12-C13-C15	120.5(13)
C2-O1-C8	117.9(8)	C14-C13-C15	119.7(16)
C10-O2-C16	117.7(10)	C9-C14-C13	121.4(14)
C18-O3-C24	117.0(9)	S3-C17-C18	122.0(9)
S1-C1-C2	120.3(8)	S3-C17-C22	120.7(10)
S1-C1-C6	120.5(7)	C18-C17-C22	117.3(11)
C2-C1-C6	119.3(8)	O3-C18-C17	115.1(10)
O1-C2-C1	116.9(8)	O3-C18-C19	126.4(12)
O1-C2-C3	123.9(9)	C17-C18-C19	118.6(12)
C1-C2-C3	119.3(10)	C18-C19-C20	121.3(14)
C2-C3-C4	119.3(10)	C19-C20-C21	121.5(13)
C3-C4-C5	122.7(9)	C20-C21-C22	116.6(13)
C4-C5-C6	117.1(10)	C20-C21-C23	118.3(14)
C4-C5-C7	121.8(9)	C22-C21-C23	125.0(15)
C6-C5-C7	121.1(10)	C17-C22-C21	124.5(13)

References

1. a) Full System Reference: E.J. Gabe, Y. Le Page, J.-P. Charland,. F.L. Lee, and P.S. White, *J. Appl. Cryst.*, **1989**, *22*, 384-387. b) Scattering Factors from *Int. Tab. Vol. 4: International Tables for X-ray Crystallography, Vol. IV*, **1974**, Kynoch Press, Birmingham, England. c) ORTEP Plotting: C.K. Johnson, ORTEP - A Fortran Thermal Ellipsoid Plot Program in *Technical Report* ,ORNL-5138, Oak Ridge, **1976**. d) Pluto Plotting: S. Motherwell, University Chemical Laboratory, Cambridge, **1978**.

2. $R = \Sigma (F_o-F_c) / \Sigma (F_o)$,
$R_w = [\Sigma (w(F_o-F_c)^2) / \Sigma (wF_o^2)]^{0.5}$ and
$GoF = [\Sigma (w(Fo-Fc)^2) / (\text{No. of reflns - No. of params.})]^{0.5}$.

Vita

Henry Luten was born in Fort Lauderdale, Florida on March 19th, 1969. He received his High School degree from Westminster Academy, in Fort Lauderdale, in June of 1987. Henry then studied at the University of Miami, in Coral Gables, Florida, where he received a Bachelor of Science degree with general honors in May of 1991. His degree included an American Chemical Society certified major in chemistry and dual minors in physics and mathematics. After graduating from the University of Miami, Henry joined the research group of William S. Rees, Jr. at the Florida State University in Tallahassee, Florida. Henry then transferred to the Georgia Institute of Technology, in Atlanta, when Dr. Rees accepted a faculty position there. Henry received his PhD. in Chemistry from the Georgia Institute of Technology in September of 1996.